

**DETECTION AND DETERMINATION OF ABUSED DRUGS  
FROM FORENSIC MATRICES BY RAMAN BASED SERS  
NANOPARTICLE SENSING METHOD**

Thesis Submitted for the Award of the Degree of

**DOCTOR OF PHILOSOPHY  
in  
FORENSIC SCIENCE**

**By  
VAIDEHI KATOCH**

**Registration Number: 11916648**

**Supervised By**

**Dr. SAURABH SHUKLA (26174)**

**Department of Forensic Science**

**(Assistant Professor)**

**School of Bioengineering and Biosciences,**

**Lovely Professional University, Punjab**

**Co-Supervised by**

**Dr. JASKARAN SINGH**

**Department of Forensic Science**

**(Associate Professor)**

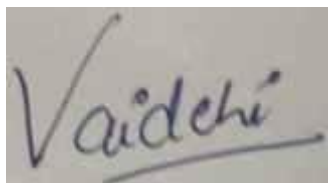
**Geeta University, Panipat, Haryana**



**LOVELY PROFESSIONAL UNIVERSITY, PUNJAB  
2024**

## **DECLARATION**

I, hereby declared that the presented work in the thesis entitled **“Detection and Determination of Abused drugs from forensic matrices by Raman based SERS Nanoparticle Sensing Method”** in fulfilment of degree of **Doctor of Philosophy (Ph. D.)** is outcome of research work carried out by me under the supervision **Dr. Saurabh Shukla**, working as **Assistant Professor** in the **Department of Forensic Science/ School of Bioengineering and Biosciences of Lovely Professional University, Punjab, India**. In keeping with general practice of reporting scientific observations, due acknowledgements have been made whenever work described here has been based on findings of another investigator. This work has not been submitted in part or full to any other University or Institute for the award of any degree.

A photograph of a handwritten signature in blue ink on a light-colored surface. The signature reads "Vaidehi" in a cursive script, with a horizontal line underneath the name.

**(Signature of Scholar)**

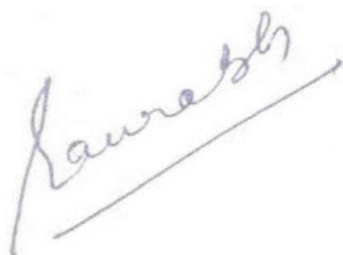
Name of the scholar: Vaidehi Katoch

Registration No.: 11916648

Department/school: Department of Forensic Science/ School of Bioengineering and Biosciences Lovely Professional University, Punjab, India.

## CERTIFICATE

This is to certify that the work reported in the Ph. D. thesis entitled **“Detection and Determination of Abused drugs from forensic matrices by Raman based SERS Nanoparticle Sensing Method”** submitted in fulfillment of the requirement for the reward of degree of **Doctor of Philosophy (Ph.D.)** in the **Department of Forensic Science/ School of Bioengineering and Biosciences** is a research work carried out by **Vaidehi Katoch**, (11916648) is bonafide record of his/her original work carried out under my supervision and that no part of thesis has been submitted for any other degree, diploma or equivalent course.



**(Signature of Supervisor)**

Name of supervisor:

Dr.Saurabh Shukla

Designation: Assistant Professor

Department/school: Forensic science

Science School of Bioengineering & Biosciences



**(Signature of Co-Supervisor)**

Name of Co-Supervisor

Dr. Jaskaran Singh

Designation: HOD & Dean

Department/school: Forensic

Geeta University, Panipat, India

## **Abstract**

Benzodiazepines, which are routinely used as anti-anxiety drugs, have been shown to be beneficial in various toxicological tests. Because of their impact on the central nervous system, drugs are also used in sexual assaults cases. Due to their potency and frequent use at low levels, the goal threshold for detection of these chemicals in bodily fluids is 10 ng/mL. To analyze these compounds at the moment, immunoassay methods are routinely utilized, although more specialist screening methods are needed. This led to the development of a rapid, reliable Surface enhanced Raman spectroscopy (SERS) which is an analytical method induced a dipole moment in the molecules when a laser emits light as this approach used for screening of benzodiazepine in forensic samples, The ability of SERS to detect extremely low quantities of pharmaceuticals in aqueous solutions has been previously proven. Historically, the selectivity and fluorescence effects of Raman spectroscopy have been constrained by surface enhancement. By placing an analyte on a metal substrate with a SERS-active characteristic, such as colloidal metal particles, the spectrum can be created. Including aggregate solutions, the signal strength of the SERS solution can be raised even more. These compounds make the nanoparticles cluster and form areas of greatest need, which amplify the signal and make the problem worse.

The colloidal particles used in this study can be split into two groups: sphere particles of zinc in an aqueous solution, having a mean dimension of about 30 nm, and iron oxide and zinc nanocomposites that with an average diameter of about 15 nm. Consequently, without calcination, extremely crystalline and mesoporous oxide of zinc oxide (ZnO) nanoparticles with a substantial area of surface were synthesized in this study. A thorough analysis of the effects of various pH values on the related to structure, physicochemical, and morphological properties of ZnO nanoparticles was also carried out. According to the Rietveld modification, the pH variation significantly affected the crystal structure of ZnO nanoparticles.

The production of ZnO as a significant phase in all nanopowders was confirmed by the phase, molecular, and elemental structures. ZnO nanoparticles have an uneven shape and a mean size of 45–9 nm (nanometer). ZnO nanoparticles were found to be polycrystalline according to phases and atomic structures. Furthermore, isotherms demonstrated the better specific surface area as well as the porosity volume of the mesoporous morphology of all ZnO nanoparticles. It was determined that the ideal aggregating agent is one that exhibits the highest signal intensity at the least amount of drug concentration and has a limit of detection among 0.5 and 127 ng/mL in order to detect benzodiazepines at the lowest levels of drug concentration.

It was possible to isolate benzodiazepines from urine using a extraction technique at pH 5 allowing for clean the extraction of drug via detection limits ranging from 6 to 640 ng/mL, and dispersive solid phase extraction (DSPE) technique that permitted a rapid clean extraction. There is proof that the benzodiazepine that is important can be preferentially detected with a pH of 6.5 by eliminating other medications that are commonly found in biological samples. It has been demonstrated that this technology, able to detect benzodiazepines in urine at very low concentrations (conc.) in a manner that is both highly sensitive and very specific. The creation of a sensitive and targeted testing approach for determining the presence of benzodiazepines has aided the forensic community in the identification of cases involving drug- facilitated attacks that involve benzodiazepines. Urine, blood, and saliva extracts from oral fluids are combined with an aggregate agent and nanoparticles made of zinc or iron oxide to detect tiny levels of these substances.

In this study the application of this method to the testing of samples as well as the optimisation of key process parameters. Numerous metabolites, including 1, 2-triazolo-benzodiazepines and 1, 4-benzodiazepines, were investigated. The findings of this investigation showed that, for each drug evaluated individually, each aggregating agent caused varying degrees of signal augmentation. Zinc nanoparticles in saliva exhibited the lowest threshold of detection for the medications at 2.5 ng/mL and linearity over a broad range of levels for these medicines.

As it has shown the practicality of SERS in this situation, there is no question that this technique can be used to detect minute amounts of Xanax and this methodology optimized to detect a variety of substances. By using this technique, benzodiazepines can be found in toxicology samples following the analyte have been removed and can be utilized to find trace amounts of the chemical.

## **Acknowledgements**

First and foremost, I would acknowledge Almighty for blessing me with strength, wisdom and positivity during my research work. It is my profound privilege to show a deep sense of gratitude to my Co-supervisor **Dr Jaskaran Singh** for his valuable guidance, consistent support, keen supervision, expertise and suggestions in conducting my research work. I am also grateful to my supervisor, **Dr Saurabh Shukla**, Department of Forensic science, Lovely Professional University, Phagwara, for his guidance, generous support and persistent motivation. I would like to acknowledge **Dr Neeta Raj Sharma**, Dean and Head of School of Bioengineering and Biosciences, for her kind support. I would like to acknowledge the generous help, co-operation and support extended by **Dr Tejasvi Pandey**, Head of Department and all the other faculty members of the Forensic science department. I would like to show my deepest concern of regards to PIMS, Jalandhar, for providing me the ethical permission to carry out some part of my research work there. Also, sincere gratitude to whole CIF faculty members. I fully acknowledge **Ms. Ruby Angurana** for her help, cooperation, moral support and propitious company during my research work. I am also thankful to my friends, seniors and lab mates for their support, co-operation and affection. I am extremely thankful to non-teaching staff of the University for their Assistance. I highly appreciate for unsolicited cooperation and cheery assistance of my family for their unflagging love and support. I owe my sincere gratitude and regards to my parents (**Mr. Vivek Katoch and Mrs. Sharmila**), my sisters, and also heartfelt gratitude to **Mr. Anubhav Thakur** my husband and my in-laws for his continuous support, encouragement and assistance throughout the course of my work. Their abundant affection and unflagging love were constant source of inspiration for me. Last but not least, I thank all those who cannot be mentioned but none of them is forgotten.

**Vaidehi Katoch**

## Abbreviations

SERS	Surface Enhanced Raman Spectroscopy
ZnO	Zinc oxide
nm	Nanometer
LOD	Limit of detection
DSPE	Dispersive solid phase extraction
Conc.	Concentration
WHO	World Health Organization
EPA	Environmental Protection Agency
FDA	Food and Drug Administration
OSHA	Occupational Safety and Health Administration
DFSA	Drug-facilitated sexual assault
BZD	Benzodiazepine
NPS	New psychoactive substance
GABA	Gamma-aminobutyric acid
Cl <sup>-</sup>	Chloride
SUDs	Substance abuse issues
SWGDRUG	Scientific Working Group for Seized Drugs
CN	Cyanine
HPLC	High-Performance Liquid Chromatography
GC	Gas chromatography
EF	Enhancement factor
PAT	Process analytical technology
PCA	Principle component analysis
APIs	Active pharmaceutical ingredients
nps	nanoparticles
DAD	Diode-array detection
µg	Microgram
µM	Micromolar
Mg	Milligram



RF	Radio-frequency
IONPs'	Iron nps
SORS	Spatially offset Raman spectroscopy
ALP	Alprazolam
GQD	Graphene quantum dots
AFM	Atomic force microscopy
Hg	Mercury
DFT	Density functional theory
EST	Estazolam
LLE-LTP	Liquid–liquid extraction with low-temperature
	partition
DZ	Diazepam
LOQ	Limit of quantification
ZNHH	Zinc nitrate hydroxide hydrate
FWHM	Full width at half maximum
$X_c$	Degree of crystallinity
SWV	Square Wave Voltammetry
Fe (NO <sub>3</sub> ) <sub>3</sub> 9H <sub>2</sub> O	Ferric nitrate
C <sub>2</sub> H <sub>6</sub> O <sub>2</sub>	Ethylene glycol
Fe <sub>3</sub> O <sub>4</sub>	Magnetite
NaOH	Sodium hydroxide
SEM	Scanning electron microscopy
pHpzc	Isoelectric point
NH <sub>4</sub> OH	Ammonium Hydroxide

## Table of Contents

<b>S.No.</b>	<b>Titles</b>	<b>Page No.</b>
1	Introduction	1
1.1	Toxicology	1-2
1.2	Forensic Toxicology	3-4
1.3	Benzodiazepines	5-6
1.3.1	Development and structure	7
1.3.2	Chemical structures of Benzodiazepines derivatives	8-9
1.4.	Pharmacokinetics and Pharmacodynamics	10
1.4.1	Absorption	11
1.4.2	Distribution	12
1.4.3	Elimination	12
1.4.4	Role of Metabolites	13
1.4.5	Mechanism of action	14-15
1.5	Epidemiology of benzodiazepine abuse	16-18
1.6	Utilization of recent detection approaches	19
1.6.1	Nanotechnology as an efficient tool in forensic science	20-25
1.6.2	Surface-enhanced Raman Spectroscopy for substance detection	25-30
2	Review of Literature	31-45
3	Hypothesis	46
4	Research Objectives	47
5	Materials and method	48

5.1	Chemicals and Reagents	49
5.2	Hydrothermal synthesis of ZnO nanoparticles and Nanocomposites	49-52
5.2.1	Coating process of synthesized nps on WF substrate	53
5.2.2	Characterization of nanoparticles samples	54-56
5.3	Utilization of nps in forensic sample	56
6	Results and Discussion	57
6.1	Phase structure	58
6.1.1	Crystal structure	59-62
6.1.2	Molecular structure	63-66
6.1.3	Mesoporous structure	66
6.1.4	Morphological and elemental structure	67-72
6.2	Particle size distribution	72-74
6.2.1	Zeta potential measurement	75
6.3	SERS Raman Validation	76-84
6.3.1	Figure of Merit	85
6.3.2	Linearity curve	86-87
6.4	Discussion	88-96
7.	Conclusion	97-100
8.	References	101-136

## List of Tables

<b>Table No.</b>	<b>Titles</b>	<b>Page No.</b>
Table 1	Physical and chemical properties of the benzodiazepines drug used in the present work	9
Table 2	BZDs' key effects and applications	15
Table 3	The pH value of solid solutions and corresponding nomenclature of synthesized Nanopowders	50
Table 4	Percentage yield of dried nanoparticles	51
Table 5	Physiochemical specification of the WF (Grade 3) paper	53
Table 6	FWHM values corresponding to (002) and (101) diffraction peaks of ZnO phase pertinent to each nanopowder	55
Table 7	Observed wave numbers ( $\text{cm}^{-1}$ ) in the surface enhanced Raman spectra of alprazolam	77
Table 8	Analytical attributes of ZnO NPs-DSPE-SERS method for alprazolam	86
Table 9	Analytical attributes of ZF NPs-DSPE-SERS method for alprazolam	87

## List of Figures

<b>Figure No.</b>	<b>Titles</b>	<b>Page No.</b>
Figure 1	Categorized areas of forensic toxicology	5
Figure 2	Base structures of (A) 1,4 benzodiazepines derivative (B) 1,2 triazolo-benzodiazodiazepine	8
Figure 3	Showing Benzodiazepines Mechanism of Action	15
Figure 4	Applications of nano-polymers and nanomaterials in forensics	21
Figure 5	Schematic representation of nanomaterials used for optical biosensors in forensic analysis	22
Figure 6	Synthesis methodology of ZnO nanoparticles	50
Figure 7	Synthesis methodology of ZF nps by sol-gel method	52
Figure 8	Visibility of the iron oxide, the zinc oxide and the various Zn/Fe oxidecomposite nanoparticles disributed from left to right.	52
Figure 9	Schematic methodology for coating of synthesized nps on WF paper	54
Figure 10	XRD patterns of (a) ZnO7, (b) ZnO8, (c) ZnO9, (d) ZnO10, and (e) ZnO12 nanopowders	59
Figure 11	XRD fitted profiles of (a) ZnO7, (b) ZnO8, (c) ZnO9, (d) ZnO10, and (e) ZnO12 nanopowders	60
Figure 12	XRD pattern of Fe <sub>3</sub> O <sub>4</sub> and Fe <sub>3</sub> O <sub>4</sub> /ZnO	61
Figure 13	XRD pattern coated nps on WF paper	62
Figure 14	FTIR spectra of (a) ZnO7, (b) ZnO8, (c) ZnO9, (d) ZnO10, and (e) ZnO12 nanopowders	63
Figure 15	FTIR spectra of ZnO/ Fe <sub>3</sub> O <sub>4</sub> and ZnO	64
Figure 16	FTIR pattern coated nps on WF paper	65

Figure 17	N <sub>2</sub> isotherms and BJH curves (inset) of (a) ZnO7, (b) ZnO8, (c) ZnO9, (d)ZnO10, and (e) ZnO12 nanopowders FESEM (a-b) ZnO (c-d) EDS mapping	67
Figure 18	(a) FESEM, (b) EDX, and (c-d) HRTEM micrographs of ZnO9 nanoparticles	68
Figure 19	FESEM (a-b) Fe <sub>3</sub> O <sub>4</sub> .ZnO (c-d) EDS mapping	69
Figure 20	FESEM (a-b) Fe <sub>3</sub> O <sub>4</sub> . (c-d) EDS mapping	70
Figure 21	FESEM micrograph of (a-b) Uncoated WF, EDX and(c-d) Coated ZnO Nnps in WF	71
Figure 22	FESEM (a-b) Coated Fe <sub>3</sub> O <sub>4</sub> .ZnO on WF (c-d) EDS mapping	71
Figure 23	HRTEM of (a-b) Fe <sub>3</sub> O <sub>4</sub> .ZnO (c)SAED pattern	72
Figure 24	Particle size distribution and zeta potential (a-b) Fe <sub>3</sub> O <sub>4</sub> .Zno (c-d) ZnO nps	73
Figure 25	Effect of pH on zeta potential of Fe <sub>3</sub> O <sub>4</sub> -NPs	74
Figure 26	A study of the effect of pH on the size (triangles) and zeta potential (circles) of ZnO particles	75
Figure 27	Surface enhanced Raman spectra of reference sample alprazolam	76
Figure 28 (a)	SERS signals for 10-50 ppm, alprazolam extracted from blood with ZnO nps preparation techniques and Dispersive solid phase extraction	79
Figure 28 (b)	SERS signals for 10-50 ppm, alprazolam extracted from saliva with ZnO nps preparation techniques and Dispersive solid phase extraction	80

Figure 28 (c)	SERS signals for 10-50 ppm, alprazolam extracted from urine with ZnO nps preparation techniques and Dispersive solid phase extraction	81
Figure 29 (a)	SERS signals for 10-50 ppm, alprazolam extracted from blood with ZF nps preparation techniques and Dispersive solid phase extraction	82
Figure 29 (b)	SERS signals for 10-50 ppm, alprazolam extracted from saliva with ZF nps preparation techniques and Dispersive solid phase extraction	83
Figure 29 (c)	SERS signals for 10-50 ppm, alprazolam extracted from urine with ZF nps preparation techniques and Dispersive solid phase extraction	84

# **CHAPTER 1**

## **INTRODUCTION**



## **Chapter 1**

### **1. Introduction**

#### **1.1. Toxicology**

The study of poisons (also called toxins) is known as toxicology, mainly focuses on how poisonous substances impact biological systems (Flanagan et al., 1990). Harmful substance administered can results in abnormal, unfavorable, or hazardous modifications in that organism is often known as a toxin (Cooper et al., 1986). The negative consequences of a toxin may vary from mild signs, such as nausea and migraines, through more serious signs, such as seizures and death in humans (Drummer et al., 2002; Gurney et al., 2014). An organic compounds fundamental characteristic includes its toxic effects. In most cases, toxins disrupt normal physiological processes by altering basic cellular metabolic functions (Leikin and Watson, 2003). They also experience metabolic changes in their systems that render them inert (purification). In terms of its complexity and interdisciplinary nature, toxicology involves the different disciplines of the sciences of chemistry pharmaceuticals, healthcare, inheritance, finance, and legal system (Skopp, 2010). Three major branches of toxicology are usually distinguished in modern toxicology:

- Clinical toxicology is the study of how toxic substances (often drugs) affect human health;
- Forensic toxicology, which deals with the detection of toxic agents used in criminal acts, and
- Environmental toxicology, which examines how industrial and agricultural toxins affect humans and the environment (Gupta, 2016).

The first practitioners of toxicology were prehistoric cave dwellers who identified deadly animals and plants and used the extracts for combat and hunt. Legends from 1500 BC claim that opponents were slaughtered or drugged with the sap of hem the drug opium arrowhead poison, and specific alloys. The use of poison has become widespread and sophisticated over time. There were many notable poisoning victims

throughout history, including Socrates, Cleopatra, and Claudius. Toxicology began to take shape period of Renaissance and Age of Enlightenment. While in 1500s AD also in 1800s AD, Paracelsus, also known as Philippus Aureolus Theophrastus Bombastus von Hohenheim, is considered as father of toxicology. Paracelsus and Orfila performed important scientific studies (Gallo and Doull, 1996; Langman and Kapur, 2006). Based on Paracelsus' findings, toxic plant or animal toxic effects were caused by specific compounds. He also showed that how much of these compounds had an impact on the body's reaction to them. While tiny amounts of a chemical can be useful or safe, greater doses could prove toxic. The dose-effect relationships connection has grown in importance as a result of this finding, which changed the field of poisoning (Eaton and Gilbert, 2008). One among the fathers of contemporary the study of toxicology he is considered as. His most well-known quotes: All chemicals are toxic substances; it's the amount they consume that renders them poisonous (Maurer, 2010).

## **1.2. Forensic Toxicology**

Forensic toxicology involves the application of poison to elucidate the questions that arise during a judicial proceeding. The maintenance of commercial, agricultural, and health regulations (to ensure the security of water, food, and air) as well as drug detection and analysis are additional important concepts in forensic toxicology. Each side should be aware of the benefits and drawbacks of each other's techniques as civil analysts may occasionally be subjected to harsh public examination in a courtroom, similar to how forensic toxicologists are in criminal cases (Anderson et al., 2005). In most cases of accidental self-poisoning and attempted suicides, the medical toxicologist or biochemist are responsible for taking care of them and work closely with a poison control center to assist them. There are cases where a forensic toxicologist is referred to, such as when there is a claim of poisoning or an inquest is ordered following a death (Gunja, 2013). An important distinction between a clinical toxicologist and a forensic toxicologist is that forensic toxicologists specialize in evidence in court. A clinical toxicologist diagnoses and treats acute and chronic poisoning by identifying drugs and poisons. The clinical toxicologist able to gather sufficient analytical information for the pathologist and

the coroner to be able to determine the cause of death based on the analytical results obtained by them if the patient dies without any suspicious circumstances surrounding the death (Levine et al., 1999; Peters et al., 2017). Forensic toxicologists are often involved in poisoning cases. In recent years, they have also been engaged in additional activities, such as animal and human doping in sports and drug screening.

Field of forensic toxicology can, therefore, be divided into three main areas of study (Figure 1):

- **Workplace or pre-employment drug testing** is performed to determine whether an applicant will be eligible for employment prior to a drug test.

- **The postmortem toxicology** procedure involves testing a deceased person's toxicology post-mortem and is a normal part of the autopsy procedure.

- **Human performance testing or criminal toxicology** to determine whether substances affect human performance or behavior. (Peters, 2007; Cina et al., 2011).

One of the most difficult tasks of forensic toxicology is to separate, purify, and measure minute harmful compound and their byproduct (Poklis, 1997). All handling procedures for forensic and toxicology specimens must be followed to reduce the risk of degradation, contamination, adulteration, and/or destruction. Samples have typically been delivered to toxicology labs physically, by mail shipments, or by private courier services. As a component of the entire chain of custody, as well as a form which will follow specimens through the point of collecting to the testing is essential (Reys and Santos, 1992).

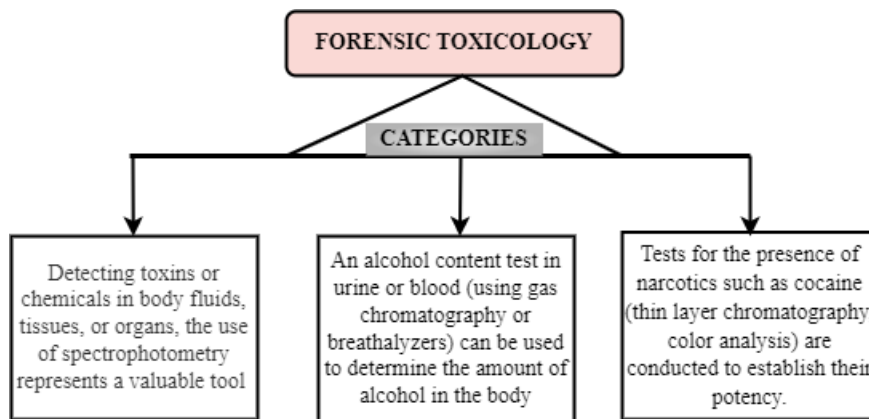


Figure 1. Categorized areas of forensic toxicology

### 1.3. Benzodiazepines

Leo Sternbach synthesized the first benzodiazepine in 1955 at the Swiss drug manufacturer Hoffmann-La Roche, the drug was named as Librium (Kanto et al., 1982). Benzodiazepines are frequently prescribed and widely available medicines that are frequently discovered during toxicology testing in cases of drug-facilitated sexual assault (DFSA). Currently among the most frequently prescribed drugs benzodiazepines are a class of psychoactive drugs misused because of their variety of color, no specific smell and can be easily available without prescription (Hirschtritt et al., 2018). Treatment for anxiety-related conditions, panic attacks, and muscle spasms all involve the medicinal consumption of sedative drugs. Other negative consequences that may lead to diminished ability include memory loss, vertigo, sleepiness, and impaired awareness. Considering their increased potential for abuse and addiction in the case of crime, driving under the impact of drugs, drug and suicides in term of sexual offences (Zin and Ismail, 2017).

Beside this reason, there is need of simultaneous analysis of benzodiazepines and their metabolites in biological matrices are of great interest to clinicians and forensic toxicologists. According to the International Narcotics Control Board, in the last ten years the most commonly BZD were: alprazolam, chlordiazepoxide, diazepam, flunitrazepam, lorazepam, nitrazepam, temazepam and triazolam (Chang et al., 2006). A study by the World Health Organization estimates that 10-20% of adults in

developing countries use these drugs every year (Manchester et al., 2018). Moreover, these types of pharmaceuticals are widely spread due to their effectiveness and safety, their low cost (Narayana et al., 2006). Overdoses of BZD occur more often than overdoses of any other drug, mainly because human bodies adjust quite quickly to an increased level of the drug in the blood. The safety of using BZD is decreased when co-administered with alcohol, sedatives, narcoleptics antidepressants, and morphine-like substances (Greenblatt et al., 2000).

The purpose of the study is to use surface enhanced Raman spectroscopy (SERS) for developing a quick screening technique intended to detect low dosage benzodiazepines in toxicology cases. While, Raman spectroscopy not just to detect the drug, but it also allows for the measurement of spectrum information, which is extremely valuable in the presumptive detection of unknown chemicals (McKernan et al., 2000). As this technique is highly promising for analyzing drug products because it is non- invasive, fast, reliable and non-destructive.

Currently there are two form BZD evaluations:

1. Qualitative or semi-quantitative techniques are used to detect the presence or absence of a chemical is determined using a qualitative test. Instead of using statistical terms to explain the results, qualitative terms like positive, negative, reactive, nonreactive, and normal are used (Chweh et al., 1984). Semi-quantitative testing is comparable to qualitative testing in that the results are presented as an estimate the amount of a detected substance; but semi-quantitative testing does not precisely measure the amount of a material.
2. Quantitative technique- Toxicological screening often necessitates the use of various screening and dosing procedures. Quantitative analysis reveals chemical as well concentration of poisons. Nonspecific instrumental investigations, also including colorimetric and UV- visible spectrometric tests, may be employed for the qualitative assessment of toxins (Wright et al., 1980). To quantify the toxins, sophisticated technologies like infrared spectroscopy, HPLC, GC-MS approaches can be employed.

### **1.3.1. Development and structure**

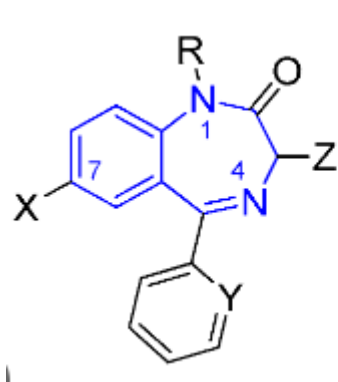
The first benzodiazepines were created in 1950. The advancement of these compounds sparked a boom in the creation of novel medications which could pharmacologically outperform existing tranquillizers such as barbiturates (Hirschtritt et al., 2018). Sternbach discovered the very first benzodiazepines, chlordiazepoxide (Librium), by unexpectedly expanding the ring of a quinazoline-3-N-oxide derivative in 1955. Since the synthesis of this initial compound's homolog and analogues was patented in 1959, pharmaceutical companies have developed and commercialized structurally related compounds for therapeutic purposes such as valium, hypnotics, and anxiolytics (Zin and Ismail, 2017). According to the International Psychoactive drug Regulation Board's alprazolam and diazepam have been the two most extensively produced benzodiazepine in the world.

In recent years, new psychoactive substance (NPS) benzodiazepines were developed for the purpose of inducing benzodiazepine medication. These drugs have a rapidly expanding market, and new compounds are being produced and reported quite frequently. There has been recent progress in developing new benzodiazepine derivatives with alternate metabolic pathways (Dourlat et al., 2007). The proposed new benzodiazepine, remimazolam, undergoes an organ-independent metabolic process through ester hydrolysis, which may make it potentially revolutionary. As a result, most benzodiazepines in the body are excreted in the urine by the kidneys as their final method of elimination (Salve and Mali, 2013). It has been reported that up to 20% of parent drug is excreted unchanged in some cases, although the glucuronidated metabolites are the most prevalent excreted form (Hamilton, 1967).

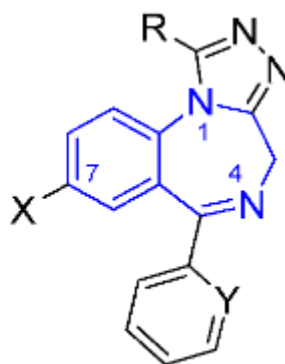
### 1.3.2. Chemical structure of Benzodiazepines derivative

- 1, 4-benzodiazepine derivative (the main group of benzodiazepines such as chlordizepoxide, diazepam, clonazepam, temazepam, oxazepam).
- 1, 5 derivatives of benzodiazepine (clobazam, triflubazam).
- Tricyclic derivatives (alprazolam, adinazolam, estazolam, loprazolam, triazolam) called trizolobenzodiazepines.
- Miscellaneous benzodiazepine (Imidazenil, Flumazenil, Clotiazepam).

Different benzodiazepines from two of the main classes: 1, 4 benzodiazepine derivatives and 1, 2 triazolo- benzodiazepines (Grossi et al., 2002). The basic structure can be seen in Figure 2, While substituents for individual drugs can be seen in Table 1.



(A) 1, 4 benzodiazepines derivative



(B) 1, 2 triazolo-benzodiazepine

Figure 2. Base structures

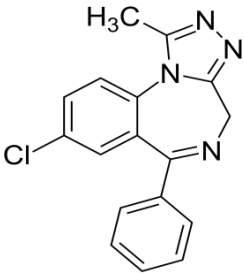
Drugs And Their Properties	Alprazolam
IUPAC name	8-Chloro-1-methyl-6-phenyl-4H-s-triazolo (4,3a) (1,4) benzodiazepine
Chemical Structure	
Molecular Formula	C <sub>17</sub> H <sub>13</sub> ClN <sub>4</sub>
Molecular Wt.	308.7 g/mol
Color/Form	Pink or peach
Odor	Unpleasant
Melting Point	228-229.5°C
Solubility	A white crystalline powder, which is soluble in methanol or ethanol but has little solubility in water at physiological pH levels (Sardana and Madan, 2002)
Stability/ Shelf Life	Stable under recommended storage conditions
pka	5.08
Other Experimental Properties	*Freely soluble in chloroform, soluble in alcohol, Sparingly soluble in acetone  Slight solubility in ethylacetate (Haiying et al., 2017)

Table: 1 Showing the chemical and physiological properties



## **1.4. Pharmacokinetics and Pharmacodynamics**

Benzodiazepine action is primarily regulated by specific benzodiazepine receptors in the central nervous system, especially the cortex and limbic system (Roberts et al., 2011). The hippocampus region of the brain contains the greatest density of benzodiazepine receptors, but its clinical significance is not yet known. As benzodiazepines interact with their receptor sites, GABA's inhibitory effects on neuronal activity are enhanced (Xia and Sun, 2012). As a result of drug concentrations at the receptor sites, benzodiazepine acts in a predictable manner. It is also important to note that drug concentration at receptor sites is dependent on the extent to which benzodiazepine is up taken by passive diffusion from plasma into the brain (Ohtake et al., 1999). A drug with high lipid solubility (diazepam and midazolam) passes easily through the blood brain barrier than a drug with low lipid solubility (clonazepam).

Additionally, pharmacokinetic properties, such as absorption rate and distribution extent, are also taken into consideration. In determining the time course and intensity of a drug's action, dose and elimination rate play a key role. After absorption into the bloodstream, benzodiazepines are distributed throughout the body. The rate at which the process takes place depends on the level of protein binding, lipid solubility, and the size of the molecules. The majorities of benzodiazepines are protein-bound and tend to redistribute to tissues rich in lipids. Benzodiazepines are highly lipophilic, which makes them widely distributed. The liver metabolizes the majority of benzodiazepines through phase I oxidative reactions. This process is facilitated by the enzymes of cytochrome P450. A CYP3A4 enzyme plays a major role in most cases, but other members of the family play an important role as well (Ashton, 1987).

### **1.4.1. Absorption**

The rate at which benzodiazepines are taken in from the intestines into the systemic blood, as opposed to the rate at which they diffuse from bloodstream into the brain, determines how active they are when taken orally (Haefely, 1985). In contrast to

oxazepam, temazepam, which are gastrointestinal medications that are gradually absorbed and have a longer onset of action, diazepam and clorazepate are quickly absorbed through the gastrointestinal tract. The rapid onset of benzodiazepines action makes them particularly suitable for patients who need to take the drugs on a regular basis (shown in Table 1). It is however, common for some patients to experience fast absorption (Miller et al., 1987). Currently staccato is being developed for intrapulmonary delivery of alprazolam to treat epilepsy seizures rapidly. Through a heating package, this drug delivery system vaporizes the drug. A normal breath delivers drug vapor into the lungs as aerosols (Greenblatt et al., 1987). During a phase 1 trial, inhaled alprazolam reached its peak concentration in smokers after 1.8 minutes at 48ng/ml, and in non-smokers at 26.72ng/ml. The majority of alprazolam's binding occurs in vitro to serum albumin (80%). The primary metabolizer of this drug is CYP3A4, which leads to the possibility of pharmacological interactions.

Four- hydroxyalprazolam and alpha- hydroxyalprazolam are two of alprazolam's main metabolites, both of which have low levels of plasma concentrations not having any pharmacological effects (Arendt et al., 1987). The main way in which alprazolam and its metabolites are excreted is through urine. During phase IIa study, five patients diagnosed with photoparoxysmal response were administered alprazolam intrapulmonarily via the Staccato system in doses ranging between 0.5 and 2 mg. An inhalation experiment was performed to measure the number of photo- epileptiform responses induced by photic stimulation frequencies (Greenblatt et al., 1983). Compared with placebo, staccato alprazolam significantly reduced photonic stimulation frequencies after 2 min, and the effect lasted 4 hours and 6 hours for the 0.5 and 1 mg doses. Inhaling 2 mg of alprazolam with the goal of achieving 31.5 ng/ml of plasma concentration within 2-minute produced plasma concentrations which is dependent on dose.

### **1.4.2. Distribution**

After a single dose, a drug must promptly and broadly reach peripheral areas to continue to be effective (Greenblatt et al., 1983). There is a high lipid solubility for midazolam, diazepam, and desmethyldiazepam (metabolite of diazepam), while there is a low lipid solubility for lorazepam, oxazepam, and clonazepam (Kales et al., 1983). Once peak concentrations of diazepam are achieved in the blood, the drug is rapidly and extensively distributed to muscle and adipose tissue. Upon dispersion into these inactive storage sites, diazepam levels in blood and brain drop, and the impacts of a single dose are rapidly ended (Greenblatt et al., 1988). Conversely, drugs with a less extensive distribution such as lorazepam continue to act longer after a single dose since they remain in the system for longer periods of time.

### **1.4.3. Elimination**

It is also important to consider the rate of drug elimination during the half-life of an individual dose when considering the time span of action of a single dose (Dietch and Jennings, 1988). A drug elimination half-life refers to the rate at which it is removed from the body during the post distribution phase; it does not take into account the rate and extent at which it is distributed into peripheral tissues (Greenblatt et al., 1989). Once the drug has been distributed to peripheral tissues, the plasma levels of the drug begin to decline steadily. It depends on how widely the drug is distributed and how quickly it is eliminated by the liver that the drug disappears at this point.

Due to the rapid and extensive distribution of the drug from blood into adipose tissue, drugs with long half-lives, such as diazepam, may actually have a short duration of action. It is important to consider drug accumulation during chronic or multiple-dose therapy, since clinical effects are influenced by its rate and extent (Ciraulo et al., 1988). Longer half-life means a slower accumulation rate. Once an interval of at least four times the half-life has elapsed since treatment commenced, a steady-state condition is achieved in more than 90% of cases. Consequently, the relative amount of accumulation increases as half-life increases (Ciraulo et al.,

1988). The rapid and sometimes superficial accumulation of short-acting benzodiazepines, the buildup of long-acting benzodiazepines occurs slowly and extensively and cannot be removed from the body as quickly as they were accumulated by body once the treatment has been discontinued (Strom, 1987).

#### **1.4.4. Role of Metabolites**

Benzodiazepine compounds are considered to have a net clinical effect taking into account the parent compound's effects, as well as any active metabolites generated during biotransformation (Miller et al., 1988). Compared with the parent compound or other metabolic products, some metabolites appear in small amounts, while other metabolites may have concentrations that are as high as or much higher than those of parent drug (Jacobson et al., 1983). It is also important to note that lipid solubility and binding to serum or plasma proteins affects the ability of metabolites to reach brain tissue. A metabolite's affinity towards benzodiazepine receptors also determines its intrinsic activity. In contrast to benzodiazepines with a long half- life, which usually have active metabolites which are pharmacologically active, benzodiazepines with an intermediate or short half- life do not usually have active metabolites. There are three metabolites of diazepam: desmethyldiazepam, temazepam, and oxazepam (Shen et al., 2019). In comparison to desmethyldiazepam and diazepam, two final metabolites are present, but at much lower concentrations its levels may potentially reach levels above those of diazepam during chronic therapy when administered in greater doses (Strom, 1987). Flutoprazepam was administered orally to 8 participants in a trial, and the results were examined by HPLC and GC-MS, concentrations started to progressively decline after two hours and were undetectable after nine hours (Cornett et al., 2018). In contrast, N- desalkylflurazepam, its metabolite, had a much higher concentration than the parent compound (Foitzick et al., 2020). An average half- life of 90 hours was associated with its rapid onset (within 2 hours). During the period of 2-12 hours, the peak concentration was achieved.

#### **1.4.5. Mechanism of action**

1,4-Benzodiazepines increase the action of the neurotransmitter gamma- aminobutyric acid, which results in effects that are sedative, hypnotic, anxiolytic (anti-anxiety), anti-convulsant, and relaxant (Sanabria et al., 2021). There are different 1, 4-benzodiazepines that stimulate the binding of GABA at the GABAA receptor, and increases the frequency of opening the  $\text{Cl}^-$  ion channel (Skolnick, 2012). Consequently, the sedative and hypnotic effects, the anti-anxiety effects, and the calming effect on many of the functions of the brain are a result of the reduction of communication between neurons and, thus, have a calming effect on many of these functions. As a result of binding to the receptors on the surface of neurons, GABA controls the excitability of these cells (Berro and Rowlett, 2020). GABA receptor is a macromolecular complex that not only binds GABA but also binds other molecules such as benzodiazepines that modulate GABA's activity. As benzodiazepines binds to a specific site on a GABA receptor, they do not directly stimulate (Engin et al., 2018). The molecules actually enhance the efficiency of the channel by causing it to open more frequently when GABA binds to its own receptor, when it binds to its own site. Consequently, a higher concentration of  $\text{Cl}^-$  ions is present in the post-synaptic neuron, which causes it to become more polarized and less excitable (Figure 3). In addition to binding to the GABA receptor, barbiturates also bind to other sites on the receptor in a similar manner (Meng et al., 2020).

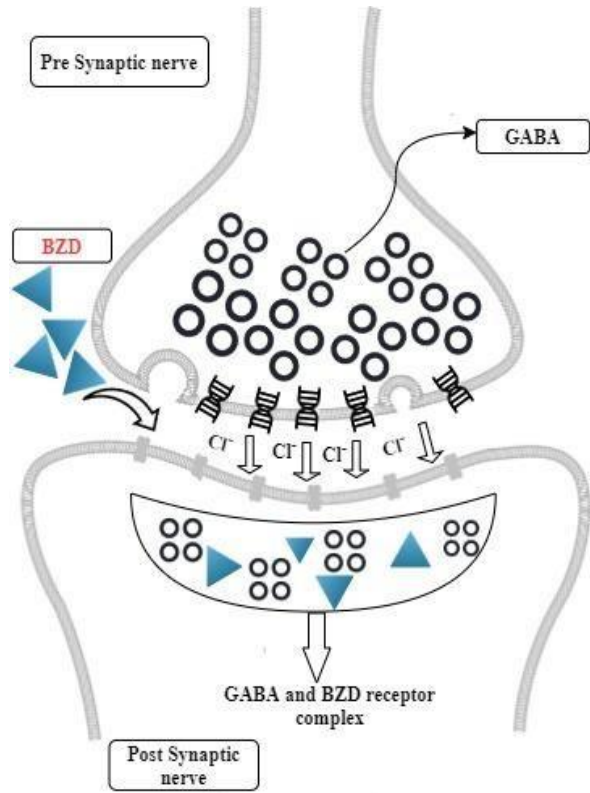


Figure 3. Showing Benzodiazepines Mechanism of Action

ACTIVITY	MEDICAL USE
Anti- fear medication	Nervousness, social phobia, mental disorders as well as drug symptoms of withdrawal.
Insomniac	Sleeplessness
Relaxant for muscles	CNS abnormalities involve muscle spasm
Anticonvulsive	Drug- induced assaults, as well as certain forms of epilepsy
Amnesic	Pre-surgery or perioperative medicine

Table: 2 BZDs' key effects and applications

## **1.5. Epidemiology of benzodiazepine abuse**

The use of benzodiazepines is significantly public health concern, an increase in antidepressant related deadly overdoses and emergency hospitalization in recent years (Gaudreault et al., 1991; Park et al., 2020). However, there has not been much focus on this expanding problem (Han et al., 2018). There are several indications that these drugs pose a risk to the public's health. The number of emergency room visits due to antidepressant increased by over 300 percent between 2004 and 2011, while the number of overdose deaths increased by over 400 % between 1996 and 2013 (Bleich et al., 1999; Blazer and Wu, 2009; Blanco et al., 2013). A survey of substance abuse disorder treatment centers reported a 109% increase in admissions for opiates abuse between 2013 and 2022. These increases coincided with an increase in the number of sedative prescriptions. Between the middle of the 1990 and 2013, the quantity of benzodiazepine prescriptions (i.e., the dosage counterparts) grew by 67% has increased three- fold. The prevalence of benzodiazepine dependence or abuse in the elderly has been documented in research study (Bleich et al., 2002).

The pattern of psychotropic drug use by elderly patients presenting to a tertiary care outpatient department in India revealed in a retrospective cross- sectional study, found that benzodiazepines were the most common drugs prescribed, with 64% of those patients who received the medication. Study reported that benzodiazepines were prescribed to elderly outpatients across diagnostic groups, with clonazepam the most frequently prescribed drug. A case series also highlights a number of elderly patients who were prescribed zolpidem and eventually developed dependence and delirium (Boggis and Feder, 2019). Despite evidence that concurrent opiate and benzodiazepine prescriptions increase the risk of death, the percentage of patients having an opioid prescription who were given BZDs increased by 41% between 2002 and 2014 (Bouvier et al., 2018). Indeed, the current opioid overdose epidemic has been considerably facilitated by the use and misuse of benzodiazepines, with benzodiazepines accounting for nearly 30% of opioid overdose death As National Institute on Drug Abuse, 2018 concerns are developing as more harmful

benzodiazepines, such as potent designer benzodiazepine and illegally manufactured tablets containing benzodiazepines and fentanyl, are available illegal in the market.

Despite the worsening public health indicators associated to benzodiazepine use, the government and the science community continue to disregard this issue (Borges et al., 2000; Grover et al., 2012). According to NDPS act, commenced on 14 November 1985, demonstrated that family of benzodiazepine including alprazolam are classified under Schedule IV prohibited substance. The recommended commercial dosage for alprazolam is 100 gm, per NDPS recommendations. Infractions involving the illegal diversion and supply of neuro-psychotropic medications are punishable by a minimum 10- year prison term and a fine under Sections 8(c), 21(c), 27(a), and 29 of the NDPS Act (Sharma et al., 2017). Although evidence indicates that benzodiazepines have had the potential to be abused, the risk was originally regarded to be low (Brady et al., 1991). This is particularly true for only certain vulnerable populations, such as individuals with a history of substance abuse issues (SUDs). Different benzodiazepines formulations are more commonly misapplied than others, but on availability (drug prescription rates) has a substantial impact (Brands et al., 2008). General populace of the United States, 73% of individuals who overused benzodiazepines in the previous year reported using the same alprazolam products (Brandt et al., 2014).

Alprazolam is the most often prescribed benzodiazepine in the United States, according to data, thus its consistent finding (Breen et al., 2004). Participants in the trials illustrate they had abused clonazepam, diazepam, and lorazepam (also among the most commonly prescribed psychiatric medications) (Calhoun et al., 1996; Chen et al., 2011). Even while there appears to be a correlation between dosage rates and estimations of prevalence for misuse of particular benzodiazepine formulations, some benzodiazepines appear to be preferred over others, indicating a larger abuse potential. Many substance-using participants said that they endorsed diazepam and flunitrazepam over other benzodiazepine medications (Boyd et al., 2018). Given that these trials were published and over 20 years ago, choice may have reflected accessibility at the time. The most popular injectable benzodiazepines are flunitrazepam and temazepam, particularly the gel-filled capsule version; the way a



drug is administered may affect a person's preference (Cochran et al., 2004). According to study, when benzodiazepine and alcohol are consumed simultaneously, expressing multiple motives is associated with higher levels of drug use severity (Comiskey and Snel, 2016). This is particularly true for those who additionally take opioids and/or inject substances.

In persons who use opioids and/or inject narcotics, benzodiazepines are frequently used to enhance the effects of the drugs agonist medicines. In similar contexts, the study also demonstrated that benzodiazepines were inappropriately used to alleviate the symptoms of opiate withdrawal and to serve as an alternative for opioids, either to help to reduce its use or taken in limited supply (Compton et al., 2000). The likelihood of benzo overdose, as well as the risk of an elevated heart rate and respiratory failure, is raised when alcohol or opioids are consumed. Similarly, benzodiazepine usage and dependency have been associated to non- fatal overdoses in retrospective studies (Cook et al., 2018). Given the association among receiving a higher methadone dosage and benzodiazepine misuse, it is particularly concerning that benzodiazepines are also implicated with methadone and buprenorphine-related overdoses (Darke et al., 1992; Dåderman and Lidberg, 1999).

The understanding of the increased risk of overdose when mixing opioids and sedatives differs dramatically across overdose samples. Furthermore, research on benzodiazepine use disorders, their treatment, and prevention is lacking. The majority of non- usage-related therapy studies have concentrated on xanax withdrawal in patients with long-term prescription for the treatment of insomnia or anxiety (Darke and Ross, 2000). It is critical to develop better therapies to reduce benzodiazepine misuse in order to reduce the danger of an overdose. It should be emphasized that combining a benzo reduction alongside cognitive-behavioral therapy (particularly, exposure-based psychotherapy) improves the chances to quit taking benzodiazepines (Darke et al., 1994). As a result, given the tight relationship among anxiety and its abuse, these strategies may also be helpful in the treatment of antidepressant abuse.

## **1.6. Utilization of recent detection approaches**

Drug abuse, particularly illicit drug abuse, is widespread across the globe, making it a concern not only for medical professionals but also for those involved in forensics (Vinyas et al., 2019). Forensic investigation often requires the analysis of drugs, for example, in the identification of seized drugs or in the analysis of post-mortem samples. In order to ensure rapid and sensitive detection methods for drug screening, simple and inexpensive detection methods are required (Blanco et al., 2018). Previously, the methods were time-consuming, expensive, and required laboratory settings for analysis, but now the methods have been affirmed by the SWGDRUG, USA (Scientific Working Group for Seized Drugs), and are sensitive and specific. In place of the labor-intensive traditional methods for detecting drugs including cocaine, cannabis, amphetamines, and opiates, drug detection employing new biosensors is proving to be a feasible option for the quick and accurate screening of drug samples (Blanco et al., 2013).

In addition, ability to utilize multiplex biosensors to simultaneously test various drugs represents a major advantage, since unidentified samples may be screened for a number of drugs at the same time. Drug detection applications using nanotechnology increasingly important in the pharmaceutical industry to prevent such problems (Bleich et al., 1999; Blazer and Wu, 2009). Due to its unique properties, nanoscience plays a vital role in the detection of illegal drugs due to its selectivity, specificity, cost effective and also time consuming (Bleich et al., 2002). In this new study, clonazepam is detected by a colorimetric sensor with very high sensitivity and selectivity. An ultrasensitive detection using gold nanoprobe capped with melamine was demonstrated in this study through a simple, quick, and rapid methodology (Boggis and Feder, 2019). In this detection, melamine and cyanine (CN) form hydrogen bonds that cause AuNPs agglomerate instantly and change color from red to blue. The presence of CN can be detected with the utilization of highly sophisticated instruments luminescence spectroscopy. For the purpose of detecting drugs in samples, this highly specific and sensitive sensing technology can

be adapted into a strip-based kit for on-site analysis (Borges et al., 2000). It can be used in forensic drug analysis, because of several advantages like, cost-efficient, rapid, precise, and real-time analysis this colorimetric technique can be used as a tentative spot test and a good substitute for on- field samples as nano-sensors can be applied to toxicological samples (Bouvier et al., 2018). As a result of the different types of evidence found at crime scenes, forensic science procedures vary considerably (Boyd et al., 2018).

### **1.6.1. Nanotechnology as an efficient tool in forensic science**

A nanometer (nm) is a unit of measurement that ranges from 1 to 100 nm. To put that into perspective, a nanometer is an estimate of about 1/80,000 of the measurement of single human hair, which is about ten billion micrometers large (Breen et al., 2004). Nanotechnology also has the potential to revolutionize the way we diagnose, treat, and prevent diseases, since nanomaterials can enter cells and deliver essential drugs, hormones, and other substance directly into the body (Cochran et al., 2004). Additionally, nanomaterials can be used to create lighter, stronger, and more efficient materials for use in the automotive, aerospace, and electronics industries.

Nanomaterials are so small that they can provide unprecedented levels of control over the structure of materials and can be used to manipulate physical and chemical properties at nanoscale levels. Ideally used in light weight and strength products are important, such as in airplanes and cars, as well as for use in electronics where precision and efficiency are a key (Comiskey and Snel, 2016). The field of nanotechnology has a wide range of technologies and techniques available for synthesizing, creating, developing, or creating nanomaterials (Compton et al., 2000). The nanoscale can also be used to engineer specified properties and characteristics in nanomaterials, such as improved strength or electrical conductivity, which makes them ideal for various uses. This is because at the nanoscale, materials have different properties than they do at a broad scale. For example, nanomaterials are stronger than their larger counterparts due to their higher surface area-to-volume ratio, and they can also be engineered to have specific electrical properties that make them useful in electronics applications (Cook et al., 2018).

In fact, it is because of the characteristics of nanomaterials that enable them to detect and analyze the crucial evidence at a nanoscale levels. Furthermore, these offer enhanced sensitivity, as well as selectivity, in analyte detection, which can provide more accurate results compared to traditional methods. Additionally, they can detect trace levels of evidence that may have previously been undetectable, thus increasing the potential for successful outcomes in criminal investigations. The use of these devices has been shown to enhance the detection and collection of evidence that was previously difficult to attain, including the detection of drug, toxicological screening, and analytical techniques (Darke et al., 1992).

Several forensic applications have used nanotechnology over the years, including fingerprinting, poison detection, narcotic detection, food contamination detection, analytical analysis of questioned documents etc. (Darke and Ross, 2000; Cochran et al., 2004). This demonstrates that nanotechnology is an important tool in forensic science, providing investigators with a powerful, reliable means of collecting and analyzing evidence in a variety of settings (Figure 4). Nanotechnology has enabled forensic scientists to take smaller samples of evidence and to better analyze them. In one of the study, scientists were able to detect and recover DNA evidence from a knife blade using a handheld Raman spectrometer (Darke et al., 1994). The use of various instrumental methods chromatography, electrophoresis, spectroscopic techniques are already in wide use for detection and analysis, however these methods are chemical, trained manpower, expensive and require a lot of time.

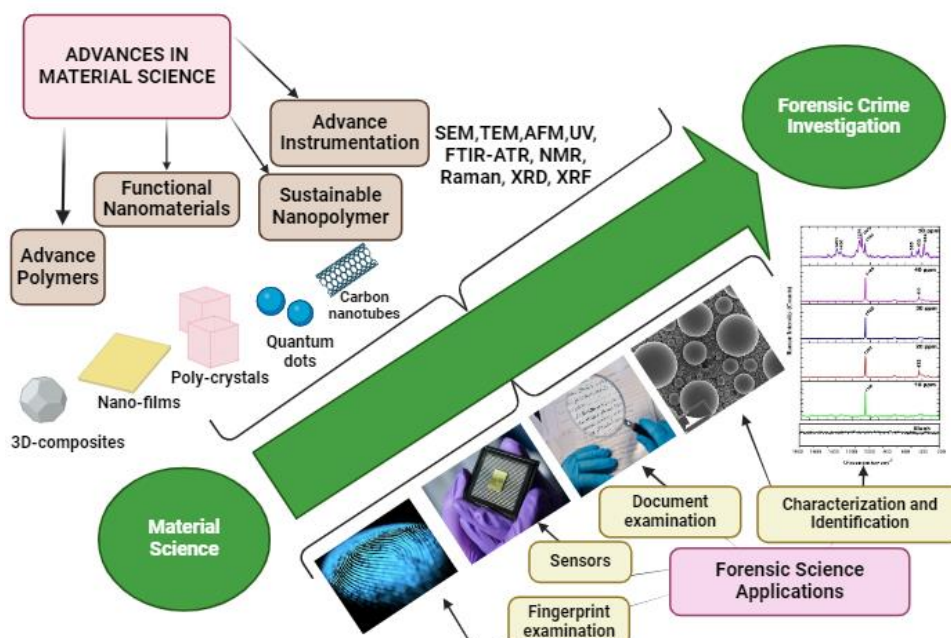


Figure 4: Applications of nano-polymers and nanomaterials in forensics

Nanotechnology is replacing these instrumental techniques in the manufacturing process. In order to overcome the limitations of various instrumental techniques in comparison with the conventional methods, various sensors have been developed that have replaced the conventional method. These nanoscale materials are highly sensitive and can detect very low concentrations of analytes. They are relatively inexpensive compared to other sensing materials and can be easily integrated into existing measurement systems. These nanoparticles sizes, shapes, and structures all influence a wide spectrum of optical properties. They have been utilized for terrorist tracking, environmental screening, biological trace detection, and illicit drug screening (Figure 5) (Compton et al., 2000).

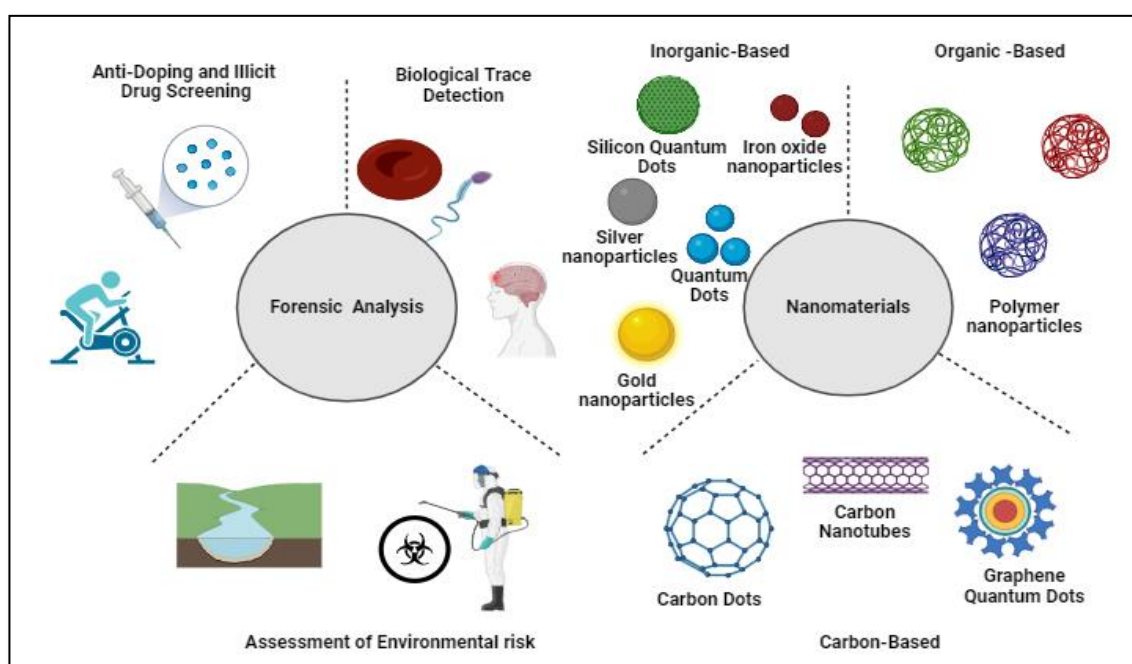


Figure 5: Schematic representation of nanomaterials used in various fields of forensic analysis

Rapid progress in field of nanotechnology, enormous improvements in biomedical sciences as nanosized and nanocrystalline mesoporous material has been developed with significant texture and bioactive characteristics (Koutu et al., 2016). An array of semiconductor materials such as silicon, germanium, gallium nitride and gallium arsenide were extensively employed in electronics and textile industry (Lalzawmliana et al., 2020), photovoltaic cells (Willander et al., 2010), antibacterial (Vaseem et al., 2010) and cosmetic applications (Podporska et al., 2017). Among these novel materials, zinc oxide (ZnO) nanoparticles have been acclaiming wide attention in solar cells, luminescence, electrical devices and chemicals sensors (Masaki and Kim, 2003).

A number of studies has been carried out in variety of ZnO nanostructures such as nanowires and nanorods (Guo et al., 2000), nanorings (Baruah et al., 2008), nano-loops (Huang et al., 2006), nano-combs (Hughes and Wang, 2005), nano-helices (Kong and Wang, 2003), nano-bows (Hughes and Wang, 2004), nanobelts and nanocages (Sun et al., 2008). ZnO is a type of inorganic semiconductor exhibiting high refractive index, thermal conductivity and many other physic-chemical properties (Snure and Tiwari, 2007). Metal oxide-based nanoparticles with their charge and high selective nature become a good conductor and largely used in application of medical sciences, as they are stable and materials at nanoscale provide high surface area which in term enhances adsorption capacity (Anand et al., 2019). Many synthesis routes including sol- gel (Snure and Tiwari, 2007; Li et al., 2010; Huang et al., 2014; Saxena et al., 2020), wet precipitation (Zak et al., 2011; Dutta and Ganguly, 2012; Kołodziejczak-Radzimska and Jesionowski, 2014), hydrothermal (Samanta et al., 2009) chemical vapor deposition (Madathil et al., 2007), and precipitation (Cheng and Samulski, 2004) methods have been reported to prepare the monolithic ZnO nanoparticles. Among these techniques, the hydrothermal route has been a versatile method owing to several advantages. For instance, an increase in molar concentration of precursors increased to both degree of crystallinity and crystal size of ZnO nanoparticles (Li et al., 2012).

The homogenous growth of ZnO particles were observed at a threshold pH value (Wahid et al., 2013). Similarly, the size of ZnO particles increased with increase in hydrothermal temperature (Bai and Wu, 2011), whereas, decreased with precursor concentration (Moghri et al., 2013). Furthermore, calcination temperature removed the organic compounds, thus produced the pure crystalline structure of ZnO nanoparticles (Bindu and Thomas, 2014). Also, the influence of pH variation on the dimensions and morphology of ZnO nanoparticles prepared using hydrothermal process (Xu and Wang, 2011). The investigation reported that the growth of ZnO nanorods- like particles was rapid in alkaline conditions, whereas, growth of ZnO particles eroded in acidic conditions (Ridhuan, 2013). Similarly, calcination temperature had a significant effect on the morphology of ZnO nanoparticles.

A study was reported that the morphology and size of ZnO nanoparticles transformed from rods- like to short prisms- like with the increase in the calcination temperature (Mahmood et al., 2016). The ageing temperature had a critical effect on the morphology of ZnO nanoparticles, and the different particle morphologies exhibited different electrical conductivity (Hada et al., 2014). The effects of varying molar concentrations (0.1- 0.4 M) of NaOH precursor on the properties of resultant ZnO nanoparticles. Results revealed that the diameter of ZnO nanoparticles decreased with the increase in molar concentration of NaOH (Koutu et al., 2016). A comprehensive literature review suggested significant effects of varied synthesis parameters on structural and physicochemical properties of ZnO nanoparticles. Apart from it, few reports have been available which have investigated the textural properties of ZnO nanoparticles. Therefore, in this study, ZnO nanoparticles were hydrothermally synthesized using solid solutions with different pH values. While nanocomposite materials offer opportunities to overcome the constraints of micro composites and monolithic, they also present challenges in terms of controlling elemental compositions and stoichiometry (Shamhari et al., 2018). As a result of unique design and combination of properties not found in conventional composites. One type of special nanocomposites can be comprised of nanoparticles with a core and shell, or nanoparticles with a surface modification.

An organic shell surrounds an inorganic core, making these nanoparticles hybrid nanoparticles (Bahari and Ramzannejad, 2012). Among the inorganic elements can be metals or metal oxides, and organic elements can be polymers, chromophores, detergents, carbons, or organic molecules (Bahari et al., 2016). Composite materials widely increasing numbers of applications and have dominated all new marketing efforts (Robertson, 2005). There is growing evidence that nanoscale composites' characteristics and properties are influenced by how they are prepared. There are a number of applications for zinc oxide nanoparticles, including electronic, optical and photonics, and in nanotechnology, transparent conductor electrodes, polymer protective covers, varistors, catalysts, solar cells, etc. therefore, they are ideal for ceramics (Martins et al., 2011). Furthermore, magnetic iron nanoparticles have cubic inverse spinel structures, which is a type of magnetic material that has attracted researchers' attention. Magnesium nanoparticles in crystalline form are becoming increasingly important in research because of their unique properties, such as super paramagnetism and low toxicity (Green et al., 2001).

In addition, these nanoparticles tend to aggregate easily in external environments, which make them difficult to store, process, and apply for long periods of time. Due to the numerous fields, it is employed in, pharmaceuticals, biological sensors, fluid sealing, orientation regulate and directional transport, MRI, mineral division, thermal transfer uses, electro-photography, and effective hyperthermia for treatment of cancer (Edelstein and Cammaratra, 1998). Prior work on iron oxide/ZnO focused on understanding the properties of the two components and the use of nanocomposites in spintronic devices (Holzwarth and Gibson, 2011). None of the studies addressed their applications in bioscience. This nanocomposite has the potential to be used in biosensing and bioimaging. It could also be used to create nano-scale drug delivery systems for targeted drug delivery.

ZF nanocomposites have been synthesized successfully by many researchers using various methods. The sonochemical method was successfully used to synthesize ZnO/Fe<sub>3</sub>O<sub>4</sub> (Yumusak et al., 2009). The hydrothermal method was used to reduce graphene oxide (RGO)/ Fe<sub>3</sub>O<sub>4</sub>-ZnO in nanocomposites. An effective method for measuring methylene blue photodegradation of nanocomposites was found using wet grinding of nanocomposites (Sudha et al., 2014). Synthesize ZF nanocomposites with 88.5% degradation efficiency against methylene blue and high stability over five reaction cycles (Cheung et al., 1986). It is an environmentally friendly method for synthesizing nanoscale particles and obtaining nanocomposites with high yields. The structural, physicochemical and textural properties of nanoparticles were comprehensively studied using XRD, FTIR, FESEM, HRTEM, EDX, and BET techniques. The crystal structure of nanoparticles was determined using Rietveld Refinement. The structure-property correlations were comprehensively discussed in the light of published results.

### **1.6.2. Surface-enhanced Raman Spectroscopy for detection**

Raman spectroscopy is a molecular vibration-based technique, studies molecular structures by utilizing the Raman scattering effect, discovered by C.V Raman in 1928. As a result, conventional Raman spectroscopy's relatively weak Raman scattering process limits its sensitivity and application range. Hence, it is necessary to utilize surface enhancement effects for Raman studies. The Raman scattering signal intensity of pyridine molecules adsorbed on rough silver electrodes was found to be 106 times



higher than silver electrodes with smooth surfaces (Fleischmann et al., 1974). Later, Van Duyne verified this phenomenon as surface enhancement (Jeanmaire and Van, 1977). An effective tool for detecting low-concentration analytes can be developed with Surface-enhanced Raman spectroscopy (SERS), because the enhancement factor (EF) can reach  $10^{10}$ .

As an analytical technique, Raman spectroscopy has gained importance in which laboratories over last decade (Długosz et al., 2021). In this method, molecules are induced dipole moments by using a laser that emits intense light. The frequency difference between the lasers scattered light and the incident beam frequency is used to form a Raman spectrum (Le and Etchegoin, 2008). Compared with commonly used spectroscopic techniques, which allowed powder samples to be analysed right away, Raman spectroscopy had some analytical advantages.

Rich spectral information can be obtained, which allows compounds with closely related structures to be distinguished. It is also possible to study small particles using Raman instrumentation coupled with an optical microscope (Vankeirsbilck et al., 2002; Bell et al., 2004). Separated from infrared spectroscopy, where water is a significant limiting factor, Raman spectroscopy can be conducted in an aqueous environment (He et al., 2023). Fluorescence obscures the spectrum, making it challenging to detect drugs with spectroscopy, and the signal is typically faint until the analyte is present in significant concentrations (Trachta et al., 2004; Rana et al., 2011). While Surface- enhanced Raman spectroscopy (SERS), permits an augmented signal that is many orders of magnitude above ordinary Raman spectroscopy and quenches fluorescence, eliminates these limitations. Adsorbate molecules are detectable using the SERS method on roughened metal surfaces, which results in a significant Raman scattering enhancement (Rivas et al., 1999; Das and Agrawal, 2011). Past few years, SERS has made a significant leap forward in terms of sensing and diagnostics. This means that it will soon be at the forefront of modern sensing and diagnostics. Studies have found that non-plasmonic enhanced Raman scattering can be achieved using dielectrics, enabling SERS experiments to be conducted invasively and reproducibly than an equivalent SERS being performed using plasmonics (Alessandri, 2013; Alessandri and Lombardi, 2016; Bontempi et al., 2018). Additionally, as operational SERS- based method was needed in diverse system and real- world situations, multivariate techniques for Raman data analysis were introduced, opening the door to a multitude

of computer and deep learning-based method (Chen et al., 2019; Fan et al., 2019; Zou et al., 2019). Advances in SERS using naked silver nanorods and oxide-coated silver nanorods (food, environment, biological molecules, and gas) were summarized (synthesis and applications in various sensing fields).

Among 39 most widely used drugs are antidepressants, cannabinoids, amphetamines, fentanyl, benzodiazepines, and other psychoactive small molecules in the SERS library (Farquharson et al., 2019). In this study, the chemical structure of related molecules was compared and analyzed. This revealed unique Raman bands, which are capable of distinguishing and separating identical compounds by their bands. In addition, there are a number of differences in the Raman spectra due to pH, medium, and the addition of various metal enhancers. In the field of bio-diagnostics, SERS-based nano-sensors have been developed and validated with the aim of distinguishing healthy cells from cancerous cells by the measurement of their extracellular pH (Capocefalo et al., 2019). The spectral signatures of benzodiazepine drugs were assessed by Raman confocal microscopy (Montalvo et al., 2014).

In PCA (Principal component analysis) there was a significant spectral difference between batches of benzodiazepine medication, mostly due to heterogeneity. This analysis calculates the factors influencing spectral variation across samples using the covariance matrix. In a study, the ability to detect midazolam and metabolites in saliva using gold- and silver-doped sol gels immobilized in glass capillaries. It can identify 50 ppb cocaine reliably in contaminated saliva with amphetamine, diazepam, and methadone (Le et al., 2012). Using a portable spectrometer and paper SERS substrate, consumers can easily analyze pharmaceutical medications containing APIs (active pharmaceutical ingredients) like oxycodone, hydrocodone, alprazolam, and codeine (Kneipp et al., 2002). On-board spectral matching of a measured sample to a library spectrum was performed by implementing a correlation coefficient algorithm, a popular spectroscopy library matching technique (Kneipp et al., 2006). To ensure maximum signal generation and enhancement, SERS require careful consideration of samples and optical setup, and is a non-destructive method of determining a small number of molecules' chemical identity and structure. Although the discipline is extremely precise and technically sound, it is still extremely novel and needs to be incorporated into a broader forensic context (Campion and Kambhampati, 1998). Despite the fact that nanodevices has many applications in forensic science, but they are not in practice frequently. This is because many of the reported advancements have

not been applied to sufficiently complex samples. Studies in the near future on nanomaterial-based methods of detecting substances abused would probably involve the use of these nanoparticles as a modifier in the process of detecting these substances (Camden et al., 2008). In spite of being extremely precise, the discipline has only been around for a relatively short period of time. Therefore, it must be incorporated into a broader forensic context to become truly effective (Sharma et al., 2013).

Gold, silver, and copper are commonly used as active metal substrates for SERS, such as roughened metal sheets or dispersed metallic particles in water-based solutions. With increase in signal intensity is caused by the interaction between the analyte and substrate (Ryder, 2005). As this type of synthesis method result in poor cost in all batches, colloidal solutions are advantageous. To further enhance the signal in Raman the combination of nanoparticles agents to provide a fresh surface for each analysis (Dijkstra et al., 2004; Mosier and Lieberman, 2005). In addition to increasing signal intensity, causes the nanoparticles to accumulate and create hot-spots. Two factors contribute to the greatest enhancement provided by ions produced by metals. The zinc ions displace the stabilizing agent to cause aggregation and they affect the ionic strength of the surrounding solution changing the surface charge of the substrate, therefore increasing the signal intensity (Abdali et al., 2007).

Detecting narcotics, amphetamines, nicotine, and benzodiazepines, the SERS technique has been tested for the detection of other controlled substances. Typically, this analysis involves drying the controlled substance onto the SERS active substrate, which is then analyzed (Inscore et al., 2011; Fox et al., 2012). Although SERS is not recommended to be used in aqueous solutions, this approach can be adapted for detection of controlled substances in toxicological samples. Silver colloid surfaces were used in aqueous solutions at a concentration of 30 ng/mL to detect diazepam and nitrazepam by SERS (Leopold and Lendl, 2003). For over 40 different compounds, toxicology laboratories must conduct quick screenings in cases of drug-facilitated sexual assault (Lucotti et al., 2012). As a member of the benzodiazepine family, alprazolam is short-acting psychotropic drug characterized by high potency and may be administered orally (Creighton et al., 1979; Rivas et al., 1999). Among people suffering from depression, alprazolam is one of the most widely used drugs. A number of therapeutic uses for alprazolam have been reported. These include anxiolytics,

tranquilizers, hypnotics, antiepileptics and muscle relaxants (Breimer, 1979; Kerker et al. 1980; Liao et al., 1981). Recreational abuse has increased as a result of the widespread use of this class of drugs. The study of methimazole adsorption on surfaces containing gold nanopowders (AuNPs). SERS experiments and various calculations suggest that the molecular interactions between methimazole and AuNPs may exist. Based on the experiment results, a rectilinear connection between methimazole concentration and Raman signal strength was discovered and found to have an excellent limit of detection and a good coefficient of correlation (Saleh et al., 2017). There is a wide range of compounds derived from this drug that may be encountered by forensic laboratories due to its widespread misuse worldwide.

It is possible to develop drowsiness, muscle numbness, coordination problems, fainting, and even death from heavy overdoses (Le Beau et al., 1999; Bonora et al., 2014). It is therefore strongly recommended that toxicologists and clinicians monitor the effects of this medication. Recently, (Alves et al., 2020) conducted a study to test the effectiveness of SERS for detecting clonazepam in beverages. Analyses of spectra from standard solutions were performed, and LDs of clonazepam were calculated. In accordance with the results of the study, SERS analysis using AuNPs was an appropriate method for the purpose intended. Using this technique, sample preparation was not required for distilled beverage samples. The process of extraction is required for more complex drinks, such as beer and energy drinks.

The use of UV spectroscopy (Salamone, 2001), high performance liquid chromatography (HPLC) (Elsohly and Salamone, 1999; Salamone, 2001), GC-MS (Forsman et al., 2009) and LC-MS (Papoutsis et al., 2010; Donoghue et al., 2010) were earlier methods for determining alprazolam in biological fluids and pharmaceutical formulations. It takes a lot of time and effort to use any of these methods. Thus, alprazolam was detected in biological fluids using coated ZnO nanoparticles for ultrasensitive clinical and forensic trials (Das and Agrawal, 2011). This method can be adapted for trace detection of benzodiazepines in poisonous samples as a specific systematic technique for detecting and identifying trace quantities of benzodiazepines in aqueous solutions. This study employed zinc oxide solutions prepared under optimal conditions at different pH levels to enhance the alprazolam signal because these solutions provided signal enhancement for the drug. Several parameters for the SERS detection were investigated includes

aggregation, its counter ion, and its absorption to maximize the sensitivity. There is no doubt that the SERS method is a highly sensitive and precise method that can become a valuable tool for forensic scientists with the development of non-invasive measuring methods. The present work was undertaken to analyze Surface Enhanced Raman Spectroscopy's (SERS) role in identifying abused drugs in a forensic matrix. Essentially, SERS occurs whenever analytes are deposited on noble metallic nanoparticles (Brady et al., 1991). A SERS method has been used to identify and quantify explosives, narcotics (illicit and pharmacological), and explosive residues (Brands et al., 2008). Single molecule detection is typically conducted using this technique at extremely low concentrations to detect and characterize analytes. Although SERS can be used as an analytical technique, substrates must be reliable and repeatable in terms of enhancing factors, which are dependent on the form, size, and aggregate of the nanoparticles (Brandt et al., 2014).

Therefore, the aim of this study is to evaluate whether SERS was adequate of distinguishing spiked alprazolam in oral fluids at toxicological levels. This work is divided into four parts. In part one, zinc oxide nanoparticles were synthesized for SERS analysis. The second objective of the study examined the coating of zinc coated strips in order to determine its composition. Also, examined the results of our method using a portable Raman spectrometer, as compared to our bench mark results in part two. Lastly, SERS's use as a toxicological screening method for urine samples that have been spiked.

**CHAPTER 2**  
**REVIEW OF LITERATURE**

## Chapter 2

### 2. Review of literature

Overview of synthesis and preparation of various metallic nanostructures

Wittwer et al. (1980) several benzodiazepines were separated and measured using an HPLC adsorption system utilizing isocratic elution coupled with 280 nm and 254 nm dual wavelength detection. A powder form and solid dosage form of 10 benzodiazepines are simply ground and extracted with chloroform. Benzodiazepines can be presumptively identified using the W absorbance ratios and chromatographic systems together with dipotassium which does not dissolve in chloroform. Clorazepate dipotassium was analyzed with a novel approach and the chloroform-soluble benzodiazepines were demonstrated.

Lloyd and Parry, (1989) suggested using high-performance liquid chromatography (HPLC) with electrochemical reductive mode detection and micro column cleanup; researchers have developed procedures for determining benzodiazepines and their metabolites from degraded and contaminated blood samples, which are typical of forensic science work. Detection limits and recovery values range from 0.3-12 ng / mL and 75-95 %, respectively, and selectivity far exceed those of HPLC techniques normally used on this type of sample.

Musshoff and Daldrup, (1992) demonstrated diode-array detection (DAD) technique having a great speed recovery and quantification for detection of benzo family of drug. C18 extraction columns were used to extract drugs from oral fluids. A brotizolam internal standard was used. Researchers recovered 75% to 94% of all the benzodiazepines they investigated using spiked serum/blood samples. Over the range of 5–1500 ng benzodiazepine/ml, excellent linearity was obtained. Approximately 2ng/ml was detected. It is also possible to detect low remedial level of serum of highly potent benzodiazepines.

Inoue et al. (2000) there were no significant differences in the SIM chromatograms or TICs between 19 benzodiazepines and two thienodiazepines, except for oxazolam to cloxazolam separation. No benzodiazepines or thienodiazepines interfered with

the blank whole blood extract from the chromatogram. The blank whole blood extract did not interfere with any of the benzodiazepines or thienodiazepines on the chromatogram. Benzodiazepines that were calibrated with fludiazepam as an internal standard displayed excellent linearity with correlation coefficients of 0.995 over the concentration range 5–500ng/ml blood. Based on the detection limits, blood samples ranged from 0.2 to 20ng/ml. As a method for determining benzodiazepines in whole blood, it is both simple and sensitive, which makes it useful in forensic science practice.

Scarisoareanu et al. (2005) Zn oxide thin films were obtained by laser ablation of a Zn target in an oxygen reactive atmosphere, where the oxygen was supplied either by an inlet valve or via radio-frequency (RF) oxygen plasma. A Pt-coated silicon substrate and a MgO substrate were used as substrates. A study was conducted on the impact of the laser wavelength (266, 355, 1064 nm), laser fluence (1.5–20 J/cm<sup>2</sup>), and oxygen pressure (1–60 Pa) on the deposition process. In addition to these tests, several configurations of the ablation plasma, the RF plasma beam, and the substrate were also investigated with respect to the influence of the RF plasma beam addition on zinc oxide films' morphological properties. AFM, X-ray diffraction, and transmission electron microscopy have been used to characterize the obtained films with thicknesses between 50 nm and 1 μm. The development of thin films with different crystalline orientations by pulsed laser deposition assisted by RF plasma beams was demonstrated by varying the direction of the RF plasma beam, the gas pressure, and the substrate. It has been possible to deposit films with the c-axis parallel to the film surface under a limited set of experimental conditions. It was determined that the crystallite orientations were grouped in two orthogonal directions.

Wu et al. (2008) In view of current medical, industrial, and commercial usage, a brief description of the production of iron oxide nanoparticles, their size and morphological manipulation, and magnetic characteristics. The hydrophobic character of monolayer polymer coating and organic ligand coating has been successfully turned into water soluble and biocompatible. Large-scale particle production techniques face difficulties with toxicity, scaling up, and safety.



Singh et al. (2011) reported a case on a comparison of Zinc oxide nanoparticles generated utilizing two different methods: the sol- gel method and the solid phase reaction method. The fluctuation in the energy band gap as a function of the particle size too was discovered using absorption spectra analysis. The sol- gel method produced highly crystalline ZnO nanoparticles. It was discovered that size affects the band gap of the synthesized nps. The results of XRD and TEM experiments are supported by a photoluminescence. Particle size-dependent variations and significant fluctuations were not appropriately accounted.

Tamang et al. (2011) presented the study; the wet chemical method was used to successfully produce ZnO nanoparticles utilizing zinc acetate. Improvements in nps production have been made using a variety of techniques, including chemical and biological ones. Further analysis revealed that *S. aureus* exhibited greater levels of antibacterial activity than *E. coli* in both qualitative and quantitative tests. Only very minimal clumping of nanoparticles was observed.

Khoshhesab et al. (2011) studied ZnO nanostructures have been effectively created by dissolving micron-sized ZnO powder from an aqueous ammonium hydrogen carbonate solution, re-precipitating it in the presence of thiourea, and then calcining it at 400°C for one hour. The Scherrer formula determined that the average size of the particles of ZnO nanoparticles ranged from 4 nm to 18 nm. The main drawbacks include the necessity for pricey chemicals like surfactants as well as requirement to wash and filter the precipitate formed in order to get rid of impurities like NaOH, Cl, etc. from the starting material.

Lee et al. (2013) demonstrated and studies that nanoparticles are produced using simple precipitation and hydrothermal processes at RT-100°C. Precipitation was performed by mixing zinc nitrate with NaOH aqueous solutions with strict controls on temperature, pH, and precursor content. Crystallite sizes and shapes might be effectively controlled by changing the processing parameters of the preparation procedures. There remains a need for aqueous medium nanoparticle synthesis techniques that take the powder's shape and phase into account.

Santhosh (2016) According to this review, nanometal oxides can effectively remove heavy metals and trace elements. Their adsorbent efficiency can be increased by optimizing working circumstances such as pH, nano-adsorbent quantity, time of exposure, and so on. The best adsorbents and photocatalysts have been found to be zinc oxide and iron oxide nanomaterials because of their large surface area, simplicity in synthesis, and good to extraordinary performance. These approaches are expensive to achieve nanoscale size, whereas bottom-up procedures use chemical technologies.

Maldonado et al. (2017) described a dependable statistical method, Taguchi's methodology, was used to reduce the number of experiments. The following elements were studied at: kinds of precursors, solvent, and precipitating agent, Zn molar content, saturating percentage, speed and period of agitation, overall synthesis temperature. It is shown that using a statistically experimental design makes it possible to quickly and accurately optimize the synthesis parameters in order to create small-sized Zinc oxide even while making the best use of the available resources, such as energy, labor, and materials. However, it is clear that more study is necessary to enhance the comprehension of the concepts behind the formation of nanoparticles.

Dien et al. (2019) demonstrated the hydrothermal procedure and the chemical solution method have been utilized to create nonmaterial with diverse morphologies. SEM, TEM, XRD, and EDS studies were performed to confirm the produced ZnO nanostructures. Although there were differences in morphology and crystalline size across all XRD signals, there was no evident change in crystal structure.

Naderi et al. (2020) demonstrated the sol-gel method was used in the current investigation to create the ZF nanocomposite. After analysis of nanostructural composition, the composite was tested on MCF-7 cancer cells to see if it may be used in treatment. As a result of their small size, colloidal durability, magnetic properties, and low toxicity, these nanocomposites could be a great candidate for application in medicine. Coercive fields of the samples, changes in temperature will increase crystallite size and crystal anisotropy.

Johari and Rafati, (2021) explained the shape of nanoparticles influences their characteristics significantly. In this study, zinc oxide and cupric oxide nanoparticles were produced using the identical co-precipitation procedures. The generated ZnO and CuO nanoparticles have sphere- like and hierarchical flower- like structures due to their different parameters of different and electrostatic interactions. Their diverse structures are the result of distinct electrostatic interactions among their ionic species and polar surfaces.

Pourmadadi, (2022) explained and demonstrated different parameters of synthesis affect the textural, optical, and micro structural properties of ZnO nanoparticles. The adsorptive behavior of ZnO nanoparticles for heavy metal removal has also been summarized, particularly at different pH levels. The shape and crystallite size of the nanoparticles of zinc oxide are significantly influenced by each of the parameters. Future studies should concentrate on immobilizing ZnO nanoparticles on appropriate supports for simple separation after use.

Bharti et al. (2022) explained the primary objective to provide an outline of the biomedical application of Fe<sub>2</sub>O<sub>3</sub>-based nano - composites, such as drug transporters, tissue engineering, and wound repair. Their magnetic properties, biocompatibility, and toxic nature also discussed. The effectiveness and drug loading capacity of tissue engineering applications were both enhanced by IONPs' (iron nps) increased surface area and porosity. By coating iron oxide NPs with the suitable polymers, extend the carrier's life span, raise the possibility of future functionalization, and boost drug loading capacity.

### **Development of Raman based SERS nanoparticles sensing method for detection of benzodiazepines in forensic samples**

Drummer, (1998) presented a method for the measurement of benzodiazepine in biological specimen published in last few years. Several immunoassays have been published and show great sensitivity and specificity and offer advantage of being able to detect these drugs with equal sensitivity. No, of confirmation tests available, most favored are HPLC, GC and GC-MS techniques were strongly represented. TLC has shown little interest over last 5 years, still suffers from lack of sensitivity and specificity, particularly for never more potent benzodiazepine.

The use of a variety of solvents for solvent extraction remains popular, offering acceptable recovery rates and minimal interference by other substances. There were also a number of papers published describing solid phase extraction procedures. There were also successful reports of samples being directly injected into a HPLC column with backflushing. This review examined 72 chromatographic methods based on HPLC, LC-MS, GC, and GC-MS. Using 1-2 ml of urine or serum (blood), HPLC was able to detect many benzodiazepines below 1-2ng/ml. It was an order of magnitude lower than NPD detection limits for ECD detectors from 1 ml of specimen. Although EI-MS was similar in sensitivity, NCI-MS was capable of detecting as low as 0.1ng/ml. A HPLC method has been described for separating enantiomers of benzodiazepines.

Manthey et al. (2010) reported that antidepressants possess anxious symptoms, they are expected to engage the stress levels. BZD use suppressed cortisol levels during short-term treatment. It has been shown that long-term Xanax administration will affect the hypothalamic-pituitary-adrenal (HPA) axis. However, little research has been done in this area. BZD use over a lifetime was investigated in subjects of them Netherlands sleeping disorder and mental study with a lifetime diagnosis of mental health issues. In this study the subjects were classified into three categories: daily BZD users, infrequent BZD users, and non-users. Various BZD use features such as dose, dependence and duration which are analyzed for possible associations with salivary cortisol levels. Seven saliva samples were collected, and four cortisol indicators were calculated: cortisol awakening response, diurnal slope, evening cortisol, and cortisol suppression after ingestion of 0.5 mg of dexamethasone. Based on the results, daily users used BZDs for a median of 26.5 months and 6.0 mg of diazepam equivalents per day. When compared to non- users, evening cortisol levels were significantly lower in daily users ( $P = 0.004$ ; effect size:  $d = 0.24$ ) and infrequent users ( $P = 0.04$ ; effect size:  $d = 0.12$ ). There were no progressive changes in alertness, pattern slope, or dexamethasone suppressive results. The authors concluded that despite the finding of slightly lower evening cortisol levels in daily and infrequent BZD users compared to nonusers, long-term use of BZD does not appear to alter the HPA axis.

Wang et al. (2011) Demonstrated a nanostructure for SERS to trace chemical detection, surface can be formed by depositing of metallic particles or clusters. In the invention, the nano-structures are designed to have functions to improve chemical adsorption to the array surfaces, thus further improving the SERS sensitivity. A method of determining measurement chemical compounds is based on their charge states. Chemicals can be attracted to array surfaces using electrical bias applied to nanostructures or to function layers built beneath the nanostructures. Depending on the chemical properties of the chemicals being measured by SERS, the bias can be negative or positive. In another embodiment, special surface bonds are used to enhance the chemical attraction to thin chemical function layers. To selectively condense the measured chemicals to the array surface, the array structure can be cooled to a specific temperature with the substrate. Magnetic fields can also be applied to the sensing surface, or the function layer at the sensing surface, containing magnetic materials, such as Fe, Co, Ni, or their compounds. Therefore, the polar molecules would have statistically aligned to a preferred orientation on the sensing surface. With the application of magnetic fields or the presence of localized magnetic materials in an active layer, chemical specific binding is enhanced, as is the molecule surface binding efficiency. By increasing the number of molecules adsorbing on the sensing surface within a unit period of time, Raman signals are enhanced. It was shown that with interactions between nanoparticles and chemicals enhanced Raman signals are obtained. Only until particle distance is close to or nearly equal to particle diameter does significant enhancement begin to take off.

Inscore et al. (2011) investigated the ability of SERS to classify and measure drugs and their metabolites in saliva. Developed and patented a process for incorporating silver and gold nanoparticles in glass structure. They claimed that the concentration of cocaine was 5000 times more robust by SERS calculation than previously reported research. Future work incorporate capillaries in lab-on-a-chip as a part of sample kit to be used by police with hand held SERS analyzer for roadside testing.

Doctor and McCord, (2013) evaluated an application of SERS to toxicological samples, obtaining SERS spectra for 11 benzodiazepines of interest in sexual assault with drugs. A total of eleven benzodiazepines byproducts were examined, also 1,2-

triazolo- benzodiazepines and 1,4-benzodiazepines. In this study, four distinguish chlorides salts, KCl, MgCl<sub>2</sub>, NaCl and CaCl<sub>2</sub> were used as aggregation for nanopowders of gold. The level of signal improvement for each compound varied depending on which aggregating agent was used. It provided linearity over a wide range of concentrations for a variety of drugs, with the lowest limit of detection at 2.5 ng/mL. Furthermore, 1.67 M of MgCl<sub>2</sub> was found to be the optimum concentration. A wide range of compounds have been tested and optimized using SERS to detect trace number of benzodiazepines in water solutions. Trace benzodiazepines can be detected in sample of toxicology after extracting the analyte using this technique. Such techniques are also used to restrict the technique of immunoassay by having lower detection limits. The methods were robust, generating reproducible intensities and frequencies of SERS. These methods show low limit detections in water-based solutions, which require proof of principle to demonstrate implementation in cases involving true biological samples.

Kannan et al. (2013) sedative drugs are mostly found in various criminal case studies which involves traffic crimes and drug overuse. Chromatoplate chromatographic analysis was performed for alprazolam, clobazam, chlordiazepoxide, clonazepam, flurazepam, diazepam, nitrazepam, olanzepam and lorazepam, which are nine most commonly used benzodiazepines. A rapid efficient and simple method for separating the drugs is developed utilizing pre-coated silica gel GUV254 as the stationary phase in this study. Separation of the previously mentioned drugs using ten different mobile phases was successful. Utilizing an appropriate mobile phase will allow you to separate each drug from the others. This study found that CHCl<sub>3</sub>: CH<sub>3</sub>OH (97:3) was found to be great solvent in above studies.

Montalvo et al. (2014) demonstrated Raman spectral signals which were used to discriminate drug product with the same benzodiazepine from different Pharma companies those manufacture it. It was concluded that bands increase with increasing doses. The study of all the drug products at the same dose was not possible because they were commercialized at different doses depending on their therapeutic effects.

Mir et al. (2015) described the applications of Raman spectroscopy in the forensic area, especially in toxicology. Various types of Raman Spectroscopic techniques have been utilized for purposes including portable Raman, micro- Raman, fiber optic Raman for on field applications SERS to increase the sensitivity and spatially offset Raman spectroscopy (SORS) for in depth sample analysis. No measurements were reported for drug of abuse the potential application of SORS forensic and national security purpose, airports, border control terminals, customs check posts were only discussed. An effective method has been introduced for fabricating a diazepam sensor. This sensor utilizes the synergetic influence of Ag nanodendrimers and graphene nanosheets. This sensor shows high repeatability and stability and offers several advantages such as simplicity, rapidity and low cost. The interference of some drugs from benzodiazepines family such as A fixed amount of diazepam was mixed with these drugs. The results indicated because of same structures and they produce voltammetric peaks overlapping with the diazepam.

Mostowtt and Bruce McCord, (2017) demonstrated the analysis of a set of similar structure synthetic cannabinoid s utilizing SERS. The procedure includes mixing analytes with gold nanoparticles made in a solution which contains basic or alkaline salt solutions. The results examines that the procedure show good potential as a method for tentative screening of synthetic cannabinoids. The wide distribution of these cannabinoids able to virtual guaranty the screening through immunoassay which causes false negatives. As immune-based assay studies are particularly not compound specific, however a positive result cannot give much guidance for particular confirmation by GC-MS or LC-MS.

Romeiro et al. (2017) in this work, two TiO<sub>2</sub> photocatalysts were prepared under different calcination conditions as mesoporous nanoparticles by a sol- gel method, characterized, and their photocatalytic activity was examined using a 366 nm laser light for the transformation of alprazolam (ALP). After 90 minutes of photolysis, about 90% degradation was observed. ALP was phot- transformed without a catalyst using 254 nm irradiation, but the transformation percentage was only 9%. In the photo-transformation of ALP, B500 TiO<sub>2</sub>, which contains both rutile and anatase phases, is more effective than B400 TiO<sub>2</sub>. After 120 min of photolysis, the efficiency of B500 TiO<sub>2</sub> is comparable to that of Degussa TiO<sub>2</sub> synthesized in this study.

Following 90 minutes of incubation, the TOC analysis shows that the ALP has been mineralized completely. When synthetic TiO<sub>2</sub> was used, mineralization ranging from 38% to 56% was achieved over the same photolysis time period. Using fluorescence spectroscopy, triazolaminoquinoline and 8H-alprazolam were identified as luminescent photoproducts. Further, HPLC-MS analysis of ALP photolysis products with B500 TiO<sub>2</sub> revealed three products with m/z values of 327, 297, and 325. The photo transformation is hypothesized to be mechanistic in nature.

Ziegler et al. (2018) identified and improve the capabilities of optically mediated laser light scattering, blood trace detection SERS, sperm, vaginal fluid and forensic sample saliva. The portability of this device makes it perfect. The goal of this project is to decide whether or not dried fluid SERS spectrum. Stain could decide how long the sample was outside the body for a crime. The outcome of using SERS to differentiate different animal blood though not complete is incredibly encouraging because they have only found a single blood check procedure it helps SERS to identify distinctly different species.

Hamideh et al. (2018) demonstrated distinct nanoparticles of silver with addition of dopant as graphene quantum dots based on nano-ink formation which were prepared, utilized in the combination to produce a novel, distinct, as well as sensitive sensing for the detection of alprazolam. This biodegradable nano-ink-based detector was found to provide electrical detection that is affordable, environmentally safe, sensitive, and quick. Although their extraordinary advantages, these substances possess drawbacks. For example, both silver and gold are expensive whenever used in huge quantities.

Pandya and Shukla, (2018) reviewed the providing information on a new field of study using nanotechnology to solve crimes locally. Possibly the most intriguing breakthrough that could further reduce laboratory contamination problems is the possible integration of all the laboratory processes onto a nanoscale platform. The various advancement in the new technology can be used in various nano devices like probes chips effective approaches to prevent crime and provide augmenting security to the society. The results showed that silicon, a material aluminium and calcium was present in some of the leftovers. But in order to do this technique, you required an instructor and a tool.



Fritea et al. (2018) electrochemically generated gold nanoparticles-coated reduced graphene oxide nanoplatfrom was developed to detect nitrazepam with high sensitivity and selectivity. Various techniques such as AFM, scanning electron microscopy coupled with energies dispersive X-ray spectroscopy, chemical methods, and infrared spectroscopy using the Fourier transform were used to analyze the nanostructure of the material. Collectively, the two nanomaterials offer an electrode substrate with a substantial surface area, high electrical conductivity, and outstanding catalytic activity. This sensor provides exceptional sensitivity for the detection of hypnotic drugs in serum, good selectivity, a high degree of stability, and a medicinal formulation with high recovery rates. Among its important characteristics are a broad linear range from 0.5 mm to 400 mm a small detection range (0.266 mm), exceptional sensitivity, good selectivity, and outstanding durability.

Kevin, (2019) demonstrated a large proportion of the earlier reported research has focused on the use of Hg-based electrodes, characterized by low detection limits in both biological and pharmaceutical samples, requiring little sample preparation. The approaches have been shown to be selective, sensitive, and capable of determining benzodiazepines in complex samples, such as serum and forensic samples. In future, the development of new benzodiazepines and applications will also drive the further development of electrochemical assays for this important class of drugs.

Segawa et al. (2019) demonstrated that forensic drug analysis requires a method with high qualification capabilities for sensitive drug detection. It can provide detailed structural information about the compounds included in samples by using simple experimental protocols through vibrational spectroscopy. The main idea was to develop a method for the rapid detection of hypnotics in a wet system using SERS with gold nanoparticle co-aggregation. A simple analytical protocol was required for the developed method. Rapid analysis was therefore enabled with a high level of sensitivity and specific. Different types of hypnotic drugs, including benzodiazepines and non-benzodiazepines, was conducted to examine the relationship between structure and spectrum. Simulations of spiked beverages containing a hypnotic (etizolam, flunitrazepam, zolpidem, or zopiclone) were analyzed as proof of concept.

Detecting these hypnotics was possible due to dilution of beverage samples, which decreased the matrix effect. Among all hypnotics, strong signals were observed except for flunitrazepam, and the estimated lower detection limit in apple juice was 50 ppm.

The developed method is a rapid screening method for hypnotics with low sample requirements.

Merlen et al. (2020) presented a gold nanoparticle-containing non-porous silicon matrices was employed as the SERS surface for recording the surface-enhanced Raman spectra of benzodiazepine molecule oxazepam. Observe spectral fluctuations in the measured spectra, with minor shifts in wave numbers, appearances and disappearance of peaks, and variations in peak shapes. The density functional theory-simulated spectra and the experimentally determined fingerprints of the molecule's numerous sites of adsorption on the surface of gold can be connected. It has also been shown that temperature and laser power can affect absorption sites, indicating that lasers can be used to activate absorption sites. SERS spectra could be misinterpreted and drug identification errors could occur as a result. In order to correctly interpret the SERS spectra of drug molecules, it should be taken into account systematically, oxazepam powder and SERS spectra differ by no means due to orientation effects, but rather fluctuations in the SERS spectrum will be caused by changes in the absorption site. The findings of the study also suggest that laser illumination can activate this mechanism as well. For the due to the molecule's distinctive relationship to metal surfaces, especially dependent on temperature sites for adsorption. From these two important conclusions are drawn: first, the SERS spectrum differs significantly from the powder spectrum and second, laser power must be precisely controlled.

Sha et al. (2020) demonstrated method SERS method was used to identify estazolam in water and beverages utilizing silver and gold core shell nanoparticles using paper as a substrate. This method allows for the quick and easy identification of medications that have been illegally added to beverages. This methodology, along with the carried out qualitative and semi-quantitative analysis, show too early identification. The results showed that drinks interact with the Laser signal; as a result, dilution should be introduced as a pretreatment step going forward to avoid interference.

Alessandri and Lombardi, (2020) reviewed In line with the development of nanotechnology, surface-boostered Raman scattering has generated both thrilling anticipation due to its great sensitivity, which can be expanded to single molecules identification, and unpleasant disappointments due to its poor data repeatability. Additional specific instances of analytical SERS were described in studies intended

for application in criminal justice, drug analysis, biological sensing, and advanced diagnostics.

Alves et al. (2020) sought to detect clonazepam in beverages by combining the extraction of liquids from with low-temperature partitioning preparation of samples method with the SERS, which is analytical methodology. The outcomes showed that analysis carried out with AuNPs was suitable for the forensic objective. For samples of distilled beverages, there was no sample preparation necessary using this analysis method. However, the simple extraction phase extract was required for more complicated drinks, such beer and energy beverages.

Chen et al. (2021) established a technique for quick, sensitive, repeatable, multiplexed, and low-cost detection of illicit substances in urine based on surface-enhanced Raman spectroscopy (SERS) and a sample preparation procedure. Studies have a great potential to be used for rapid screening of illegal drugs in urine.

Azimi & Docoslis, (2022) SERS has made tremendous development in the last decade as a non- destructive, fast, and sensitive technique for drug detection and categorization. This has aided in the preservation of forensic evidence obtained at crime scenes, as well as the maintenance of the chain of custody. It is possible to identify and quantify trace samples using this method. SERS will move out of the lab and into the field for forensic and strategic applications due to rapid advancements in equipment.

Paschoarelli et al. (2023) an electrochemical detection device for diazepam (DZ) and midazolam (MZ) of BZ drugs in commercial drink samples was fabricated using laser-scribed graphene (LSG). SEM shows morphological examinations revealed the LSG material to be porous, which increased the electroactive area. The experiments using a Raman cyclic voltage measurement (CV), and electrical impedance spectroscopy (EIS) show that the PEI-LSG is highly disorganized and has high electron mobility properties. Square Wave Voltammetry (SWV) was used to detect MZ and DZ employing its analytical curve with two linear ranges in concentrations that ranged from 2.5 to 25.0 mole and 25.0 to 100.0 mols.

The maximum level of detection, or LOD for short, and estimation (LOQ) for DZ and MZ, respectively, were 0.66 and 2.01. DZ and MZ were present in samples of fluid, whisky, and sugarcane spirits, which resembled potential forensic proof of crimes related to drugs.

Ramalingam and Singh, (2023) evaluated food industries around the world continue to worry about toxicity through food and feed. The detection of these contaminants in food matrices is still an emerging science, even in developed countries. It focuses on the design and fabrication of an electrochemical microfluidic biosensor that detects trace levels of Aflatoxin-M1 (AF-M1) in milk samples using aptamers. With graphene quantum dot composite and Au nanoparticles, aptamers are anchored to the sensor surface and their signal conductivity is improved. In order to promote portability and improve mixing effects, screen-printed carbon electrodes modified with graphene quantum dots- gold nanoparticles are placed between polydimethylsiloxane layers. The linear range of the sensor was between 100 pM and 2 nM, indicating a detection limit of 0.3 nM based on differential pulse voltammograms. To evaluate sensor selectivity, interference molecules of similar size were analyzed.

### **3. Hypothesis**

Due to their higher chances of addiction and abuse, separating and identifying these compounds is of great importance. A method capable of identifying benzodiazepines in different matrixes must be developed along with an efficient sample preparation technique. SERS (surface-enhanced Raman spectroscopy) is a sensitive and analytical technique for detecting and identifying number of benzodiazepines in water solutions. It has been proven to be effective in detecting trace quantities in toxicological samples as well. Because of their signal enhancement and great recovery rate, metal oxide nanoparticles were used for this study to enhance signal detection and recovery rates. By studying the variables for SERS detection, the technique's sensitivity was optimized. In the study, trace quantities of drugs in aqueous solutions will be detected, which can be used to detect ultra-trace amounts in toxicology samples. It is currently not possible to diagnose limited quantities of drugs detected on crime scenes. It can therefore be employed for detecting and determining trace amounts of drugs, which can later be developed into sensing kits. Therefore, a new type of test strip that is cost-effective needs to be developed. Detecting benzodiazepine in drug facilitated assault cases requires a sensitive, specific screening method.

#### **4. Research objectives**

1. (a) Synthesis of novel nano dimensional pure and composite metallic particles.  
(b) And their coatings on some novel substrate.
2. Comprehensive characterization of synthesized nanoparticles and their coatings for structural, physico-chemical and textural attributes.
3. Utilization of synthesized and coated nanoparticles in forensic sample.
4. Development of Raman based SERS nanoparticles sensing method for detection of benzodiazepines in forensic samples

**CHAPTER 5**  
**MATERIALS AND METHOD**

## **5. Materials and method**

### **5.1. Chemicals and Reagents**

All chemicals and reagents are used were of analytical high grade (99%) pure, Zinc nitrate hexahydrate ( $\text{Zn}(\text{NO}_3)_2 \cdot 6\text{H}_2\text{O}$ ), sodium hydroxide ( $\text{NaOH}$ ), Ferric nitrate ( $\text{Fe}(\text{NO}_3)_3 \cdot 9\text{H}_2\text{O}$ ), ethylene glycol PEG ( $\text{C}_2\text{H}_6\text{O}_2$ ), sodium citrate ( $\text{Na}_3\text{C}_6\text{H}_5\text{O}_7$ ), Whatman filter (WF) paper (Table 4), HPLC grade methanol, sodium phosphate, procured from Merck Sigma-Aldrich Chemical Co. (India). Alprazolam was purchased from the Pharmaceutical Co. (India) as a reference substance under Lot no. IPRS/75/18. Stock standard solutions of alprazolam were prepared by dissolving the appropriate amount in (HPLC grade) methanol.

Also, for samples ethical permission granted from PIMS Jalandhar. Blood, urine and saliva samples of volunteer were collected and kept in screw- capped bottles and stored in a refrigerator at 4–8 °C.

### **5.2. Hydrothermal synthesis of ZnO nanoparticles and Nanocomposites**

The hydrothermal assisted wet precipitation route was employed for the synthesis of ZNH was used as  $\text{Zn}^{2+}$  ion source, and SH was used to control the pH value of the precursor. The synthesis methodology has been schematically depicted in Figure 6. Typically, 1 M hydrous precursors of ZNH and SH were separately prepared at room temperature (27°C). Later, SH precursor was added drop-wise in ZNH precursor under continuous stirring. The pH value of the solid solution was continuously monitored using a calculated digital pH meter. The five solid solutions of  $\text{Zn}^{2+}$  ions were separately prepared with different pH values. After homogeneous mixing, the milky-white suspension was put in Teflon bottle which is sealed in a metallic autoclave and further heated at  $110 \pm 3^\circ\text{C}$  in an electric furnace for 24 hours. After annealing, the resultant crystals underwent five rounds of centrifugation and washing with distilled water. The finished powder was then dried at  $100^\circ\text{C}$  for 24 hours in an air oven before milled into a fine powder. The nomenclatures of synthesized products categorized based on the pH value of their solid solutions have been given in Table 3.



pH value	Nomenclature
7	ZnO7
8	ZnO8
9	ZnO9
10	ZnO10
12	ZnO12

Table 3: pH value of solid solutions and corresponding nomenclature of synthesized nanopowders

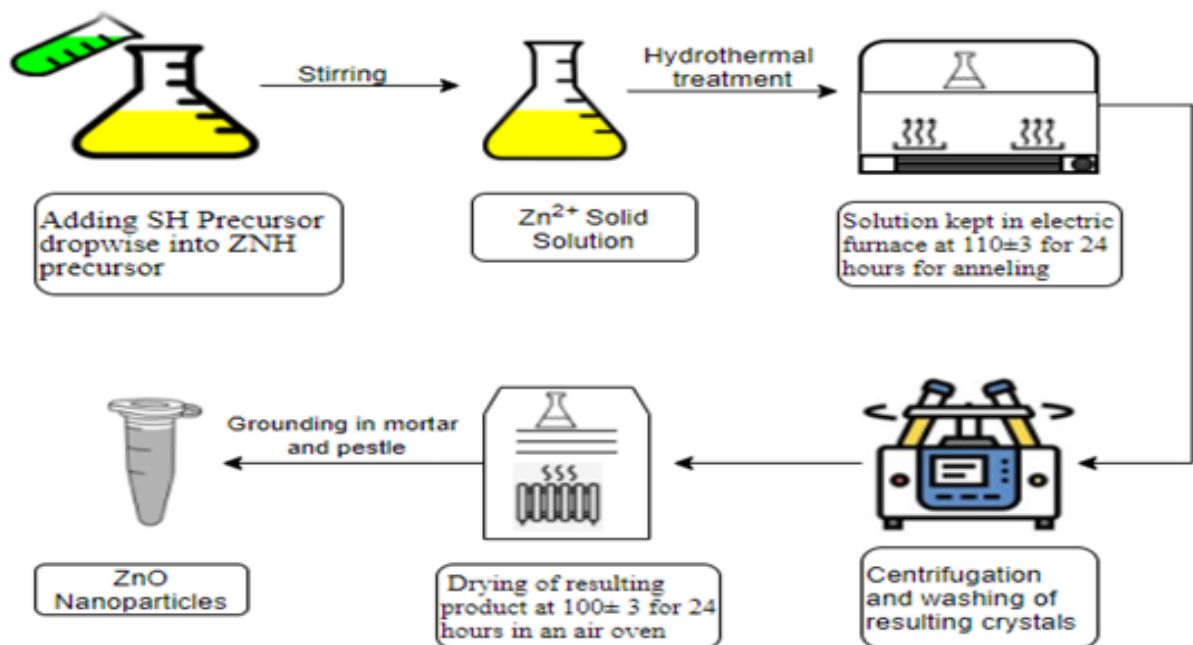


Figure 6. Synthesis methodology of ZnO nanoparticles

**Fe<sub>3</sub>O<sub>4</sub> nanoparticles:** The chemical co-precipitation method, which entailed stirring 1M of PEG and iron nitrate at 40°C for 02 hours, was used to create Fe<sub>3</sub>O<sub>4</sub> nanoparticles. After drying, they undergo two- hour calcination at 400°C. The produced iron oxide was mixed with sodium citrate, 0.5 M, and stirred in an ultrasonic bath for 12 hours. Modified nanostructures were created by utilizing a magnet to collect the prepared silt (Figure 7).

**Fe<sub>3</sub>O<sub>4</sub>.ZnO (ZF) nanocomposite:** ZF was created via the hydrothermal method, which involved suspending 10 mg of synthesized Fe<sub>3</sub>O<sub>4</sub> nanoparticles in 5 mL of milli Q water and ultrasonically processing it for 10 minutes. A second ZnO solution was made, and the two were mixed and stirred magnetically for 30 minutes. After that, the pH was kept constant by gradually adding 3.2 g of NaOH while stirring for 10 minutes. The aforementioned solution was then dried in an oven at 100°C for 24 hours before being finely ground to produce a ZF nanocomposite (Figure 7). The percentage yield of the nanoparticle was calculated using equation 1 and the calculated values are presented in Table 4 (Wang et al., 2021). The weight of the dried nanoparticles with respect to the mixture-volume ratio shows thig yield percentage.

$$\text{Percentage yield} = \frac{\text{weight of dried nanoparticles}}{\text{calculated weight of the salt}} \times 100\% \quad \text{Eq. 1}$$

Sample Label	Mass of salt (g)	Wt. of nanoparticles	Percentage
<b>ZnO</b>	0.78	0.39	50.0
<b>Fe<sub>3</sub>O<sub>4</sub></b>	0.52	0.29	55.8
<b>Fe<sub>3</sub>O<sub>4</sub>.ZnO</b>	0.78	0.53	68.0

Table 4: Percentage yield of dried nanoparticles

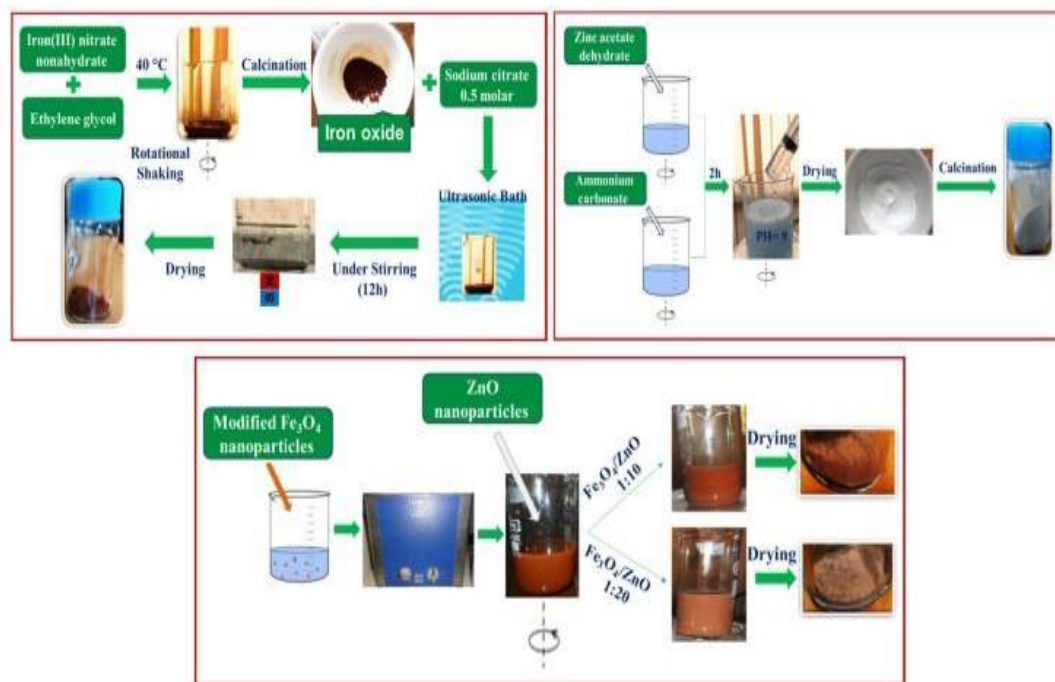


Figure 7. Synthesis methodology of ZF nps by sol-gel method

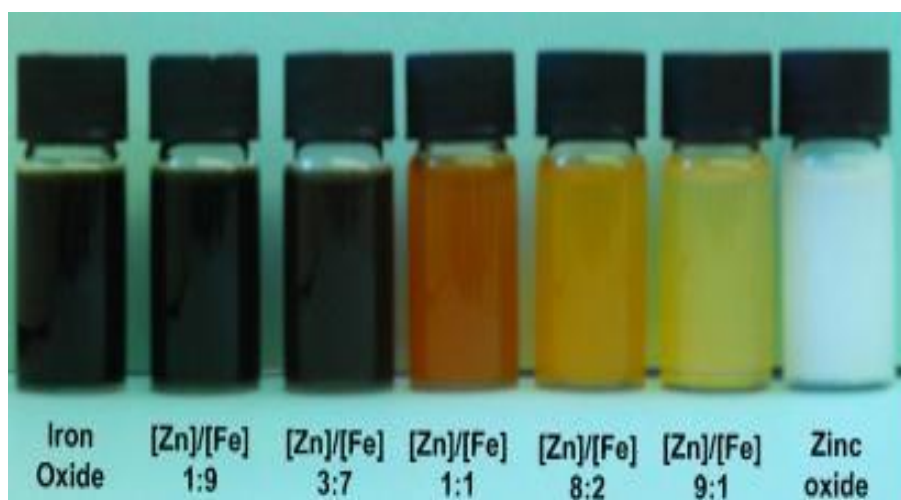


Figure 8. Visibility of the iron oxide, the zinc oxide and the various Zn/Fe oxide composite nanoparticles distributed from left to right.

### 5.2.1. Coating process of synthesized nps on WF substrate

Catalog number	Description	Pore size	Max. Operating temp.	Wettability	Thickness	Application
1600-003	Having high particle retention and excellent loading capacity.	5 $\mu\text{m}$	550°C	Hydrophilic	176 $\mu\text{m}$ .	Offers high absorbency and increased wet strength

Table 5: Physiochemical specification of the WF (Grade 3) paper

Briefly the prepared solution was warmed till boiling with vigorous stirring, for layering nanoparticles on the filter paper: As a result, 02 grams of ZnO nanoparticles (NPs) as well as ZF were sonicated in 200 mL of deionized water for 10 minutes, using a fixed power sonicator (L&R Ultrasonics, Quantrex 140, 150 W, 45 kHz). Afterwards, it was sonicated for an additional 10 minutes, and  $\text{NH}_4\text{OH}$  was added drop wise until the pH of the mixture matched the alkalinity of the paper, and the mixture was then sonicated for an additional 10 minutes before each experiment. The study reveals it is acceptable to use  $\text{NH}_3$  in place of  $\text{NH}_4$ . Coating was needed on a white paper surface from Taiwanese company YFY Papers. The paper was positioned so that it barely touched the scattered solution, and the substrate was attached face down. The spin coater was used for coating the paper surface evenly with synthesized nps. After coating the paper strips were air dried and further kept in desiccators (Figure 9). Each experiment used a different amount of sonication time-5, 10, 15, 20, 25, and 30 minutes. The fabricated paper was then separated, overdried to 80°C, and then characterized.

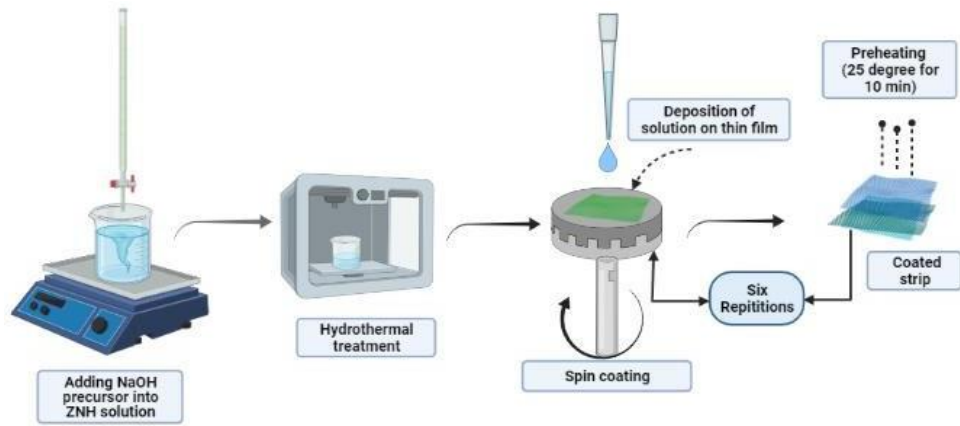


Figure 9. Schematic methodology for coating of synthesized nanoparticle filter paper

### 5.2.2. Characterization of nanoparticles samples

The patterns used for XRD were produced with the Bruker D8 (Cuk radiations, 1.54) between 20 and 70. Rietveld refining was carried out using the MAUD 2.7 programme. The fifth-order polynomial function and Pseudo-Voigt algorithm were used to fit the XRD patterns. The patterns of the JCPDS, i.e., 005-0664 for ZnO, 024-1460 for Zinc nitrate hydroxide hydrate (ZNHH), and 025-1028 for Zinc nitrate hydroxide (ZNH) phases. The crystalline size ( $X_s$ ) was evaluated utilizing the Debye

Scherrer formula (Equation. 2):  $X_s = \frac{0.9}{\beta \cos \theta}$

Where  $\lambda$  is the wavelength of radiations,

$\beta$  is full width at half maximum (FWHM),

and  $\theta$  is the diffraction angle.

In order to determine the size of ZnO crystals, atomic planes (100), (021), (002), (101), (102), and (110) were considered. Also, Williamson Hall-ISM (Eq. 2) model was used to confirm the crystal size and lattice strain in ZnO crystals. The degree of crystallinity ( $X_c$ ) was calculated using the peak-area method.

$\beta_{hkl} \cos(\theta_{hkl}) = \frac{0.9\lambda}{X_s} + 4\varepsilon \sin(\theta_{hkl})$  (Equation 3), where  $\varepsilon$  is the lattice strain in ZnO crystals.

Nanopowder	FWHM	
	(002)	(101)
ZnO7	0.1076	0.1135
ZnO8	0.0689	0.1082
ZnO9	0.0492	0.1082
ZnO10	0.0492	0.1079
ZnO12	0.0787	0.2952

Table 6: FWHM values corresponding to (002) and (101) diffraction peaks of ZnO phase pertinent to each nanopowder

Further, for molecular structure FTIR spectrums of pellets made from KBr were captured using the Bruker Tensor 27 spectrometer for synthesized nps. Also, Perkin Elmer (System 2000 FTIR) was used to record FTIR spectra of paper coated with synthesized nanoparticles and blank paper. This technique uses infrared radiation to measure how molecules rotate and vibrate can identify changes in functional groups, which can indicate changes in biomolecule composition. The presence of molecules' interactions can be detected by detecting differences in their structures. The most popular FTIR based characterization methods are ATR-FTIR, transmittance FTIR, and micro-spectroscopy FTIR. Wavenumber is used to quantify the FTIR spectrum and makes spectrum interpretation easier because of its strong correlation with both energy and frequency. The atomic structure and morphology of nanoparticles were examined using FESEM (JEOL JSM-7610F Plus). The size of nanoparticles was measured using the Image-J programme. The elemental composition of nanoparticles was ascertained using BrukerXFlash 4010 EDX tool. The Autosorb-1-C Quantachrome was employed to measure the porosity and specific surface area of nanoparticles. HRTEM (FEI Tecnai) electron microscopy to examine the morphology

and elemental characteristics. This uses a technique called phase-contrast imaging, which creates an image by combining transmitted and scattered electrons. HRTEM requires a bigger objective aperture than traditional TEM imaging when using scattered electrons. For identifying atom arrays in crystalline structures, phase-contrast imaging offers the highest resolution currently accessible. For instance, ordinary electron microscopies do not have the resolution needed to scan the single particle crystal structure that HRTEM provides, even while they are capable of providing statistical evaluations of NP shape. Because of this, HRTEM is now the method most frequently employed to characterize the interior structures of NPs. The software Image J has been used to assess the dimensions and size of nanoparticles.

### **5.3. Utilization of nps in forensic samples**

As a result of optimization of the above method, a spiked forensic sample (urine, blood, and saliva) containing alprazolam at concentrations ranging from 10 to 50 ppm in pure methanol was analyzed using dispersive solid phase extraction (DSPE). For quality controls, standards of known concentrations, and real samples, the volume of each sample was kept at 1 mL before extraction. The extraction process was carried out in 15 mL screw-capped plastic tubes.

On a vortex machine, 4 ml of extraction solvent methanol and 5 mg of synthesized NPs were added to each tube and stirred for 10 seconds. All tubes were then filled with 2 g anhydrous Epsom salt, vortexed for 10 seconds, rotated for 5 minutes on the auto rotator, and centrifuged for 10 minutes at 3500 rpm. A pipette was used to transfer the supernatant of methanol into a new tube for evaporation (the solvent is vaporized in two ways: hot water baths are placed at the bottom of the tube and pressurized air is pressed against solvent surfaces at a set temperature and pressure) in a digital turbo vaporizer machine. A vortex machine was then used to agitate the tubes for ten seconds after 50 liters of methanol had been spiked into each tube. SERS analysis was conducted by centrifuging the supernatant for 5 minutes at 3500 rpm. For analysis for Surface enhanced validation method: A confocal micro-Raman Spectroscopy measurement was conducted using a 785nm laser at 100mW power with resoluteness of  $4\text{cm}^{-1}$  (FWHM) for five scans with four seconds laser exposure for the spiked biological samples of drugs (Make: Renishaw, United Kingdom) (Model: Renishaw In Via Reflex Raman Spectrometer).

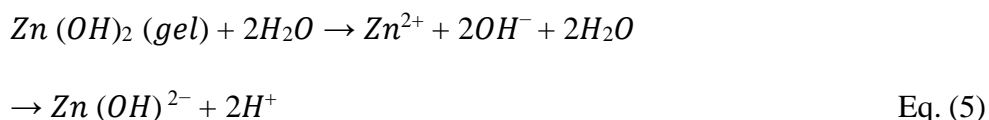
**CHAPTER 6**  
**RESULTS AND DISCUSSION**



## 6. Results and Discussion

### 6.1. Phase structure

ZnO nps- XRD pattern of all nanopowders has been shown in Figure 10. Rietveld refinement suggested biphasic structure (ZnO and ZNH phases) of ZnO at pH 7, 8, 9, and 10 nanopowders, whereas, ZnO at pH 12 nanopowder was triphasic (ZnO, ZNH and ZNHH) in composition. The presence of the distinctive ZnO peaks (100), (002), (101), (102), (110), and (103) in all nanopowders demonstrated that ZnO was the predominant phase and ZNH and ZNHH were the minor impurities. Comparison of FWHM values corresponding to (002) and (101) characteristic peaks of ZnO phase (Table 6) indicated that size of ZnO crystals increased with the increase in pH value of ZnO solid solution up to 10. At a pH value of 12, FWHM increased, thereby, indicating the decrease in ZnO crystal size. Thus, the critical analysis implied that the pH variation within 7 to 10 did not transform the phase structure, but affected the size of ZnO crystals (Figure 10). Thus, with the increase in pH value of the ZnO solid solution, resultant ZnO crystals grew. The speculated chemical reaction supporting the formation of ZnO phase has been given in Eq. (4-6).



### 6.1.1. Crystal structure

The fitted XRD profiles obtained after Rietveld refinement have been shown in Figure 10. The goodness of fit parameters ( $\sigma$ , Rwp, Rb) and crystal structure parameters of each nanopowder. The value of  $\sigma$  for all nanopowders were significantly less than four and was acceptable. With the increase in pH value from 7 to 10, the concentration of stoichiometric ZnO phase increased, whereas, the concentration of ZNH phase decreased. It has been clear that the pH value of 9 and 10 were optimal to produce the maximum concentration of ZnO crystals. Although some disparity in the standard ( $a=3.250 \text{ \AA}$  and  $c=5.206 \text{ \AA}$ ) and experimental lattice parameters of ZnO crystals were observed, interestingly, the distortion ratio ( $c/a$ ) of experimental lattice parameters was close to the standard value of 1.60.

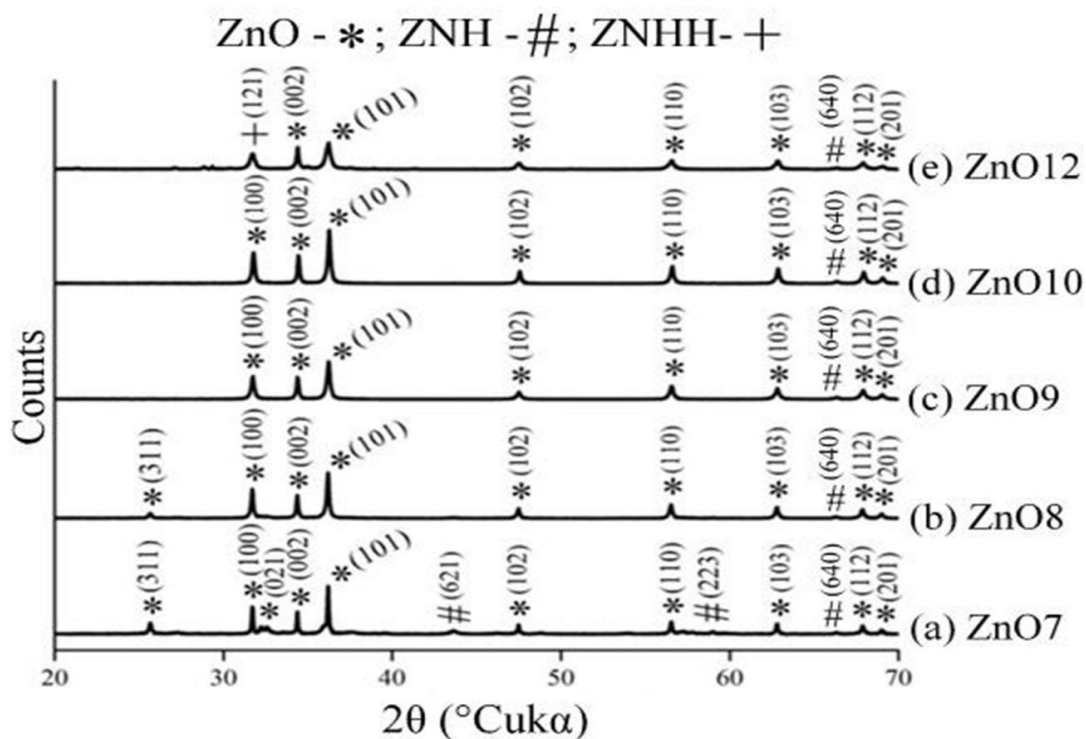


Figure 10. XRD image of (a) ZnO7, (b) ZnO8, (c) ZnO9, (d) ZnO10, (e) ZnO12 nanopowders

The ZnO9 nanopowder exhibited stoichiometric lattice parameters of  $a = 3.250 \text{ \AA}$  and  $c = 5.206 \text{ \AA}$ . The size of ZnO crystals increased in the increase in pH value up to 10 as calculated by various models. Apart from it, all other model confirmed the nanodimensional regime of ZnO crystals. Furthermore, the degree of crystallinity increased with the increase in pH value up to 10, as given in Table 4. The ZnO at pH 9 and ZnO at pH 10 nanopowders exhibited maximum crystallinity of 98%. Thus, the overall analysis concluded that variation in pH value had a significant influence on the crystal structure of ZnO crystals (Figure 11). The solid solution of nine pH value produced a maximum concentration of ZnO crystals with stoichiometric lattice parameters, nanodimensional size and maximum crystallinity.

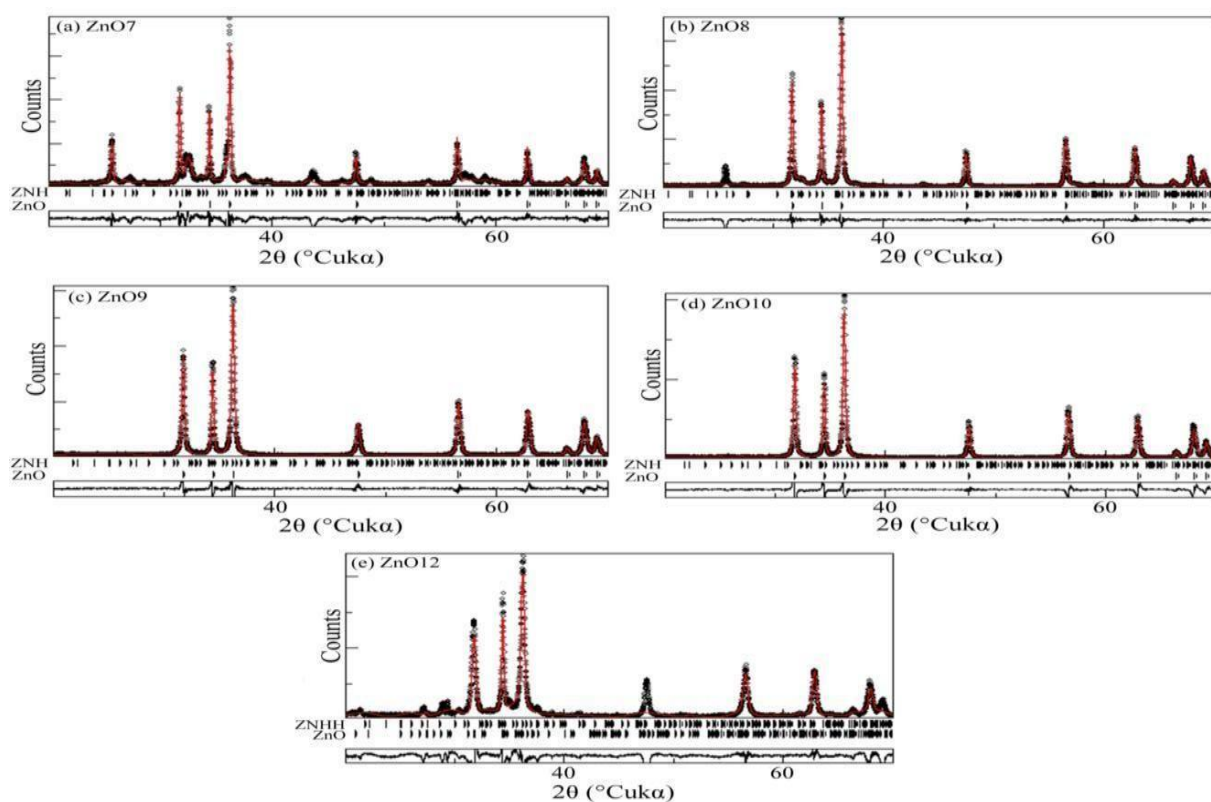


Figure 11. XRD fitted profiles of (a) ZnO7, (b) ZnO8, (c) ZnO9, (d) ZnO10, (e) ZnO12 nanopowders

Various stages of  $\text{Fe}_3\text{O}_4$  and  $\text{ZnO}/\text{Fe}_3\text{O}_4$  were indicated by the refining. No peaks of impurity or other substance presence were observed which indicates that the synthesized nanoparticles were crystalline and thus reducing the particle size increases the aspect ratio. Figure 12 shows that the magnetic nanocomposite has larger diffraction pattern towards  $\text{ZnO}$  with having hexagonal crystalline structure. Its additions do not alter the crystal phase as shown in Figure 10.

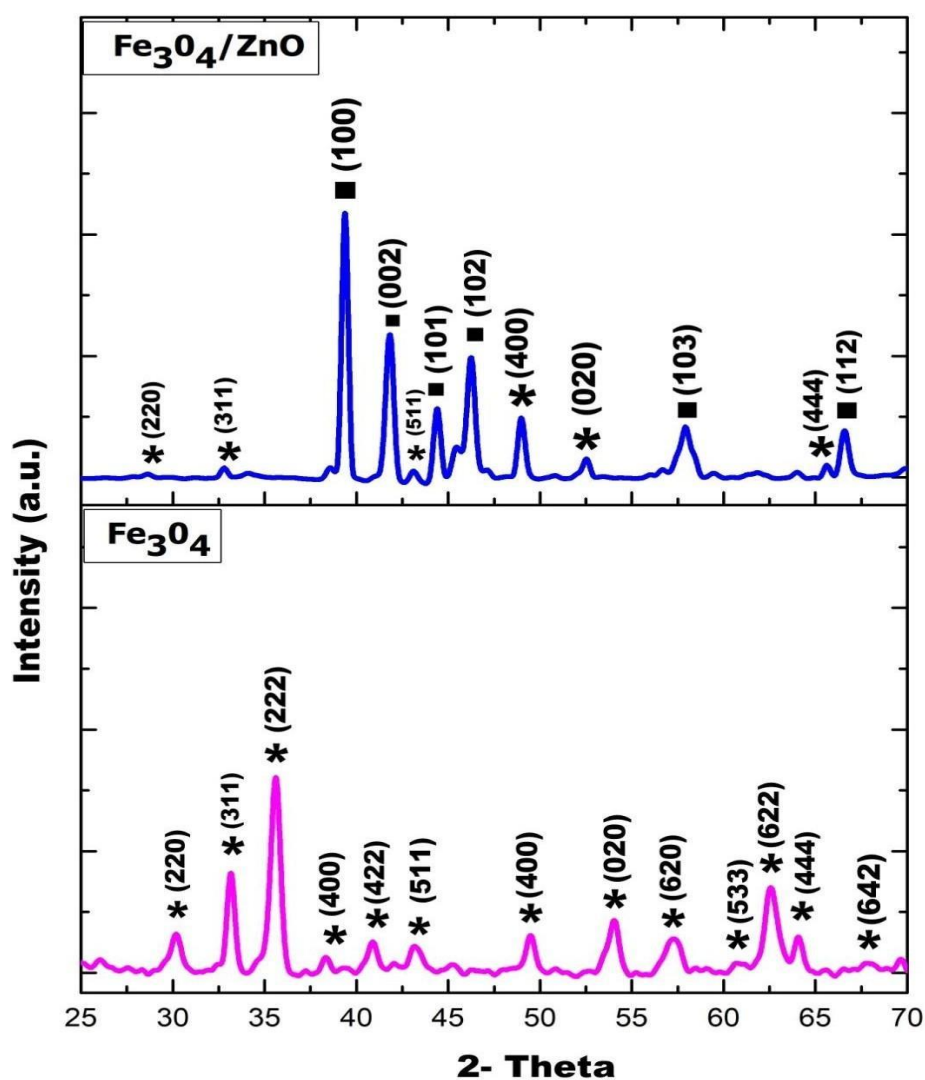


Figure 12. XRD patterns of  $\text{Fe}_3\text{O}_4$  and  $\text{Fe}_3\text{O}_4/\text{ZnO}$

XRD spectra were obtained in order to verify the covering of ZnO nanoparticles on the surface of the paper and its crystallinity. Figure 13, depicts representative XRD spectra recorded from plain paper and paper coated with ZnO nanoparticles after sonication as the fabric of paper is complex. However, paper is primarily composed of cellulose,  $\text{CaCO}_3$ , silicates, thickening agents, and binders. The residual spectral peaks have been assigned to cellulose and  $\text{CaCO}_3$ , as illustrated in Figure 13 b, c. The structural features of paper coated with ZnO-NPs and uncoated paper were analyzed using XRD. The diffraction peak of ZnO-NPs decorated on paper were obtained at various angles, including  $2\theta = 31.92^\circ, 34.62^\circ, 36.44^\circ, 47.80^\circ, 56.89^\circ, 63.23^\circ, 66.73^\circ, 68.33^\circ, 69.47^\circ, 73.04^\circ, 77.41^\circ, 81.93^\circ,$  and  $89.99^\circ$ . These peaks corresponded to the crystal lattice planes (100), (002), (101), (102), (110), (103), (200), (112), (201), (004), (202), (104), and (203), respectively, of the ZnO material, as illustrated in Figure 13 (c).

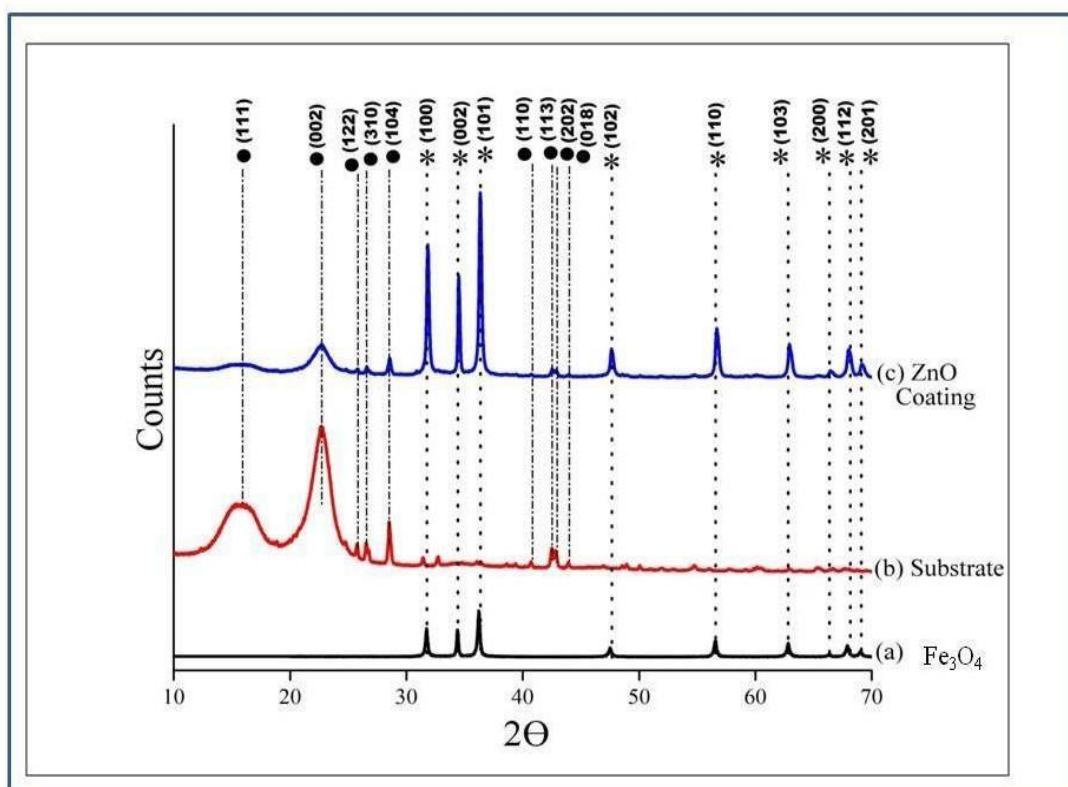


Figure 13. XRD pattern coated nps on WF paper (a) ZnO (b) substrate (c)  $\text{Fe}_3\text{O}_4$

### 6.1.2. Molecular structure

The FTIR spectra of all nanopowders have been shown in Figure 14. The peaks observed below  $500\text{ cm}^{-1}$  and  $1558\text{ cm}^{-1}$  confirmed the formation of Zn-O molecules. In addition to Zn-O ions, vibrations at  $910\text{ cm}^{-1}$  and  $1020\text{ cm}^{-1}$  suggested the presence of C-O and C-H bonded ions. In-addition, surface adsorbed water (O- H ions) at  $3500\text{ cm}^{-1}$  were also present in all nanopowders. These OH- ions remained entrapped in the surface of as-synthesized nanoparticles and would have been removed upon sintering at high temperature.

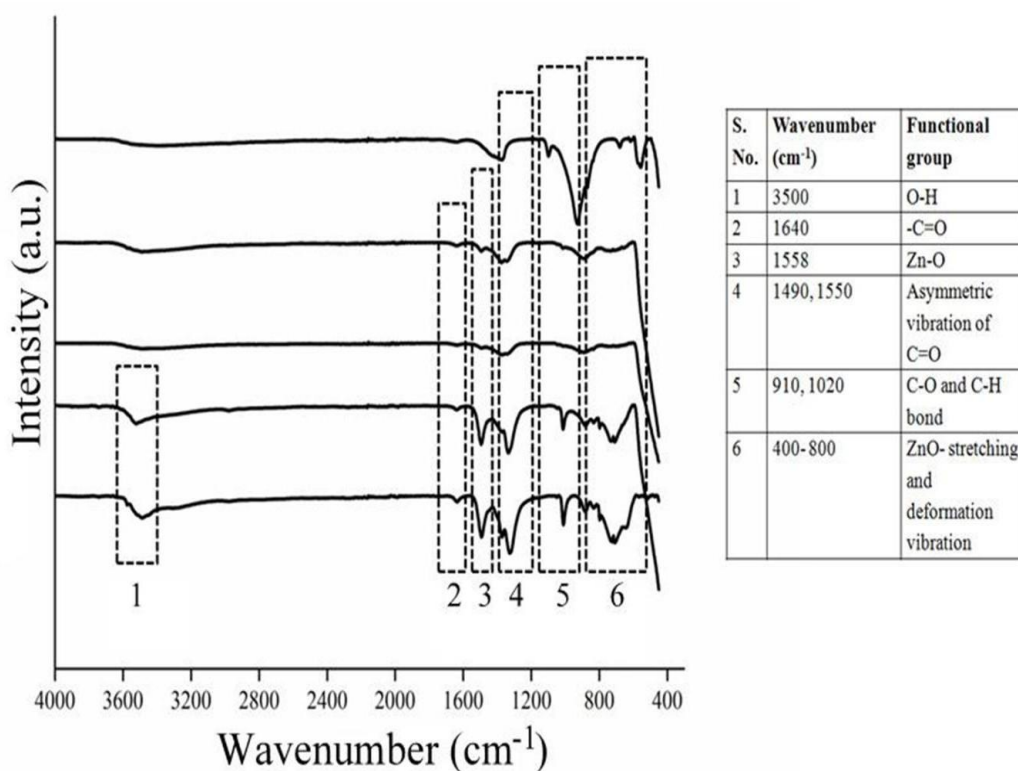


Figure 14. FTIR spectra of (a) ZnO7, (b) ZnO8, (c) ZnO9, (d) ZnO10, and (e) ZnO12 nanopowders

Figure 15 displays the FTIR spectra of ZnO and Fe<sub>3</sub>O<sub>4</sub> nanocomposites ranging from 400 to 4000 cm<sup>-1</sup>. The CO<sub>2</sub> bond type in the air could also be seen at a vibration peak that was apparent at a wavenumber of 2376 cm<sup>-1</sup>. The characterization of Fe-O bond peak is seen in wavenumber of 550 cm<sup>-1</sup> and 676 cm<sup>-1</sup>, which support the type of Fe<sub>3</sub>O<sub>4</sub> spinel inverse structure, and 465, 551, 420, and 490 cm<sup>-1</sup>, which support the form of Fe<sub>2</sub>O<sub>3</sub>.

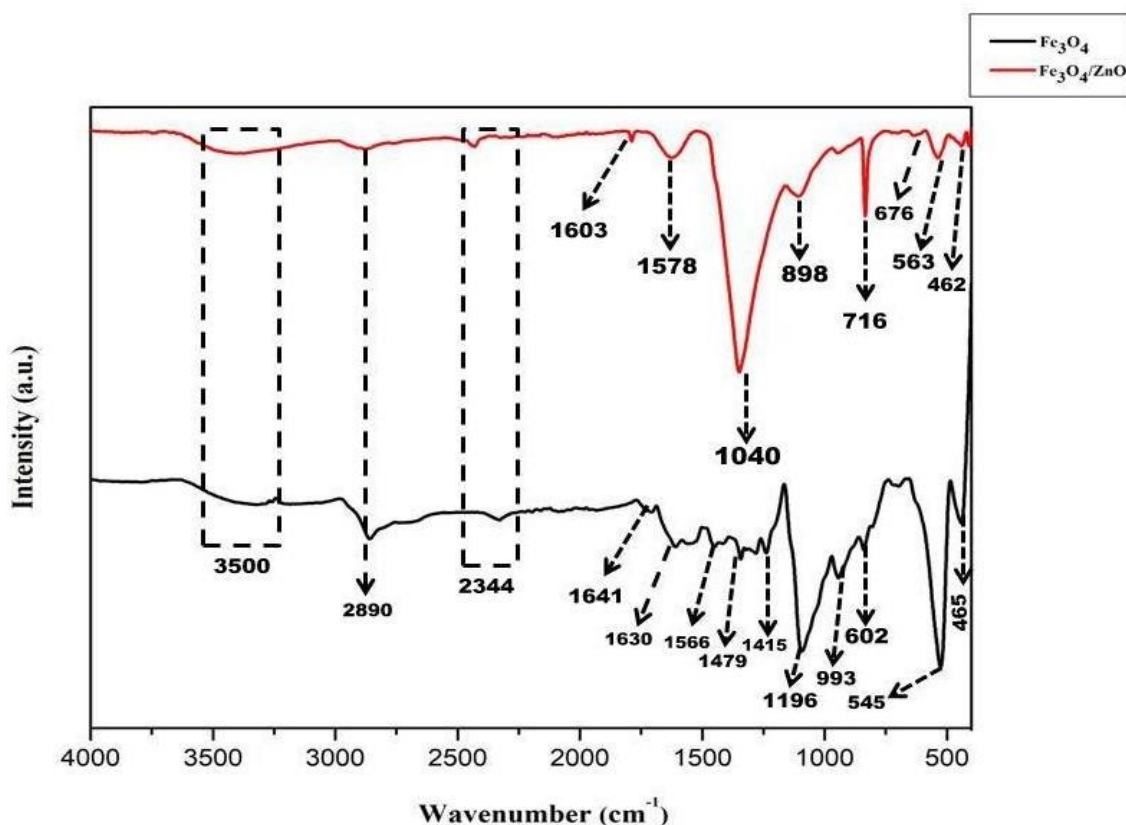


Figure 15. FTIR spectra of ZnO/ Fe<sub>3</sub>O<sub>4</sub> and ZnO

Figure 15 shows the FTIR of Fe<sub>3</sub>O<sub>4</sub>-ZnO nanocomposite. O-H tensile vibrations are shown in this spectrum by the peaks that appear between 3422.31 cm<sup>-1</sup> and 2929.46 cm<sup>-1</sup>. The C=C and O=C=O bonds may be seen in the peaks at 2366.99 cm<sup>-1</sup> and 1430.24 cm<sup>-1</sup>, respectively. The Fe-O bond's tensile vibration is associated with the peak at 676.16 cm<sup>-1</sup>, while the Zn-O bonds' fluctuation is associated with the peak at 454.66 cm<sup>-1</sup>. The modified Fe<sub>3</sub>O<sub>4</sub>, ZnO, and ZF (1:10) nanocomposites spectra are displayed. The ZnO and FeO absorption maxima, according to measurements, would be at 453.1 and 540.2 cm<sup>-1</sup>, respectively. Acetate bonds and OH hydroxyl group stretching

vibration could be responsible for peaks in the range of  $3500\text{ cm}^{-1}$ .

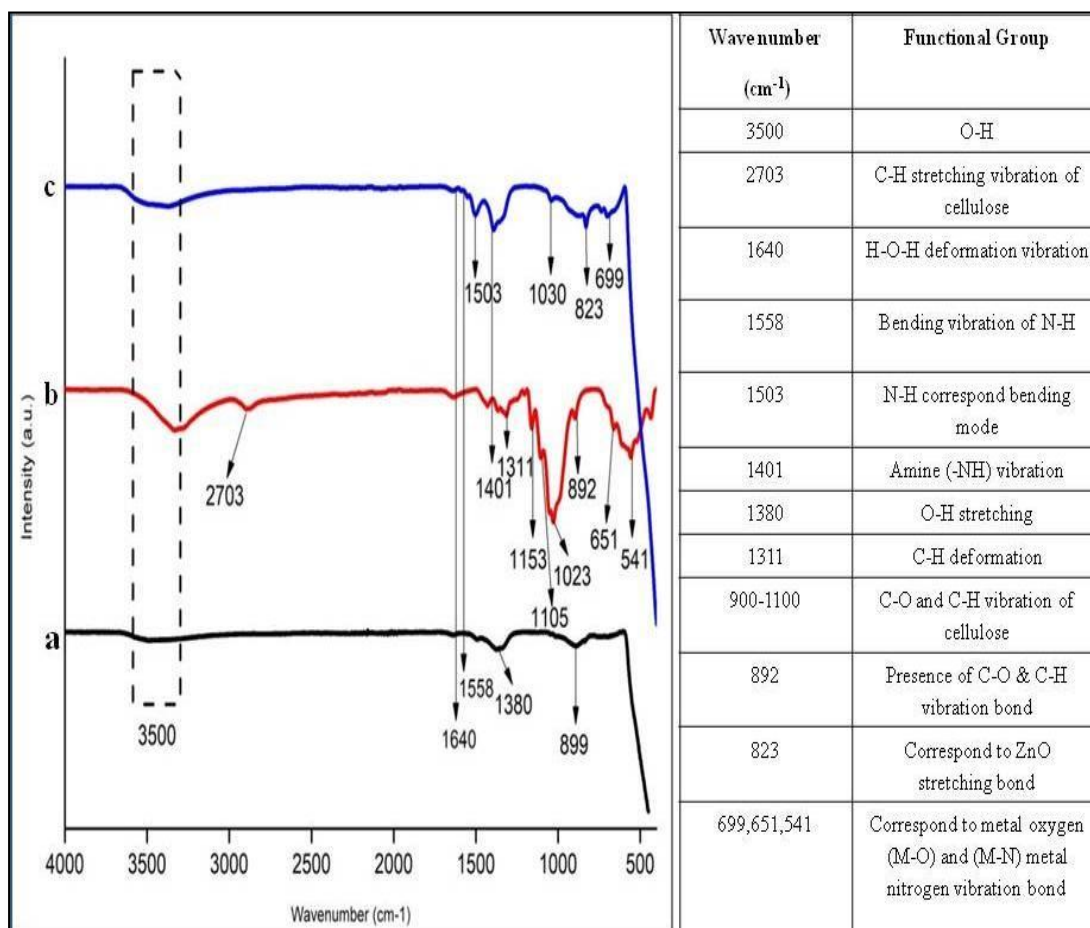


Figure 16. FTIR pattern coated nps on WF paper

The FTIR spectra of all nanopowders have been shown in Figure 16. The peaks observed below  $500\text{ cm}^{-1}$  and at  $1558\text{ cm}^{-1}$  confirmed the formation of Zn-O molecules. In addition to Zn-O ions, vibrations at  $910\text{ cm}^{-1}$  and  $1020\text{ cm}^{-1}$  suggested the presence of C-O and C-H bonded ions. In-addition, surface adsorbed water (O- H ions) at  $3500\text{ cm}^{-1}$  was also present in all nanopowders. These OH- ions remained entrapped in the surface of as-synthesized nanoparticles and would have been removed upon sintering at high temperature. The  $\text{CO}_2$  bond type in the air could also be seen at a vibration peak that was apparent at  $2376\text{ cm}^{-1}$ .



The characterization of the peak of the Fe-O bond vibration is seen  $550\text{ cm}^{-1}$  and  $676\text{ cm}^{-1}$ , which support the type of  $\text{Fe}_3\text{O}_4$  spinel inverse structure, and in the wavenumbers of  $465$ ,  $551$ ,  $420$ , and  $490\text{ cm}^{-1}$ , which support the form of  $\text{Fe}_2\text{O}_3$ . The present study employed FTIR spectroscopy to identify the functional groups, how they interact, and the chemical the fingerprint of ZnO-NPs that were decorated on filter paper. The FTIR spectrum of all samples are illustrated in Figure 16 (a, b, c), wherein the highest peak is observed at  $470\text{ cm}^{-1}$ .

The spectral bands observed at  $950$ ,  $1110$ ,  $1179$ ,  $1274$ , and  $3590\text{ cm}^{-1}$  are commonly associated with cellulose, which is a major constituent of paper. The evidence presented indicates that the functional groups of hydroxyls have been used by the ZnO nanoparticles. The generation of ZnO and ZF crystals on the base material was supported by the analysis of crystal and molecular structures using XRD and FTIR techniques.

### **6.1.3. Mesoporous structure**

The isotherms and pore size distribution curves (inset) of all nanopowders have been shown in Figure 17. The isotherms of all nanopowders were of type IV with H3 hysteresis loop, suggested the mesoporous structure of nanomaterials. Furthermore, isotherms depicted that the gas adsorption capacity of nanoparticles in increasing order was  $\text{ZnO10} < \text{ZnO12} < \text{ZnO9} < \text{ZnO8} < \text{ZnO7}$ . Moreover, the BJH curves (inset) suggested the range of diameter of pores between  $5\text{--}40\text{ nm}$ , which further confirmed the mesoporous structure of all nanoparticles. Except for ZnO12, the specific surface area of nanoparticles in increasing order  $\text{ZnO10} < \text{ZnO9} < \text{ZnO8} < \text{ZnO7}$ .

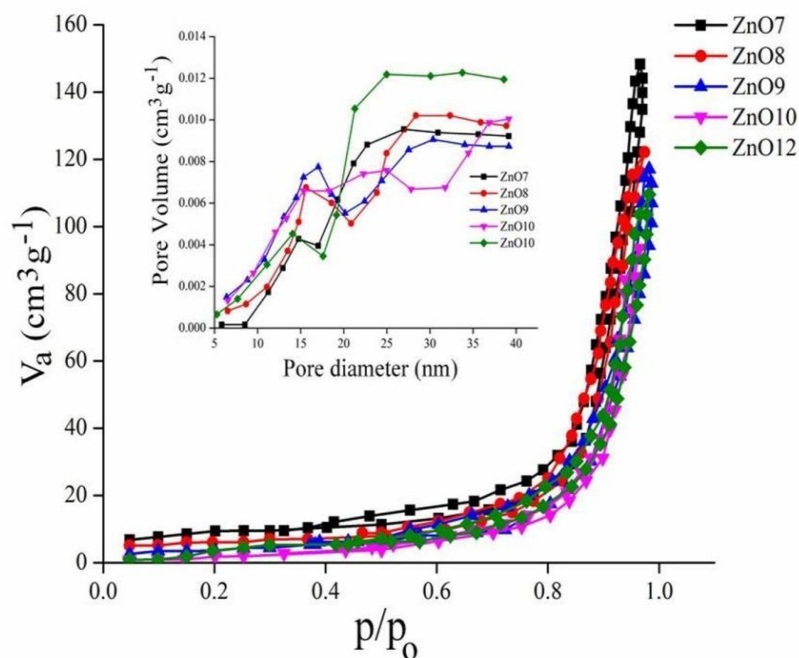


Figure 17. N<sub>2</sub> isotherms and BJH curves (inset) of (a) ZnO7, (b) ZnO8, (c) ZnO9, (d) ZnO10, and (e) ZnO12 nanopowders

#### 6.1.4. Morphological and elemental structure

The FESEM micrograph of ZnO at pH 9 nanoparticles has been shown in Figure 18 (a). Particles were irregular in shape and agglomerated. The average size of individual nanoparticles was  $45 \pm 9$  nm, which was in agreement with the crystal sizes calculated using different models. The EDX micrograph of ZnO9 nanoparticles has been shown in Figure 18 (b). Particles of vivid shapes and size were present in ZnO9 nanopowder. No other element like N and C were detected, whereas, observed in phase and molecular structures. Elements in traces sometimes could not be detected in EDX analysis. The weight and atomic concentrations of Zn and O elements is shown in Figure 18. The HRTEM micrographs showing particle morphology and atomic structure of ZnO9 nanoparticles have been shown in Figure 18, (c-d). Particles were confirmed to be irregular in shape and agglomerated. The average size of particles was  $47 \pm 9$  nm. Furthermore, the SAED pattern (Figure 18, (d) also supported the polycrystalline structure of ZnO crystals in agreement with the XRD phase analysis (Figure 10). The hexagonal pattern of spots indicated the crystalline nature of the particles.

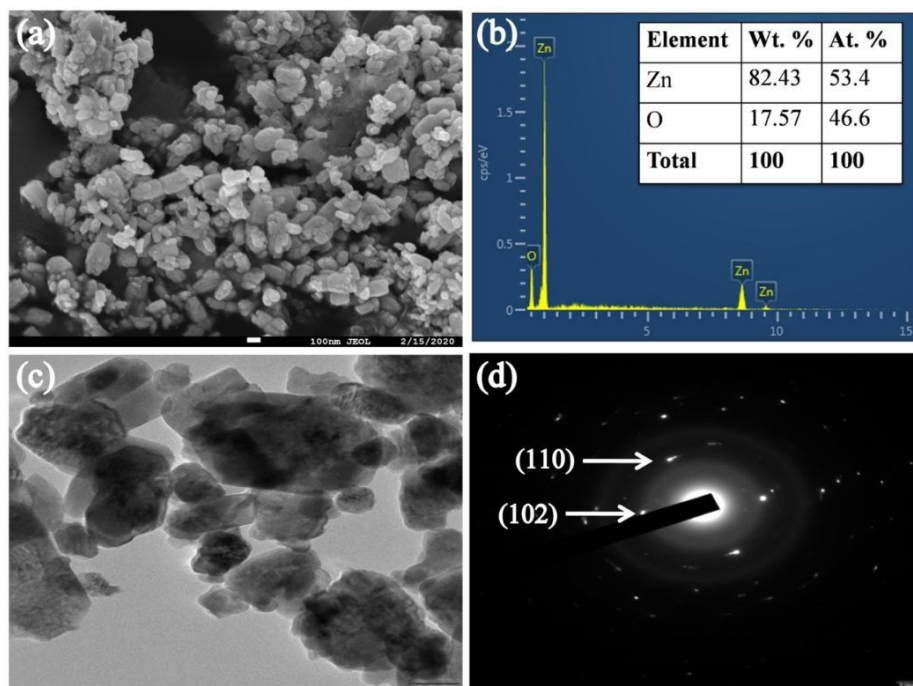


Figure 18. (a) FESEM, (b) EDX, and (c-d) HRTEM micrographs of ZnO9 nanoparticles

Figures 19 (a,b) display the synthetic SEM images of the filled  $\text{Fe}_3\text{O}_4\cdot\text{ZnO}$  nanostructures with varying weight ratios. The ZnO and  $\text{Fe}_3\text{O}_4$  formations were found to be composite, as evidenced by the SEM image. The nanoparameters of the composite frameworks were also verified by TEM examination. Many sorts of structures were found during the TEM study. The surface morphology and distribution of the sample were investigated using the field effect electron microscopy with scanning electron microscopy (FE-SEM) and the Digimizer software.

With a diameter between 40 and 50 nm, the nano-crystallite is larger than the one discovered using the XRD. This might be as a result of the varied crystallite phases or index miller or the presence of several crystal particles in the pictures from the scanning electron microscope. Contact point parameters change as a result of morphological changes.  $\text{Fe}_3\text{O}_4$  and ZF morphology was investigated using SEM.

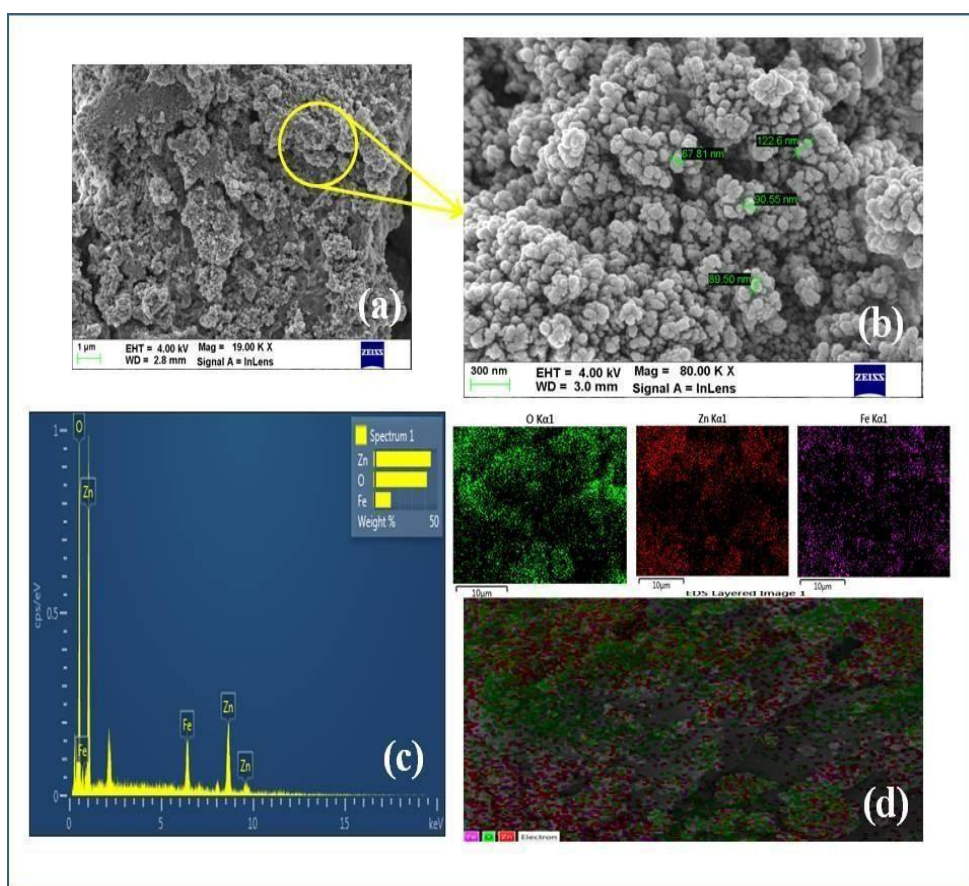


Figure 19. FESEM (a-b)  $\text{Fe}_3\text{O}_4/\text{ZnO}$  (c-d) EDS mapping

The bare  $\text{Fe}_3\text{O}_4$  nanoparticles are monodisperse without agglomeration and have a spherical morphology, as shown in Figure 19, the diameter of the particle size is 370 nm on average. The  $\text{Fe}_3\text{O}_4/\text{ZnO}$  nanocomposite's morphological structure is barely different from bare  $\text{Fe}_3\text{O}_4$ . The coating of ZnO over  $\text{Fe}_3\text{O}_4$  nanoparticles proved that smooth-surfaced nanoparticles can aggregate (Figure 21). The ZF nanocomposite was generated and evenly dispersed in aqueous solutions as a result of the hydrophilic property of ZnO's outer surface being transferred to  $\text{Fe}_3\text{O}_4$ .

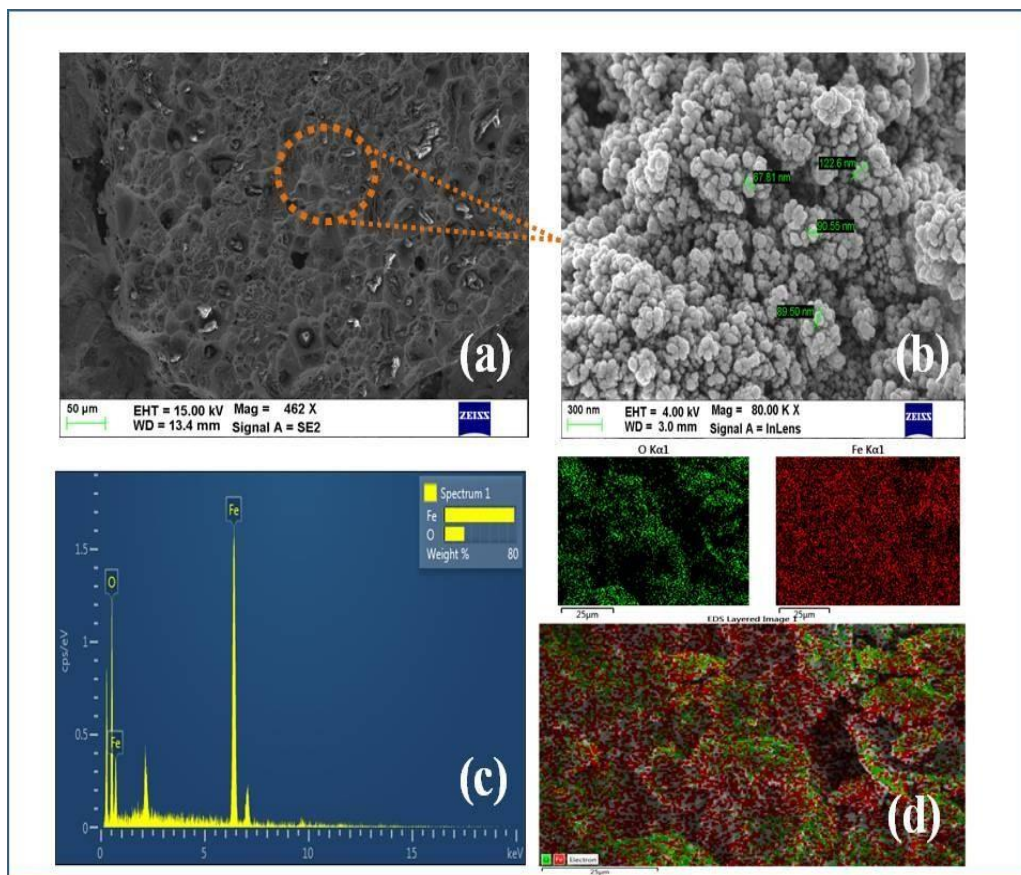


Figure 20. FESEM (a-b)  $\text{Fe}_3\text{O}_4$ (c-d) EDS mapping

As shown in Figure 21 (a,c), various magnifications of FE-SEM pictures of the ZnO-NPs layered and blank filter paper were examined to determine structural analysis, their distribution, and effects on the paper. This results in filter paper having a huge surface area and vacant volume space, which may be observed. The large void volume space allowing for such a huge amount of fabricated on ZnO– NPs, in such a large population may have little effect on pores.

Using higher magnification FE- SEM images, the size of ZnO–NPs was measured. The size manually measured utilizing Image J software, and found that it varied between 70 to 280 nm with a median of 163.64 nm. Figure 21 (b-d) illustrates how an EDX study showed that the elemental compositions of the ZnO-NPs adorned paper and the blank paper were comparable. The presence of components C and O can be used to identify the composition of filter paper. The ZnO nanoparticles could be seen to be deposited on the outermost layer of the cellulose fibers in the SEM's

magnified pictures. With the deposition of ZnO nanoparticles, Zn, C, and O were also visible in the EDS study. The SEM images in (22 a, b) show the ZnO particles coated on the paper surface after 20 and 30 minutes of sonication. A decrease in interstitial voids between fibers can be seen in SEM images as sonication time is increased. The connection between fibers of cellulose by SEM is displayed in the Figure 21 c.

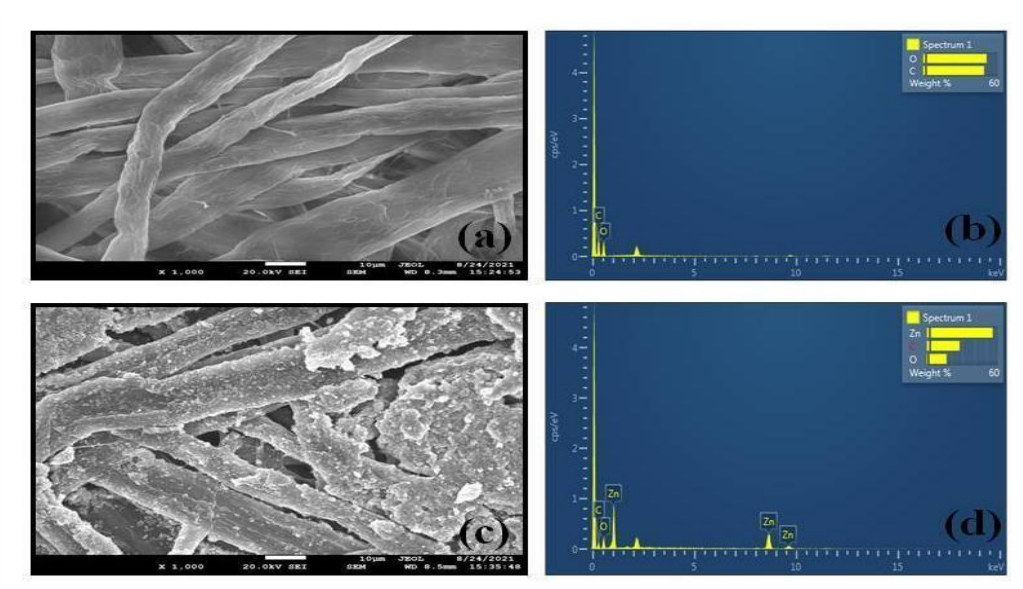


Figure 21. FESEM micrograph of (a-b) Uncoated WF, EDX and (c-d) Coated ZnO nps in WF EDX shows atomic weight percentage

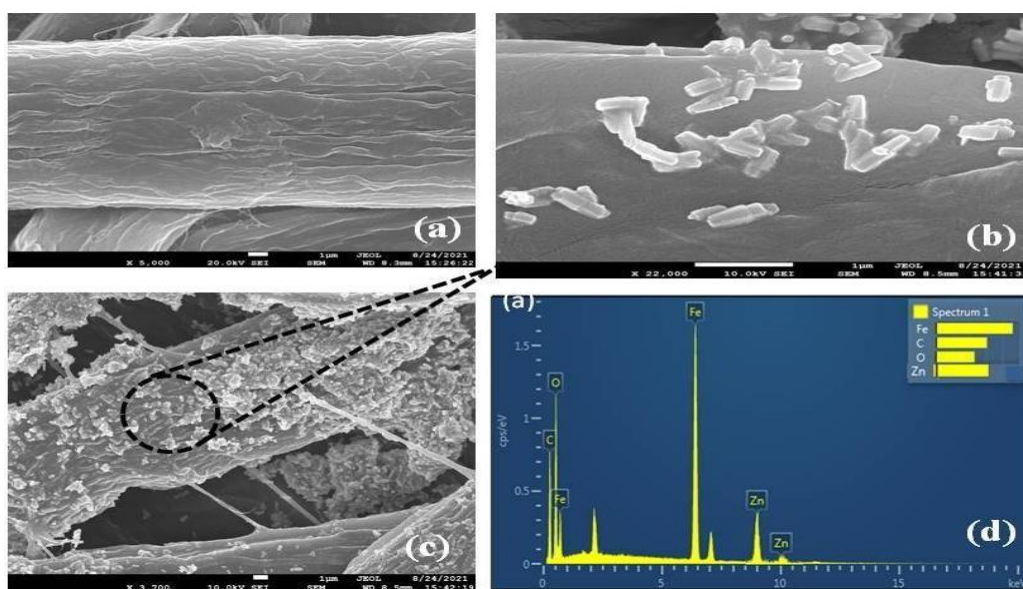


Figure 22. FESEM (a-b) Coated Fe<sub>3</sub>O<sub>4</sub>/ZnO composite on WF (c-d) EDS mapping

As seen in Figure 23, TEM images were used to further evaluate the morphological and structural properties of nanocomposites. On top of the  $\text{Fe}_3\text{O}_4$  nanoparticles' surface, a thin layer of ZnO was successfully produced as a coating. The light grey color of the ZnO matrix on the  $\text{Fe}_3\text{O}_4$  cores could be readily seen after a high-resolution HRTEM was overlaid.

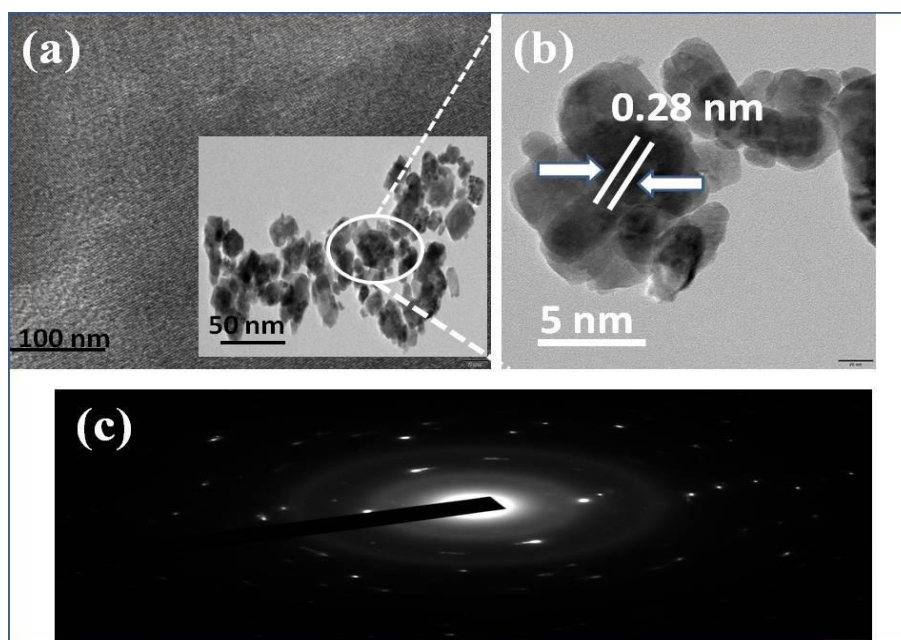


Figure 23. HRTEM of (a-b)  $\text{Fe}_3\text{O}_4\cdot\text{ZnO}$  (c) SAED pattern

## 6.2. Particle size distribution

The zeta potential of the bio fabricated  $\text{Fe}_3\text{O}_4$ -NPs and ZnO NPs was seen as a single, sudden peak with a highest intensity ranging from 25.8 to 48 mV (Figure 24). This suggested that the outermost layer of  $\text{Fe}_3\text{O}_4$ -NPs contains charge- negative moieties. The dispersion of the NPs may be attributed to the repulsive nature of the values that were negative, which also suggested stability of the  $\text{Fe}_3\text{O}_4$ -NPs. Reduced capacity to assemble and little or absent flocculation are indicated by lower zeta potential values. The effect of pH on metal ion binding on  $\text{Fe}_3\text{O}_4$  was substantial.

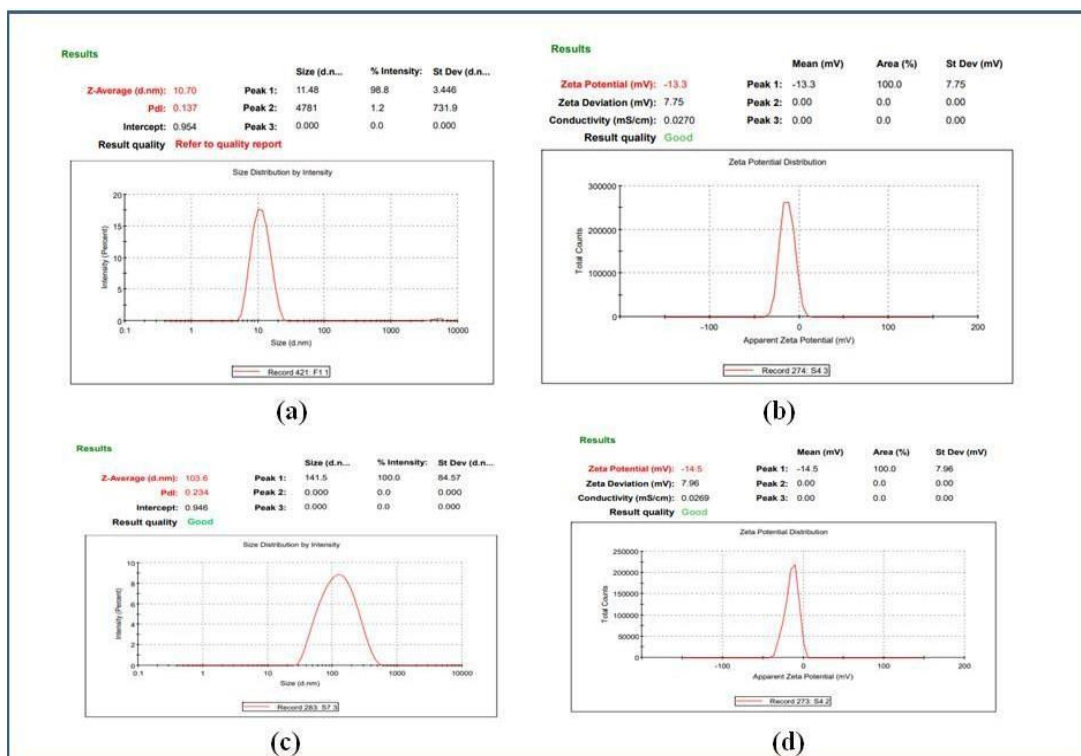


Figure 24. Particle size distribution and zeta potential (a-b) Fe<sub>3</sub>O<sub>4</sub>.ZnO (c-d) ZnO

The pH level affected the outside zeta potential of nanoparticles. The particle's surface zeta potential decreased as pH rose from 2.0 to 11.0. When the pH was between 3.0 and 4.0, the isoelectric point (pH<sub>pzc</sub>) of surface shifted from positive to negative (Figure 25). Iron oxides are covered with groups of Fe OH, etc. in an aqueous solution. Using DLS, one can determine the particle size and distribution of a component was determined by DLS using a Malvern Zetasizer Nano ZS (Malvern Instruments Ltd., GB). The DLS results for the biofabricated iron oxide -NPs indicate a 20-200 nm size range (Figure 25. a-b). It was found that average particle size of 76.5 nm. Particle size and distribution as indicated by DLS analysis are consistent with those discovered through SEM and TEM investigation.



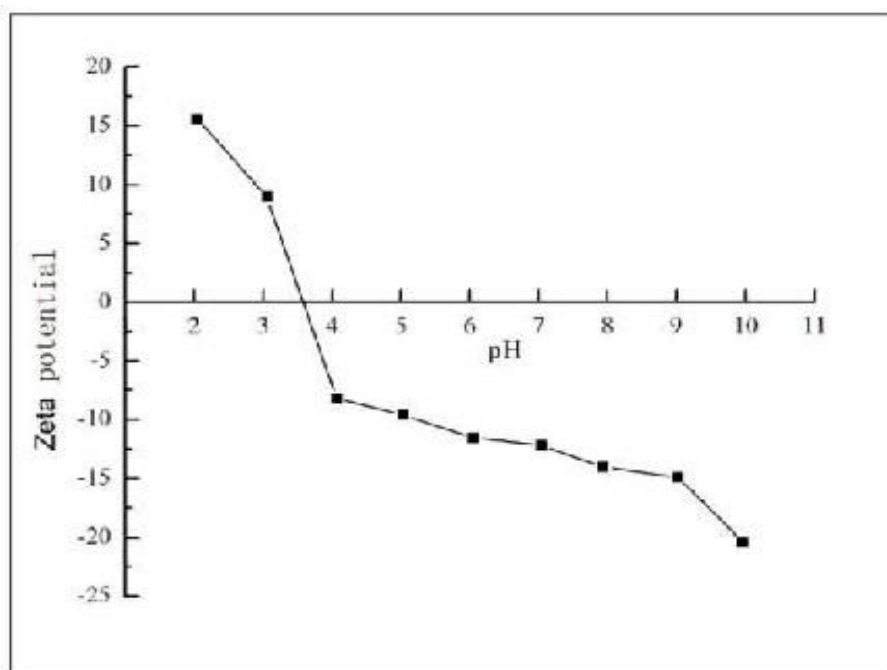


Figure 25. Effect of pH on zeta potential of  $\text{Fe}_3\text{O}_4$ -NPs

DLS measurements were taken on a 12mm type cell (DTS 0012). The cell was then filled with 50 ml of stock dispersion after 1 milliliter of distilled water (or ethylene glycol) was added, sonication for 05 minutes. The proper parameters for ZnO and dispersants were determined (viscosity, absorbance, and refractive index). Results with ZnO, water, and ethylene glycol revealed that the absorption value was 0.1, the refractive index was 2.0, the viscosity was 1.0031 cP, and the refractive index was 1, respectively. The pH value of each suspension was then changed by either adding NaOH or HCl to it. Histograms were produced in order to document the distribution of sizes.

### 6.2.1. Zeta potential measurements

Zeta potential was ascertained by analyzing 0.1 gram of zinc oxide in 10 milliliters of water (or other solutions). Prior to zeta potential measurements, each sample were subjected to ultrasonication for 5 minutes. Laser Doppler Velocimetry is used by the Zetasizer Nano ZS to detect electrophoretic mobility. This automatic titrator also used sodium hydroxide (0.25 mol/l) and hydrochloric acid (0.25 and 0.025 mol/l) to automatically change the pH of the concentrations. Figure 26 shows the zeta potential changes that occurred during the titration of NaOH.

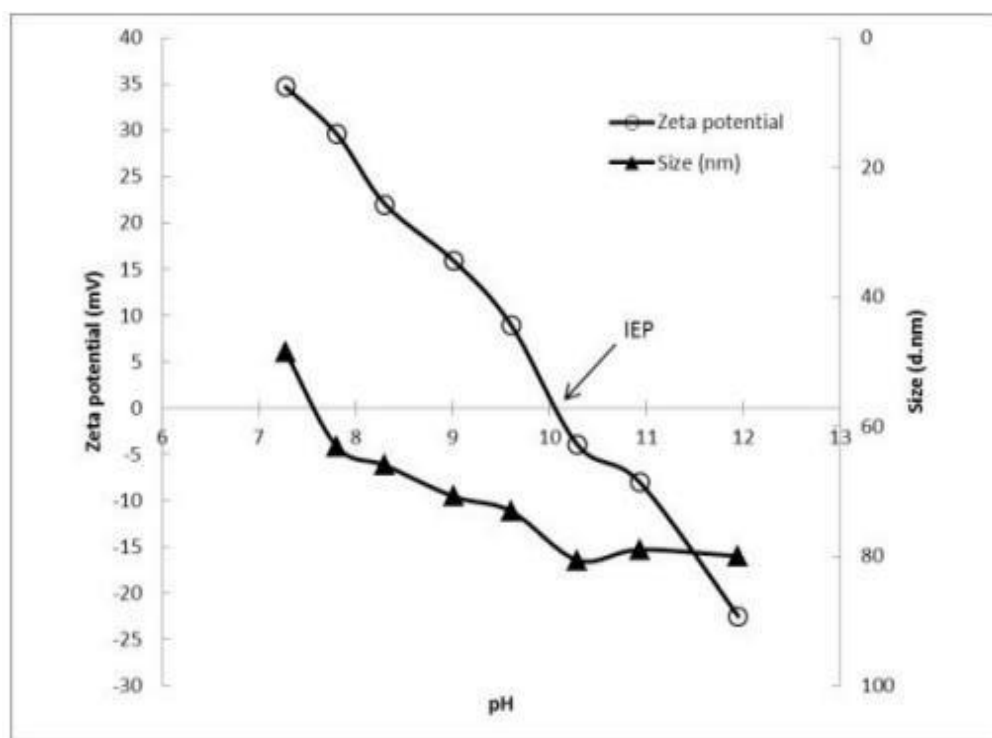


Figure 26. A study of the effect of pH on the size (triangles) and zeta potential (encircled) of ZnO particles

### 6.3. SERS Raman Validation

The study was conducted to know whether these tiny particles would generate any extraneous spectra on Whatman filtration paper coated with zinc nanoparticles that would interfere with subsequent analyses of the drugs. As explained in the methods, water was subsequently added to the particulates and aggregating agent, and SERS spectrum were produced. These blanks provided flat baselines with a significant peak at 200  $\text{cm}^{-1}$  owing to the presence of water; whereas, this peak doesn't interfere with the spectrum limit required for the analysis of drugs (1800 – 200  $\text{cm}^{-1}$ ), as shown in (Figure 27).

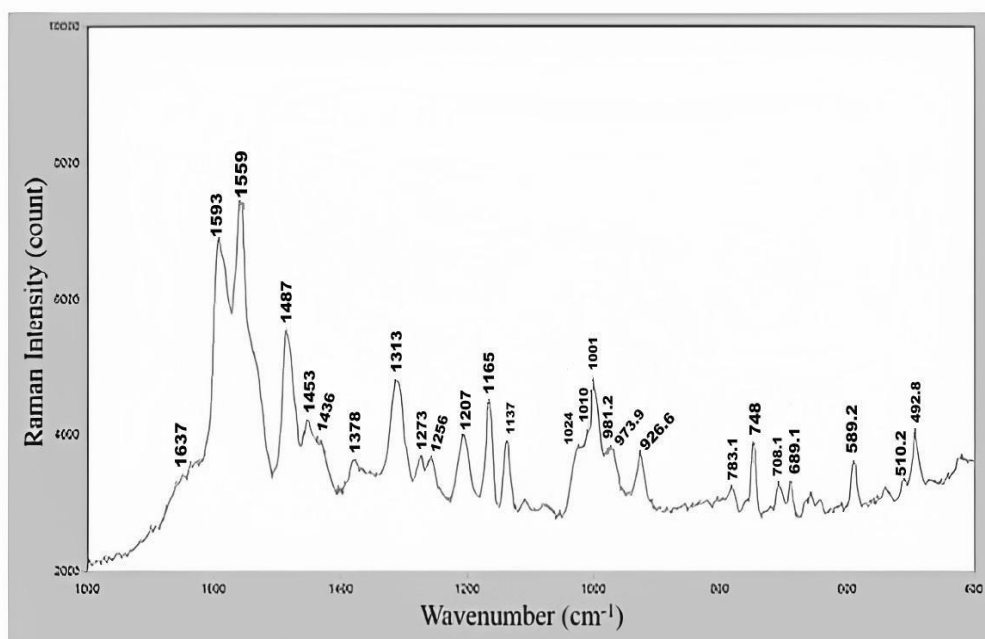


Figure 27. Surface enhanced Raman spectra of reference sample alprazolam

Each benzodiazepine is characterized by a distinct mixture of peaks, as well as other peaks indicated in the table. The wave numbers and relative intensities for these peaks in comparison with the other peaks in the spectral fingerprint each benzodiazepine. The SERS of each benzodiazepine are showing a table giving their wave numbers, relative intensities, and peak identification (Table 7).

Wavenumber (cm <sup>-1</sup> )	Assignment
1593	Arom C≡N str (diazepine ring)
1559	Arom C=C str (a-ring)
1453	Arom C=C str (a-ring)
1436	CH <sub>3</sub> str (N-ring)
1378	In plane CH def (a-ring)
1368	C=N-C sym. str (diazepine ring)
1193	Monosubstituted breathing (b-ring)
1137	Ring breathing (N-ring)
1256	Ring breathing
1207	C <sub>6</sub> H <sub>5</sub> -C vibr. (b-ring)
1165	C-C-N str (diazepine ring)
973.9	CH deformation
783	Ring vibration (b-ring)
589	C-Cl str (a-ring)
510	Out-of-plane CH deformation (b-ring)
492	C-Cl str (a-ring)
432	CH deformation
384	Ring vibration (b-ring)

Table 7: Observed wave numbers (cm<sup>-1</sup>) in the surface enhanced Raman spectra of alprazolam

The drug was extracted from various samples (blood, urine, saliva) using the DSPE method and subsequently evaluated and SERS was obtained. Alprazolam is thought to have two mild to moderate ring breathing peaks at  $1257\text{ cm}^{-1}$  and  $1138\text{ cm}^{-1}$ , which are attributed to the N-ring with three nitrogen atoms. Regardless of class, the majority of benzodiazepines exhibit two main spectrum bands as well as two minor spectrum bands. These bands have a significant correlation with the carbon- nitrogen linkage in the diazepine ring.

The presence of weak bands between  $856$  and  $880\text{ cm}^{-1}$  indicates this stretch. Due to the stretching of nitrogen bonds, between two atoms of carbon there is a final faint peak near  $820\text{ cm}^{-1}$ . The wave numbers for these two conspicuous peaks are listed in Table 8 for the alprazolam analyzed in this study. In addition to providing recognition for each compound at their lowest possible concentration, the optimized ZnO nps generate a linear response. In addition, since our objective was to obtain ultra-detection for use in drug- facilitated assault cases, we aim for a detection limit of  $50\text{ ng/mL}$  or less.

In contrast, the spectral signature of nanocomposite ( $\text{Fe}_3\text{O}_4\text{-ZnO}$ ) exhibits a number of highly significant peaks. Under the same conditions, it was observed that the nanocomposite generated similar alprazolam spectra with variable strengths at different concentrations (Figure 28 a, b, c). Regardless of this, the Raman spectrum of the nanoparticles of zinc was substantially different from those of the nanocomposite material (Table 7). The parameters utilized in these investigations were identical to those used in all other studies. Despite the fact that zinc particles improved the results; the observable detection limits are significantly higher than what is required for drug- facilitated assault-related analysis ( $10\text{ng/mL}$ ).

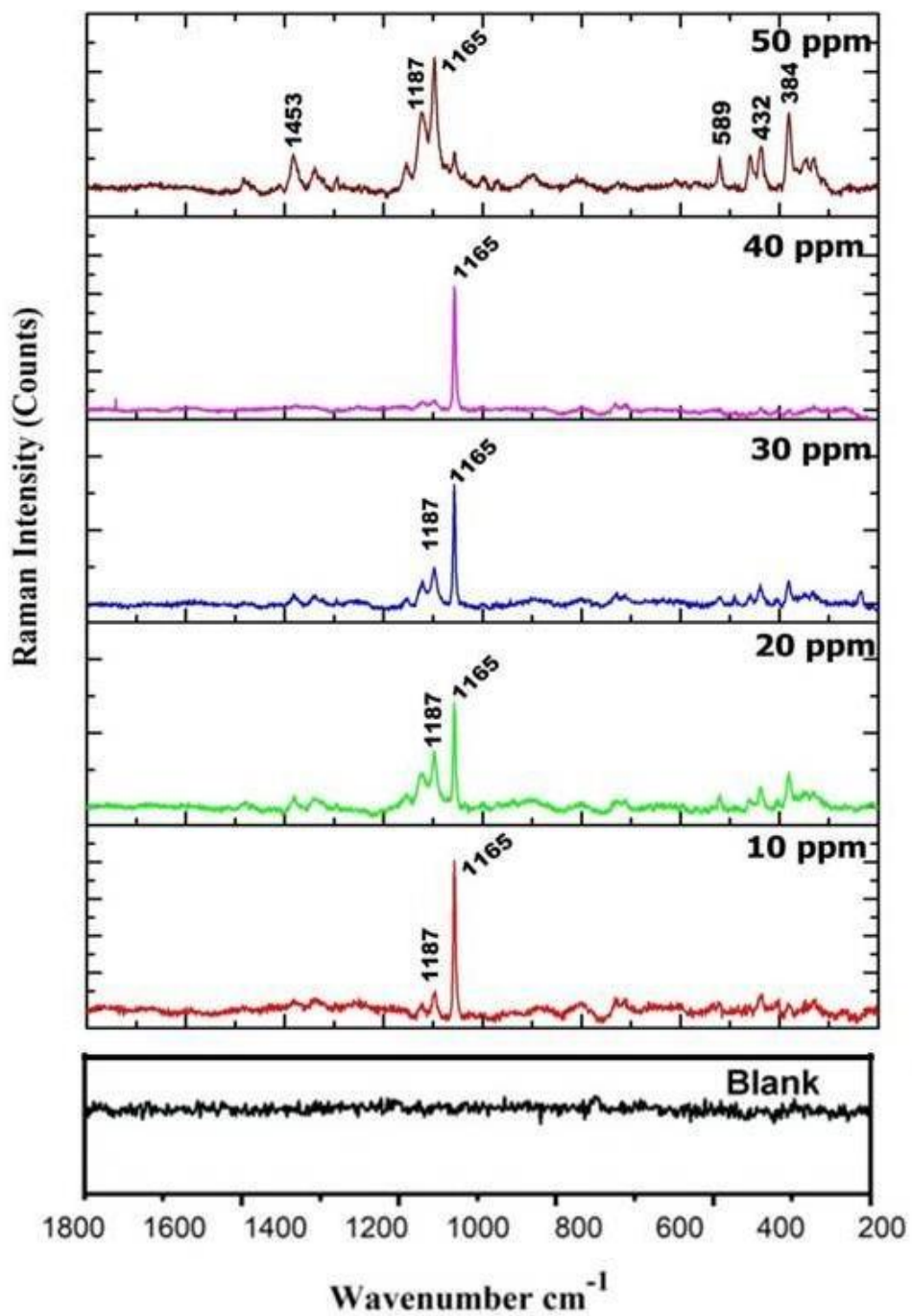


Figure 28 a: SERS signals for 10-50 ppm, alprazolam extracted from blood with ZnO nps preparation techniques and Dispersive solid phase extraction

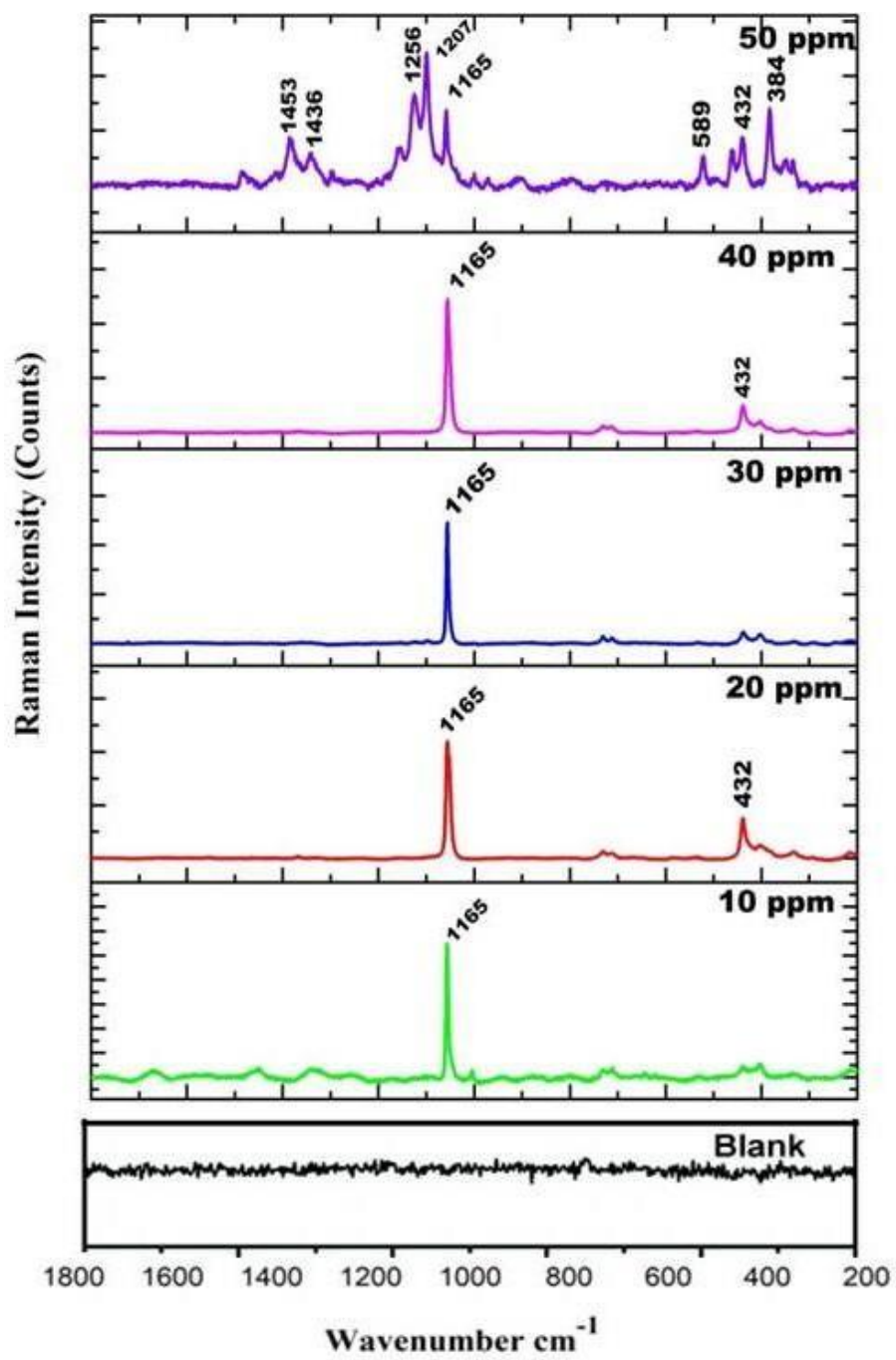


Figure 28 b: SERS signals for 10-50 ppm, alprazolam extracted from saliva with ZnO nps preparation techniques and Dispersive solid phase extraction

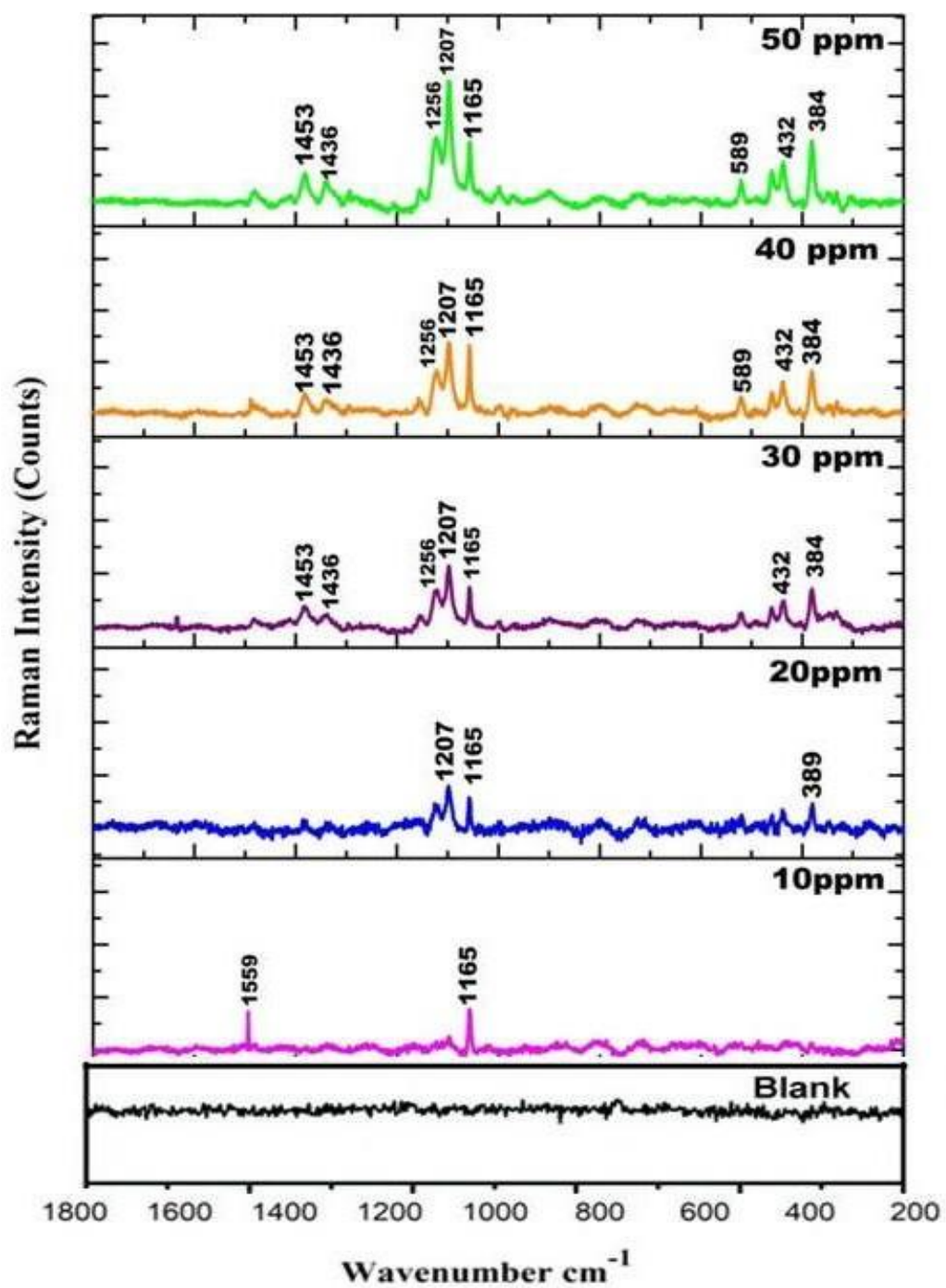


Figure 28 c: SERS signals for 10-50 ppm, alprazolam extracted from urine with ZnO nps preparation techniques and Dispersive solid phase extraction



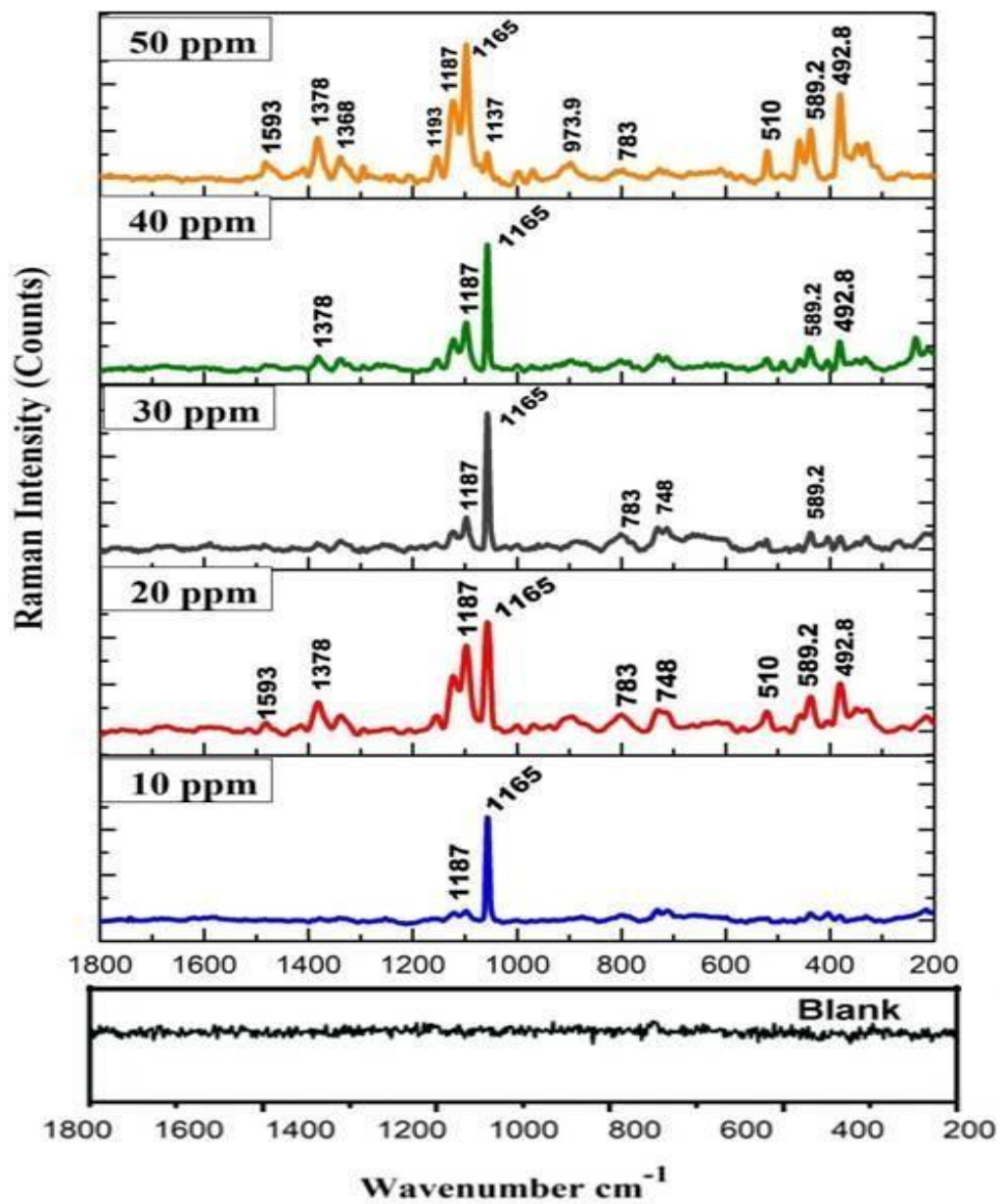


Figure 29 a: SERS signals for 10-50 ppm, alprazolam extracted from blood with ZFNPs preparation techniques and Dispersive solid phase extraction

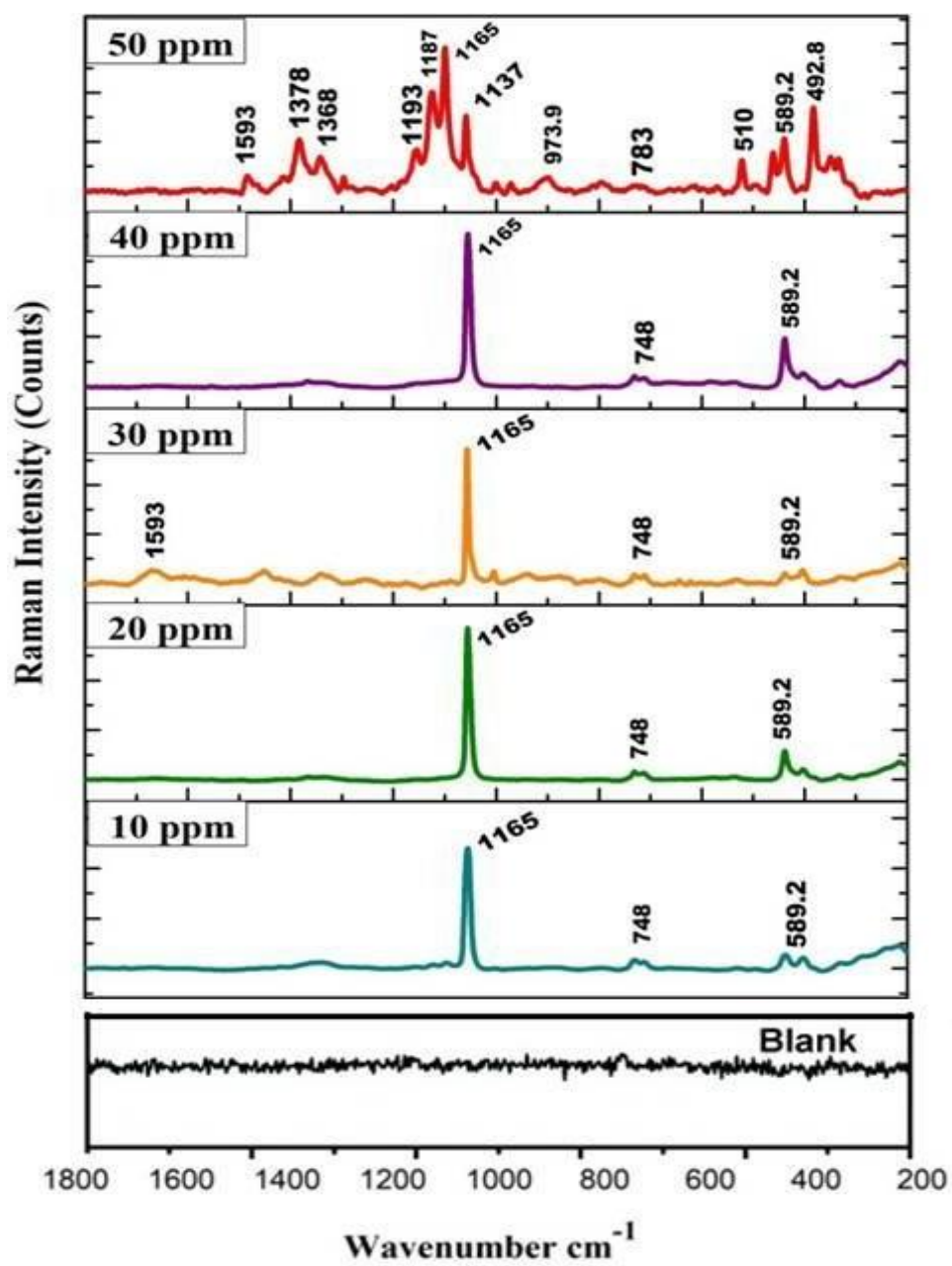


Figure 29 b: SERS signals for 10-50 ppm, alprazolam extracted from saliva with ZFNPs preparation techniques and Dispersive solid phase extraction

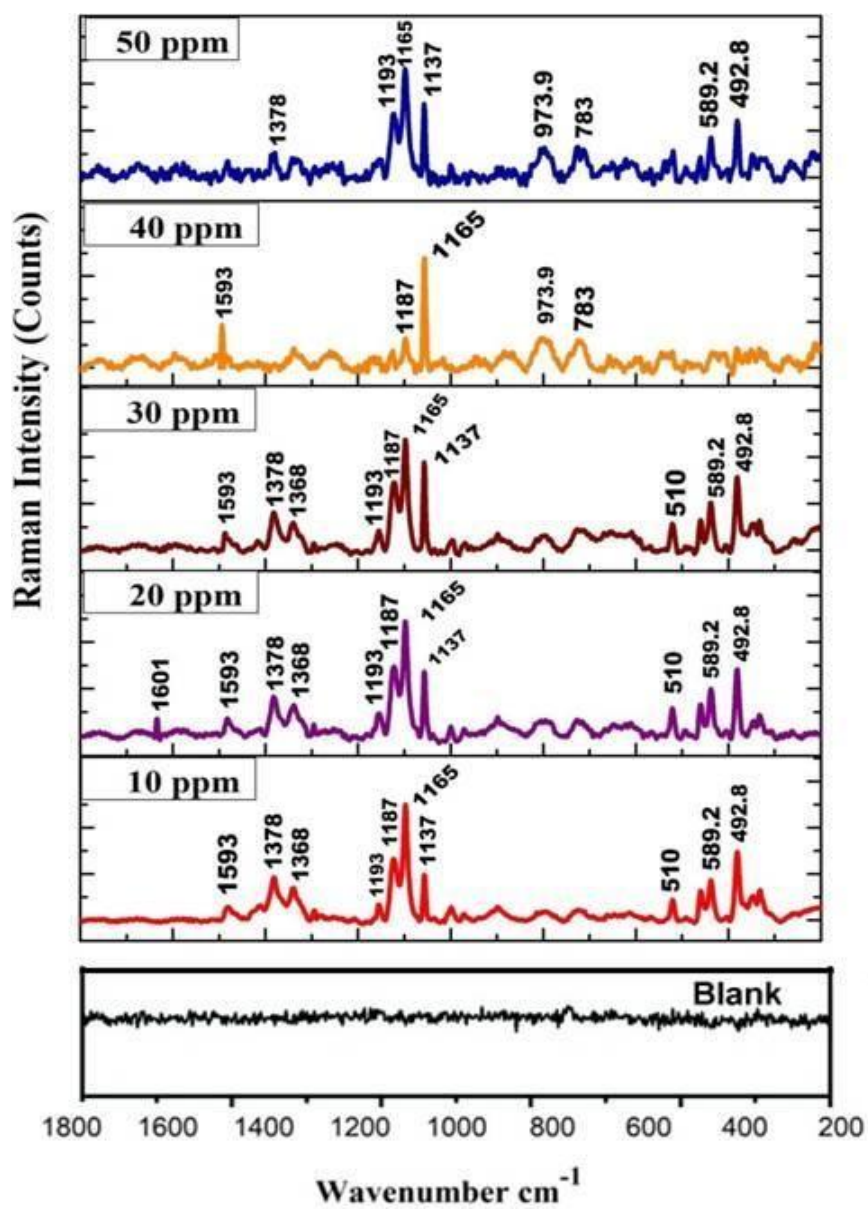


Figure 29 c: SERS signals for 10-50 ppm, alprazolam extracted from urine with ZF nps preparation techniques and Dispersive solid phase extraction

### 6.3.1. Figures of Merit

Using the spectral peaks, calibration curves were generated for every concentration of alprazolam dispersed on coated filter paper (Figures 28 and 29). From the calibration curves for administered drugs, the linear dynamic ranges and LOD have been calculated (Tables 8 and 9). The nanoparticle- induced increase in sensitivity varied depending on the concentration of the drug. Zinc nanoparticles have been displayed to generate the lowest observed and calculated detection limits for a wide variety of drugs (1 - 250 ng/mL). Observing the high intensity peaks at  $1233\text{ cm}^{-1}$ ,  $1613\text{ cm}^{-1}$ ,  $1074\text{ cm}^{-1}$ , and  $1352\text{ cm}^{-1}$ , it is apparent that the two spectra are similar. 10 ng/mL to 50 ng/mL drug concentrations have been successfully introduced into blood, urine, as well as saliva, retrieved by DSPE extraction, in addition, recognized by DSPE extraction using SERS detection.

On the basis of the findings of all three sets of samples, a curve to calibrate the samples was produced. Additionally, it was noted that the cation might add to the enhancement. Blood and urine signals were more intense than mucous signals. This is illustrated in Figure 28. At a concentration of 50 ng/mL, higher signal strength is observed in Urine than in Blood. Consequently, as the quantity of extracted alprazolam increases, the intensity of the spikes produces wider and sharper peaks, whereas it has been observed in figure that even at lesser concentrations, 10 ng/ml, the intensity of urine and blood is significantly higher. Smaller cations enabled nanoparticles to shift closer to one another, thereby increasing the probability of hotspot formation and signal intensity.

### 6.3.2. Linearity curve

To validate the proposed method, linearity, accuracy, LOD and limit of quantification (LOQ) were evaluated under optimum condition (Table 8). Calibration in urine, blood and saliva was performed with increasing concentrations of alprazolam as 10, 20, 30, 40 and 50  $\mu\text{g mL}^{-1}$ . Good linearity was noted in urine and blood through the complete concentration range with the regression coefficient of  $R^2 = 0.9935$  and  $0.9979$  respectively, with LOD and LOQ were  $0.0053$  and  $0.0171 \mu\text{g mL}^{-1}$  respectively in blood samples. Similarly, LOD and LOQ in urine were observed to be  $0.0072$  and  $0.0241 \mu\text{g mL}^{-1}$  respectively.

	Matrices	Dynamic Range (ug/mL)	$R^2$	LOD ( $\mu\text{g mL}^{-1}$ )	LOQ ( $\mu\text{g mL}^{-1}$ )	Slope
<b>ZnO</b>	<b>Blood</b>	10-50	0.9935	0.0053	0.0171	249x+ 630
	<b>Urine</b>	10-50	0.9979	0.0072	0.0241	173x+310
	<b>Saliva</b>	10-50	0.9875	0.0033	0.0152	101x+1530

Matrices	Accuracy % ( $\mu\text{g mL}^{-1}$ )				
	10	20	30	40	50
<b>Saliva</b>	55.02	73.69	81.25	86.04	91.32
<b>Urine</b>	94.5	102	100	104	110
<b>Blood</b>	93.7	99.2	98.6	102	108

Table 8: Analytical attributes of ZnO NPs-DSPE-SERS method for alprazolam

<b>ZF Nano-composite</b>	<b>Matrices</b>	<b>Dynamic Range (<math>\mu\text{g/mL}</math>)</b>	<b>R<sup>2</sup></b>	<b>LOD (<math>\mu\text{g mL}^{-1}</math>)</b>	<b>LOQ (<math>\mu\text{g mL}^{-1}</math>)</b>	<b>Slope</b>
	<b>Blood</b>	10-50	0.9968	0.0063	0.0186	156x+ 1170
	<b>Urine</b>	10-50	0.9989	0.0078	0.0334	225x+1030
	<b>Saliva</b>	10-50	0.9987	0.0030	0.0142	135x+1310

<b>Matrices</b>	<b>Accuracy % (<math>\mu\text{g mL}^{-1}</math>)</b>				
	<b>10</b>	<b>20</b>	<b>30</b>	<b>40</b>	<b>50</b>
<b>Saliva</b>	65.71	76.48	94.28	99.84	100.86
<b>Urine</b>	96.64	106	110	119	120.9
<b>Blood</b>	95.7	99.286	100.6	102.2	116.2

Table 9: Analytical attributes of ZF NPs-DSPE-SERS method for alprazolam

#### **6.4. Discussion**

In last few decades, in every field of science including nanotechnology has become more prevalent, engineering, to medical science, to plant and animal science, environmental science (Calhoun et al., 1996). In the area of science and technology, nanotechnology is making significant contributions. It can be defined as the application of nanotechnology to various disciplines of knowledge and development through the use of nanosized materials that have both high strength and durability (Chen et al., 2011). Nanotechnology is the study and manipulation of matter on an atomic and molecular scale. This has enabled the development of new materials and products, such as nanofibers and nano sensors, having wide range of application, such as medicine to energy. Forensic science and criminal investigation has seen nanotechnology as a key technology over the last couple of decades as it has replaced old laboratory-based evidence analysis with cost-effective and on-the-spot investigations.

In comparison with traditional methods, nanotechnology can provide precise evidence analysis, as it offers an unprecedented level of accuracy and detail, allowing investigators to identify tiny traces of material. In almost every discipline of forensic science, nanotechnology has made a significant contribution (Dåderman and Lidberg, 1999). In the field of chemical and biosensors, nanoscale materials such as gold and silver nanoparticles are being used as chemical and biosensors owing to their chemical structure, optical and colorimetric properties, among many. The nanodimensional semiconductor crystals have been extensively investigated in recent years owing to their novel properties, including controllable particle morphology and size, low toxicity, novel electrical and catalytic abilities (Lanje et al., 2013). In the present study, the metal oxides-based material owing due to the charge, high conductivity, and greater surface retention employed in the application of medical sciences.

The various methods employed for the synthesis via wet precipitation as well hydrothermal route includes the formation of novel nanohybrid and nanocomposite materials (Rouhi et al., 2014), low-temperature synthesis; cost-effective, strong capacity for scale-up (Martínez et al., 2016) and high temperature-sensitive application could be created (Shinde et al., 2012).

Furthermore, hydrothermal synthesis of ZnO nanoparticles critically depends on varied synthesis parameters such as molar concentration (Li et al., 2012; Moazzen et al., 2013) and pH value (Wahid et al., 2013) of precursors, hydrothermal temperature (Bai and Wu, 2011) and calcination temperature (Bindu and Thomas, 2014) etc. Therefore, in our study we observed for the formation of highly crystalline the process is dependent on pH value which effects the morphology of ZnO nanoparticles. The hexagonal shape of the wurtzite structure was the source of the diffraction peak patterns of the ZnO phase (Rosi and Mirkin, 2005; Rastogi and Arunachalam, 2011; Wang et al., 2013). Similar results were shown by (Sawai et al., 1998; Sabir et al., 2014; Shah et al., 2014) had similarly identified similar dispersion peaks. It had been proved from the results that ZNH and ZNHH contaminants originated from the first ZNH precursor and were trapped in the crystals formed as a result of the centrifuged and wash processes.

On the other hand, the characteristic peaks of the ZnO phase were distinct, narrow and sharp, which suggested their crystalline structure. Thus, the results revealed that when an increase the pH of sample solutions does not affect the phase but size decreases. While in the preparation of nanocomposite the variation in route of synthesis used and diffraction peaks were observed. In earlier studies, it was also noted that similar diffraction peaks existed the Fe<sub>3</sub>O<sub>4</sub> phase was characterized by peaks at 24.10, 33.10, 40.80, and 50.15 that correlated to (012), (104), (440), and (024) (Aliahmad and Nasiri Moghaddam 2013; Han et al., 2014).

For the improvement of ZnO nanoparticles properties, it would be a suitable choice as a reinforced phase. Because of this, the combination of these two materials (Fe<sub>3</sub>O<sub>4</sub> and ZnO) can be used in a variety of nanotechnology applications. It is possible to prepare ZF nanocomposite by a variety of methods, including co-precipitation, solvothermal synthesis, and deposition. As a result of its cost effectiveness, ease of handling, and control capabilities, in this investigation, the sol-gel technique was employed (Jeong et al., 2005). Magnetite distinctive diffraction peaks were found to have a reverse cubic spinel arrangement and a 19 nm crystal size. The ZF sample's XRD analysis revealed all of the aforementioned



peaks, which demonstrated the presence of both ZnO and Fe<sub>3</sub>O<sub>4</sub> in the original material. The similar results were observed where no peaks of impurity of any substance indicate that synthesis is crystalline and reduced particles size.

It is evident that the nano crystallite sizes are higher than those found using the (XRD) technique range between 40 and 50 nm. Several crystal particles can also appear in scans of SEM because of different index millers or phases of crystallites. XRD patterns and FESEM images indicate that Fe<sub>3</sub>O<sub>4</sub> nano crystallite with quasi-amorphous structure performs better with regard to tissue properties due to morphological changes. These reflections may easily be attributed to the lattice structures of Fe<sub>3</sub>O<sub>4</sub> and Zn/ Fe<sub>3</sub>O<sub>4</sub> based on the XRD study of the nanopowders (PDF 03-065-3107, a = 8.39Å and 8.44Å, respectively). The high-resolution image could not distinguish these oxides because they are structurally similar. However, this image analyzing technique indicates that these oxide composite nanoparticles lack content of Fe<sub>3</sub>O<sub>4</sub> and have high crystallinity. Therefore, the size of nanocrystallites with smaller particle size values of the nanocrystallites significantly influences crystallinity structure as well as in particle size (Beitollahi et al., 2008).

In earlier study described ZnO/TiO<sub>2</sub>/SiO<sub>2</sub> composites as (6:3:1) forming hexagonal phases with wurtzite morphology because ZnO is higher than Fe<sub>3</sub>O<sub>4</sub> (Chinnaraj et al., 2015). The growth pattern of ZnO crystals, as suggested by various crystallographic models (Rietveld, Scherrer, and WH-ISM) agreed with the change in crystal size, as suggested by FWHM interpretation. The ZnO crystals in all nanopowders were subjected to tensile strain. In the XRD spectra, of coated strips we have concentrated on identifying main components such as cellulose and CaCO<sub>3</sub> for the sake of simplicity. The XRD spectra of plain paper revealed peaks that correspond to cellulose (JCPDS 03-0289) along with CaCO<sub>3</sub> (JCPDS 85-1108). The peaks in Figure 10 (blank paper) without an asterisk correspond to cellulose, while those with an asterisk (labeled "CaCO<sub>3</sub>") correspond to CaCO<sub>3</sub>. The pattern of XRD images obtained from paper coated with ZnO nanoparticles (Fig. 23c) revealed peaks with 2θ values of 31.7 (100), 34.4 (002), 36.2 (101), 47.5 (102), 56.6 (110), 62.8 (103), 66.4 (200), 67.9 (112), and 69.1 (201) characteristics of ZnO (indicated with an asterisk and labeled "ZnO") for which there was substantial agreement.

The phenomenon can be ascribed to the shapeless nature of cellulose paper, as documented in sources (Prabhu et al., 2014). The congruence between the  $2\theta$  and (hkl) values and the established data on PDF card 01-074-9940 (International Centre for Diffraction Data, 2013) is notable. The wurtzite hexagonal lattice arrangement of the ZnO-NPs (Katoch et al., 2021) was verified through the confirmation of crystal elements and peak positions. The diffraction pattern acquired from the ZnO-NPs-coated paper indicates the existence of ZnO-NPs that possess a high degree of crystallinity. The intensity of the cellulose peak is minimal owing to the intense ZnO peaks present in the ZnO-NPs that embellish the paper. The absence of any diffraction peak other than ZnO and filtration paper indicates the high purity of the ZnO-NPs-coated WF paper.

To reveal the molecular structure FTIR spectra of synthesized nanopowders shows, various peaks observed asymmetric vibrations at  $1490\text{cm}^{-1}$ ,  $1550\text{cm}^{-1}$ , and  $1640\text{cm}^{-1}$  were attributed to carboxylic acid (C=O) ions. Carbon had been speculated to come from the atmosphere and entrapped in ZnO crystal structure during stirring and ageing process. The similar frequencies for metal oxides are also shown by other respective metal oxides (Li et al., 2008; Sinha et al., 2011; Leroy et al., 2011; Suntako, 2015; Shanker et al., 2016; 220-224). Thus, both phase and molecular structures revealed by XRD and FTIR analysis corroborated formation of ZnO crystals in nanopowders along with some allied impurities. The FTIR spectra of ZnO and  $\text{Fe}_3\text{O}_4$  nanocomposites with wave numbers ranging from  $400$  to  $4000\text{cm}^{-1}$ . Using this characterization, the functional groups that are inorganic as well as bonding of ZnO/ $\text{Fe}_3\text{O}_4$  nanocomposites that were studied. The  $3430$ ,  $1647$ , and  $1547\text{cm}^{-1}$  absorbance peaks, which indicate the mode of vibrating of the O-H bond produced by vibrations of water absorbance and hydroxyl surface, are used to demonstrate the organic bond of the material of ZnO/ $\text{Fe}_3\text{O}_4$  nanocomposite.

In a study  $\text{Fe}_3\text{O}_4$ -ZnO composites were synthesized by co precipitation with ratios of 1:4 and methylene blue degradation efficiency of 97.9%. It was concluded that the differences in the synthesis methods have influenced the activity of the photo catalyst (Lincot and Hodes, 2006; Chiu et al., 2010; Bahari and Gholipur, 2013). This situation is connected to research that showed O-H bond vibrations at wavenumbers of  $3500\text{cm}^{-1}$  and  $1628\text{cm}^{-1}$  (Hornyak et al., 2018). Additionally, the H-O-H vibration could be picked up at  $1630\text{cm}^{-1}$  (Vinogradov and Wei, 2012).

At wavenumbers of roughly  $1384\text{ cm}^{-1}$  and  $1630\text{ cm}^{-1}$ , the carboxyl bond stretch of zinc vibrated. Additionally, asymmetric and symmetric iron's carboxyl bond stretch ( $\text{C}=\text{O}$ ) vibrated between  $1393\text{ cm}^{-1}$  and  $1587\text{ cm}^{-1}$  (Zhou et al., 2006; Wan et al., 2009; Ahadpour and Jafari, 2014).

As similar result has been observed revealed the stretch vibrations of this  $\text{C}=\text{O}$  bond first appeared as a result of reactive carbon during the process of synthesis. For the comprehensive study, observed at  $526\text{ cm}^{-1}$  of  $\text{Zn}/\text{Fe}_3\text{O}_4$  served as a defining feature of its shape. The  $\text{Zn}-\text{O}$  bond's vibration was produced around  $426-440\text{ cm}^{-1}$  and  $453\text{ cm}^{-1}$  (Gordon et al., 2011). The spectral regions ranging from  $900$  to  $1300\text{ cm}^{-1}$  and  $1300$  to  $1500\text{ cm}^{-1}$  are indicative of the vibration modes associated with  $\text{C}-\text{O}$  and  $\text{C}-\text{H}$  bonds in cellulose. The absorption band observed at  $1640\text{ cm}^{-1}$  can be ascribed to the presence of absorbed water, as previously reported in literature (Ghule et al., 2006; Wasim et al., 2020).

The faint broad band observed at  $732\text{ cm}^{-1}$  could potentially be attributed to the overlap of the bands corresponding to the 1b and 1a stages of cellulose, which are typically identified at  $710$  and  $750\text{ cm}^{-1}$ . This observation suggests that they may be present in the composition of the paper as a composite. The spectral indicates spanning from  $900$  to  $1300\text{ cm}^{-1}$  and  $1300$  to  $1500\text{ cm}^{-1}$  are indicative of the  $\text{C}-\text{O}$  and  $\text{C}-\text{H}$  oscillations of cellulose, respectively (Sawai, 2003; Vafaei and Ghamsari, 2007). It had already been attributed to the fact that the smaller the particle size, greater is their surface area. Interestingly, the surface area of synthesized nanoparticles was greater than the results reported elsewhere (Baruah and Dutta 2009; Wahab et al., 2007; Singh et al., 2016). Notably, particles with large particle surface area and porosity volume the drug delivery and other similar therapeutic applications requiring superior adsorption capacity. The pH dependent nanopowders differ from each other shows the agglomeration and smaller particle size usually agreement in calculation the particle size through different models.

For the concept of textural attributes, it is necessary to study the morphological and elemental structure of synthesized and coated materials. Particles of vivid shapes and size were present in ZnO at pH 9 nano powder. Bigger particles were an agglomeration of numerous smaller particles. Agglomeration of nanoparticles has been a common feature owing to their high surface energy. Particles of vivid shapes and size were present in ZnO nano powder. Bigger particles were an agglomeration of numerous smaller particles. Agglomeration of nanoparticles has been a common feature owing to their high surface energy. The weight and atomic ratio of Zn:O were 4.69 and 1.14, respectively, which are agreement with the results reported (Padmavathy and Vijayaraghavan et al., 2008; Lipovsky et al., 2011). Also, through HRTEM conferment the particle agglomeration and found to have irregular and vivid shape which is similarly shows in the previous study (Singh et al., 2016).

The SAED pattern which is used to calculate the d-spacing and lattice structure also confirm the polycrystalline structure of nanoparticles the spots in the pattern of hexagonal indicates the crystalline composition. In case of ZF nanocomposites it was evident from the SEM images that 50–100 nm amorphous branches on Fe<sub>3</sub>O<sub>4</sub> structures with 10–20 nm irregular sphere ZnO NPs surrounded them. The findings of the hydrothermally synthesized ZnO/ Fe<sub>3</sub>O<sub>4</sub> nanostructures' EDS-spot and EDS-mapping measurements are depicted in Figure 19 respectively. The acquired EDS spectra revealed Fe, Zn, and O. Prior to the SEM investigations, the samples were exposed to Au sputter a typical practice employed to enhance the SEM's performance. This procedure will result in a distinct Au peak appearing in the EDS spectra. This peak is unrelated to the structure of the nanoparticles. Although they were actually 62.7, 16.8, and 19.4 in the ZnO/Fe<sub>3</sub>O<sub>4</sub> (1:1) nanostructure, the proportions of Fe, Zn, and O components were 38.9, 35.4, and 23.5, respectively. The inclusion of iron oxide in various weight ratios nearly increased the structure's Fe ratio.

Additionally, the presence and chemical makeup of the Fe, Zn, and O components in the composite ZnO/ Fe<sub>3</sub>O<sub>4</sub> framework affect the color intensities visible in the EDS-mapping images. Because of the quasi-amorphous structure of the Fe<sub>3</sub>O<sub>4</sub> nano crystallite, which is consistent with the XRD patterns and FESEM images, the

spherical ZF nanocomposite has a superior effect on tissue characteristics (Uvarov et al., 2007; Prabhu et al., 2014).

Further TEM were used to evaluate the structural attributes of nanocomposites which confirm the binding of nanocomposites is firmly done in the matrix. Regardless of whether the pH was below or above p<sub>Hpzc</sub>, hydroxyl groups on Fe OH surfaces protonate or deprotonate to form FeOH<sup>2+</sup> or FeO functional groups. It was p<sub>Hpzc</sub> and pH of solution that maintained equilibrium between protonation and deprotonation. Adsorption was easier between the pH range of 3.0 and 4.0 when the zeta potential was at its lowest point (Franklin et al., 2007). Using the Smoluchowski equation, the zeta potential was calculated from the mobility of electrophoretic (Win and Feng, 2005). Started the titration process with the pH at 7.3, zeta potential at +35 mV, and diameter at roughly 50 nm as similarly it was observed in the previous study (Bahtiar et al., 2019).

A larger particle size and a lower zeta potential were produced by the addition of NaOH. The highest size was found to occur close to the isoelectric point at pH 10.2. To put it another way, maintaining a stable pH for ZnO suspensions requires knowledge of pH and its ability to be modified (Siregar et al., 2020). Due to the excellent strength of the fibers, ultrasonic irradiation does not adversely affect the structure or network, porosity of the fibers. Despite the same pore size (5 μm), Whatman paper (WF) is different from other filter papers because of its thin fibers and extensive network. Magnified SEM pictures of the ZnO nanoparticle-coated paper surface were taken to compare the particle size effect of sonication. It appears that the particle size is not significantly different after 30 minutes, except the ZnO nanoparticles are tightly packed afterward, presumably due to collapse of the nanoparticles.

Therefore, it can be evident from the characterization techniques that highly crystalline structure was prepared and utilized as a useful substrate in SERS analysis. For the optimisation of nanoparticles for the uses in SERS, alprazolam was utilised as this drug is water-soluble and does not require organic solvents which show interference for dissolution. Alprazolam drug samples were dissolved to nanoparticles decorated with ZnO and coated on filter paper. However, the Raman spectra generated by the Zinc nps were significantly different from those produced when drug

was extracted from matrices. This is presumably the result of various interactions among the drug and particles. Due to the drastically diminished amounts of peaks in the spectra, it is probable that the drug is binding to the outermost layer of the zinc particles while being in close range to the filter paper surface. The aromatic extension of the carbon-nitrogen double bond results in a peak between 1590 and 1613  $\text{cm}^{-1}$  that is strong to very strong.

This peak alters due to the close proximity of components at the ortho position of the freely rotating b-ring. As a consequence of the carbon-to-carbon-to-nitrogen exertion, the second band has an intensity between 1166 and 1175  $\text{cm}^{-1}$  that ranges from moderate to very strong. Due to the significantly diminished number of peaks in the zinc spectra, it is likely that the drug is binding to the surface of the zinc particles and is only in very close proximity to the surface of the Iron zinc nanoparticles as a result of this binding. By investigating the range of visible detection for the concentrations that were prepared, it was also determined if SERS spectra could be produced below the high concentrations prepared.

The nanoparticles did not generate a SERS spectrum for alprazolam at concentrations below 50,000 ng/mL, regardless of the composite's concentration. However, a significant intensity was observed. Despite the fact that the gold particles formed spectra at all ratios examined, it has been obtained spectra for these particles at concentrations as low as 50 ng/mL. The objective of this technique is to be able to recognize benzodiazepines at concentrations below 10 ng/mL in order to detect their existence. In light of this, it has been found that gold nanoparticles are the optimal colloids for use in the subsequent investigation of benzodiazepines, as they are the finest colloids for this analysis. This may be due to the simple fact that the substance interacts differently with the particles than it does on its own. According to the wavelength of incident energy, a molecule on the surface of metal experiences a local field intensity improvement factor (LFIEF), which plays a crucial role in the SERS mechanism. On zinc spheres, the greatest effects of local field intensity enhancement occur more frequently in extremely narrow wavelength ranges, with the maximum local field intensity enhancement factor appearing at wavelengths of approximately 350 nanometers. Due to the paucity of local field intensity, there is virtually no enhancement factor at 785 nm. Nanocomposite, on the other hand, generates a high local field intensity enhancement factor over a broad wavelength range, with a maximum around 550 nm.

At 785 nm, the local field enhancement factor is approximately 11.31. Here, we demonstrate that zinc and nanocomposite adhere to theory, whereas Whatman filter paper is the optimal substrate for incident wavelengths of 785 nm. Without interference, benzodiazepines can also be dispersed through methanol solutions up to 10%. When a substance is dissolved in methanol, a 10% concentration of methanol invades its SERS spectrum, causing spectral peaks to become visible. The dynamic range of all three substances was between 0.98 and 0.92, with detection limits that ranged from 2 to 10 ng/mL, which was lower than our target of 50 ng/mL. This enhanced SERS technique can detect benzodiazepines obtained from urine.

Through all conditions of biologic fluids, their detection limits varied between 0.5 to 127ng/mL, with nanocomposite spiked with urine demonstrating the maximum signal intensities. Except for blood and saliva, all compounds tested were traceable at concentrations below 50ng/mL. The present work has demonstrated the importance of selecting an aggregation agent appropriately for determining the presence of SERS in suspension. The smaller the nanoparticles size, the greater the likelihood that the nanoparticles will move closer together, resulting in the formation of hotspots and an increase in signal intensity.

At a concentration of 50 ng/mL, the signal intensity is greater for urine and blood than for saliva. It has been reported that benzodiazepines are lipid-soluble; the liver must convert them to a water-soluble form before they can be released in the urine. Blood and breath offer the earliest and quickest detection opportunities for drugs because they reveal the current serum concentrations of a substance that has been consumed.

The substance can however be detected in sweat and saliva after several hours. The detection window for narcotics in urine extends from one day to several weeks after consumption. By altering the ionic strength of the ambient solution and the surface charge present on the substrate, the presence of metal oxide also contributes to an increase in signal intensity. This effect has been observed in previous studies (Vafaei and Ghamsari, 2007; Leopold et al., 2004) and may be attributable to the size of the cation; however, it has not been studied as extensively as the influence of anions on the SERS signal.

**CHAPTER 7**  
**CONCLUSION**



## 7. Conclusion

The ZnO nanoparticles were successfully derived from ZnO solid solutions with different pH values. A facile hydrothermal route was employed to prepare the ZnO nanoparticles. The pH variation had little effect on phase and molecular structures of ZnO nanoparticles. On the other hand, pH variation had a significant effect on crystal structure parameters like weight fraction of ZnO nanoparticles constituent stages lattice structure factors, crystal size, stress in the lattice, and crystallisation. Results implied that the pH value of nine produced the highest concentration of ZnO phase with stoichiometric lattice parameters, nanodimensional crystal size and highest crystallinity. Moreover, ZnO nanoparticles were irregular in shape with an average size of  $45 \pm 9$  nm. The particle sizes calculated using Rietveld, Scherrer, WH-ISM, FESEM and HRTEM models were close to each other.

All nanoparticles exhibited a mesoporous structure with superior surface area and porosity. The variation of pH had a significant effect on particle size, and therefore, particle surface area attribute was also dependent on their pH condition during synthesis. Interestingly, the particle surface area of synthesized nanoparticles was superior to the results reported in the literature. Thus, due to the amalgamation of high crystalline, mesoporous structure, and large particle surface area, the resultant nanoparticles can be employed for several multifunctional therapeutic applications, including drug delivery agents. A study was conducted in this study to examine the structural, morphological, elemental, optical, and magnetic properties of hydrothermally produced ZnO/ Fe<sub>3</sub>O<sub>4</sub>-NPs nanostructures.

Successfully fabricated ZF nanostructures using hydrothermal methods. We analyzed ZnO and Fe<sub>3</sub>O<sub>4</sub>-NPs structures using structural characterization, and we did not detect any impurities. Stability of ZnO suspensions can be influenced in several ways. Particles coagulated by dispersants, pH, and/or additional chemicals are affected by these factors. The stability of suspensions can be monitored by measuring the zeta potential. In the morphological images, the presence of composite nanostructures was revealed by both SEM and TEM microscopy. Zeta potential measurements can be used to assess the stability of suspensions. The morphological pictures of the composite nanostructures were detected by microscopy. The stability of ZnO suspensions can be impacted by a number of variables. The pH, kind of dispersant,

and other compounds present all have an impact on how well particles coagulate. By calculating the particles of zeta potential, one can determine a solution's stability.

The dispersion formulation can be optimized to provide the highest level of stability. In addition, it can be used to track how the particle size and charge vary over time. It's crucial to make sure the suspension can be used for the intended purpose in order to increase stability. Changes in the suspension that would suggest a need for extra treatment, such as a pH adjustment or the addition of more dispersants, may also be an indication. The identification of drug blood concentration is a current and ongoing research topic; therefore, efforts should be made to improve the procedure for accurately determining drug blood concentration in actual samples. The ultrasensitive detection of low-quantity medications is essential to personalized cancer therapy. This thesis goal is to provide a preliminary evaluation of the use of surface enhanced Raman spectroscopy with hazardous materials. SERS analysis of a wide range of clinically important urine samples demonstrated its applicability and resistance to false positives, which is critical for law enforcement applications. Furthermore, this small kit is simpler to operate than typical analytical equipment.

Alprazolam, a medicine that has been linked to sexual assaults made possible by drugs, has a SERS range. To produce consistent Raman signal enhancement and, therefore, ensure precision and reproducibility in clinical applications, a very regular SERS substrate is essential. This method enables the identification of pharmaceuticals at trace quantities in aqueous solutions since enhancement levels are several orders of magnitude higher than those achieved with ordinary Raman spectroscopy. Owing to the substantial research being done on developing materials for the construction of active SERS substrates, merging technologies, and building the Raman spectra database, anticipate a bright future for the use of SERS in the detection of medicines, proteins, and DNA.

Additionally, this technology overcomes some of the drawbacks of some of the current immunoassay techniques by offering lower detection limits and precise spectral-based findings. SERS utility and resilience to false positives were proven by its analysis of clinically meaningful urine samples, which is crucial for law enforcement applications. In addition, this small kit is easier to use than most analytical tools. The prior research assessed the kit's dual-analyte detection capabilities, practicability, reproducibility, consistency, and sensitivity. These

investigations also showed how well our portable kit can separate and identify amphetamines in actual human urine samples. This approach yielded SERS frequencies and intensities that were repeatable over a wide range of concentrations. The previous experiments, which evaluated sensitivity, repeatability, uniformity, practicability, and dual-analyte detection, demonstrate our portable kit's remarkable ability to distinguish and detect amphetamines in real-world human urine samples.

Among all aggregating agents tested with detection limits, ZnO nps generated the strongest SERS signals. The findings of this study highlight the significance of carefully choosing an aggregating agent when identifying SERS in suspension. It has been demonstrated that DSPE combined with surface enhanced Raman spectroscopy is an efficient method for screening for alprazolam in various matrices and at concentrations relevant to drug-facilitated sexual assaults. Additionally, this method gives scientists spectral data rather than just data about a drug class or class of pharmaceuticals, giving them insight into the particular chemical discovered. SERS analysis of clinically significant urine samples proved helpful and resistant to false positives, which is critical for law enforcement applications. This tiny kit is also easier to use than most analytical tools. Previous studies, which assessed the kit's sensitivity, reproducibility, uniformity, practicability, and dual-analyte detection capabilities, showed that our portable kit can separate and identify amphetamines in real human urine samples. This sensing kit has the potential for rapid and on-the-spot quantitative sensing, or ultra trace, in a range of fields, including public safety and healthcare.

# **CHAPTER 8**

# **REFERENCES**

## References

- Aardema, M. J., & MacGregor, J. T. (2003). Toxicology and genetic toxicology in the new era of toxicogenomics: impact of -omics technologies. *Toxicogenomics*, 171-193.
- Abdali, S., Johannessen, C., Nygaard, J., & Nørbygaard, T. (2007). Resonance surface enhanced Raman optical activity of myoglobin as a result of optimized resonance surface enhanced Raman scattering conditions. *Journal of physics: condensed matter*, 19(28), 285205
- Ahadpour Shal, A., & Jafari, A. (2014). Study of structural and magnetic properties of superparamagnetic Fe<sub>3</sub>O<sub>4</sub>-ZnO core-shell nanoparticles. *Journal of Superconductivity and Novel Magnetism*, 27, 1531-1538.
- Alessandri, I., & Lombardi, J. R. (2020). surface enhanced Raman scattering: new theoretical approaches, materials and strategies. *Frontiers in Chemistry*, 8, 63.
- Al-Hada, N. M., Saion, E. B., Shaari, A. H., Kamarudin, M. A., Flaifel, M. H., Ahmad, S. H., & Gene, S. A. (2014). A facile thermal- treatment route to synthesize ZnO nanosheets and effect of calcination temperature. *PloS one*, 9(8), e103134.
- Alves, I. M., Melo, N. O., Marinho, P. A., & Almeida, M. R. (2020). Liquid- liquid extraction-assisted SERS-based detection of clonazepam in spiked drinks. *Vibrational Spectroscopy*, 110, 103112.
- Alves, I. M., Melo, N. O., Marinho, P. A., & Almeida, M. R. (2020). Liquid- liquid extraction-assisted SERS-based detection of clonazepam in spiked drinks. *Vibrational Spectroscopy*, 110, 103112.
- Anderson, B., Peyster, A. D., Gad, S. C., Hakkinen, P. J., & Kamrin, M. (2005). *Encyclopedia of toxicology*. Academic Press.
- Arendt, R. M., Greenblatt, D. J., Liebisch, D. C., Luu, M. D., & Paul, S. M. (1987). Determinants of benzodiazepine brain uptake: lipophilicity versus binding affinity. *Psychopharmacology*, 93, 72-76.

- Ashton, H. (1987). Benzodiazepine withdrawal: outcome in 50 patients. *British journal of addiction*, 82(6), 665-671.
- Bahari, A., & Gholipur, R. (2013). Electrical and optical properties of  $Zr_x La_{1-x} O_y$  nanocrystallites as an advanced dielectric for the next FET devices. *Journal of Materials Science: Materials in Electronics*, 24, 674-686.
- Bahari, A., & Ramzannejad, A. (2012). Nanostructural properties of  $La_2 O_3/HfO_2$  gate dielectrics. *international journal of modern physics b*, 26(14), 1250080.
- Bahari, A., Babaeipour, M., & Soltani, B. (2016). Theoretical investigation of quantum tunneling and self-energy phenomena in  $Al_2 O_3/PVP$  nanocomposite. *Journal of Materials Science: Materials in Electronics*, 27, 2131-2137.
- Bahtiar, S., Taufiq, A., Utomo, J., & Hidayat, N. (2019, April). Structural characterizations of magnetite/zinc oxide nanocomposites prepared by co-precipitation method. In *IOP Conference Series: Materials Science and Engineering* (Vol. 515, No. 1, p. 012076). IOP Publishing.
- Bai, S. N., & Wu, S. C. (2011). Synthesis of ZnO nanowires by the hydrothermal method, using sol-gel prepared ZnO seed films. *Journal of Materials Science: Materials in Electronics*, 22, 339-344.
- Baruah, S., & Dutta, J. (2009). Hydrothermal growth of ZnO nanostructures. *Science and technology of advanced materials*.
- Baruah, S., & Dutta, J. (2009). pH-dependent growth of zinc oxide nanorods. *Journal of Crystal Growth*, 311(8), 2549-2554.
- Baruah, S., Thanachayanont, C., & Dutta, J. (2008). Growth of ZnO nanowires on nonwoven polyethylene fibers. *Science and Technology of Advanced Materials*.
- Beitollahi, H., Karimi- Maleh, H., & Khabazzadeh, H. (2008). Nanomolar and selective determination of epinephrine in the presence of norepinephrine using carbon paste electrode modified with carbon nanotubes and novel 2-(4-oxo-3- phenyl-3, 4-dihydro-quinazoliny)-N'-phenyl- hydrazinecarbothioamide. *Analytical Chemistry*, 80(24), 9848-9851.

Bell, S. E., Beattie, J. R., McGarvey, J. J., Peters, K. L., Sirimuthu, N. M. S., & Speers, S. J. (2004). Development of sampling methods for Raman analysis of solid dosage forms of therapeutic and illicit drugs. *Journal of Raman spectroscopy*, 35(5), 409- 417.

Berro, L. F., & Rowlett, J. K. (2020). GABAA receptor subtypes and the reinforcing effects of benzodiazepines in remifentanyl-experienced Rhesus monkeys. *Drug and alcohol dependence*, 213, 108076.

Bharti, J., Kumar, S. S., Kumar, V., Kumar, A., & Kumar, D. (2022). A review on the capability of zinc oxide and iron oxides nanomaterials, as a water decontaminating agent: Adsorption and photocatalysis. *Applied Water Science*, 12(3), 46.

Bindu, P., & Thomas, S. (2014). Estimation of lattice strain in ZnO nanoparticles: X-ray peak profile analysis. *Journal of Theoretical and Applied Physics*, 8, 123-134.

Blanco, C., Han, B., Jones, C. M., Johnson, K., & Compton, W. M. (2018). Prevalence and correlates of benzodiazepine use, misuse, and use disorders among adults in the United States. *The Journal of clinical psychiatry*, 79(6), 1865.

Blanco, C., Rafful, C., Wall, M. M., Jin, C. J., Kerridge, B., & Schwartz, R. P. (2013). The latent structure and predictors of non- medical prescription drug use and prescription drug use disorders: a national study. *Drug and alcohol dependence*, 133(2), 473-479.

Blanco, C., Rafful, C., Wall, M. M., Jin, C. J., Kerridge, B., & Schwartz, R. P. (2013). The latent structure and predictors of non- medical prescription drug use and prescription drug use disorders: a national study. *Drug and alcohol dependence*, 133(2), 473-479.

Blazer, D. G., & Wu, L. T. (2009). Nonprescription use of pain relievers by middle-aged and elderly community-living adults: National Survey on Drug Use and Health. *Journal of the American Geriatrics Society*, 57(7), 1252-1257.

- Bleich, A. V. I., Gelkopf, M., Schmidt, V., Hayward, R., Bodner, G., & Adelson, M. (1999). Correlates of benzodiazepine abuse in methadone maintenance treatment. A 1 year prospective study in an Israeli clinic. *Addiction*, 94(10), 1533-1540.
- Bleich, A., Gelkopf, M., Weizman, T., & Adelson, M. (2002). Benzodiazepine abuse in a methadone maintenance treatment clinic in Israel: Characteristics and a pharmacotherapeutic approach. *Israel Journal of Psychiatry*, 39(2), 104.
- Boggis, J. S., & Feder, K. (2019). Trends in and correlates of tranquilizer misuse among adults who misuse opioids in the United States, 2002–2014. *Drug and alcohol dependence*, 198, 158-161.
- Bonora, S., Pisi, A., Ottani, S., Cesini, D., Maris, A., & Di Foggia, M. (2014). Raman and SERS study on ibuprofen metal complexes with biomedical interest. *Vibrational Spectroscopy*, 73, 45-55.
- Borges, G., Walters, E. E., & Kessler, R. C. (2000). Associations of substance use, abuse, and dependence with subsequent suicidal behavior. *American journal of epidemiology*, 151(8), 781-789.
- Borges, G., Walters, E. E., & Kessler, R. C. (2000). Associations of substance use, abuse, and dependence with subsequent suicidal behavior. *American journal of epidemiology*, 151(8), 781-789.
- Boudiba, A., Zhang, C., Debliquy, M., Snyders, R., Lahem, D., & Olivier, M. G. (2012). P1. 7.11 Highly sensitive and rapid NO<sub>2</sub> gas sensors based on ZnO nanostructures and the morphology effect on their sensing performances. *Tagungsband*, 1089-1091.
- Bouvier, B. A., Wayne, K. M., Elston, B., Hadland, S. E., Green, T. C., & Marshall, B. D. (2018). Prevalence and correlates of benzodiazepine use and misuse among young adults who use prescription opioids non- medically. *Drug and alcohol dependence*, 183, 73-77.



- Boyd, C. J., West, B., & McCabe, S. E. (2018). Does misuse lead to a disorder? The misuse of prescription tranquilizer and sedative medications and subsequent substance use disorders in a US longitudinal sample. *Addictive Behaviors*, 79, 17- 23.
- Brady, K. T., Johnston, A. L., Cunningham, M., & Malcolm, R. (1991). Profiles of hospitalized benzodiazepine abusers. *Journal of psychoactive drugs*, 23(1), 71-72.
- Brands, B., Blake, J., Marsh, D. C., Sproule, B., Jeyapalan, R., & Li, S. (2008). The impact of benzodiazepine use on methadone maintenance treatment outcomes. *Journal of addictive diseases*, 27(3), 37-48.
- Brandt, S. A., Taverna, E. C., & Hallock, R. M. (2014). A survey of nonmedical use of tranquilizers, stimulants, and pain relievers among college students: Patterns of use among users and factors related to abstinence in non-users. *Drug and alcohol dependence*, 143, 272-276.
- Breen, C. L., Degenhardt, L. J., Roxburgh, A. D., Bruno, R. B., & Jenkinson, R. (2004). The effects of restricting publicly subsidised temazepam capsules on benzodiazepine use among injecting drug users in Australia. *Medical journal of Australia*, 181(6), 300-304.
- Breimer, D. D. (1979). Pharmacokinetics and metabolism of various benzodiazepines used as hypnotics. *British journal of clinical pharmacology*, 8(Suppl 1), 7S.
- Cai, Q., Gao, Y., Gao, T., Lan, S., Simalou, O., Zhou, X., ... & Dong, A. (2016). Insight into biological effects of zinc oxide nanoflowers on bacteria: why morphology matters. *ACS applied materials & interfaces*, 8(16), 10109-10120.
- Calhoun, S. R., Wesson, D. R., Galloway, G. P., & Smith, D. E. (1996). Abuse of flunitrazepam (Rohypnol) and other benzodiazepines in Austin and South Texas. *Journal of Psychoactive Drugs*, 28(2), 183-189.

- Camden, J. P., Dieringer, J. A., Zhao, J., & Van Duyne, R. P. (2008). Controlled plasmonic nanostructures for surface-enhanced spectroscopy and sensing. *Accounts of chemical research*, 41(12), 1653-1661.
- Campion, A., & Kambhampati, P. (1998). Surface-enhanced Raman scattering. *Chemical society reviews*, 27(4), 241-250.
- Campo-Soria, C., Chang, Y., & Weiss, D. S. (2006). Mechanism of action of benzodiazepines on GABAA receptors. *British journal of pharmacology*, 148(7), 984-990.
- Chen, C., Liu, P., & Lu, C. (2008). Synthesis and characterization of nano-sized ZnO powders by direct precipitation method. *Chemical Engineering Journal*, 144(3), 509-513.
- Chen, K. W., Berger, C. C., Forde, D. P., D'Adamo, C., Weintraub, E., & Gandhi, D. (2011). Benzodiazepine use and misuse among patients in a methadone program. *BMC psychiatry*, 11(1), 1-7.
- Chen, Y. C., Hong, S. W., Wu, H. H., Wang, Y. L., & Chen, Y. F. (2021). Rapid formation of nanoclusters for detection of drugs in urine using surface-enhanced Raman spectroscopy. *Nanomaterials*, 11(7), 1789.
- Cheng, B., & Samulski, E. T. (2004). Hydrothermal synthesis of one-dimensional ZnO nanostructures with different aspect ratios. *Chemical Communications*, (8), 986-987.
- Cheung, S. K., & Cheung, N. W. (1986). Extraction of Schottky diode parameters from forward current-voltage characteristics. *Applied physics letters*, 49(2), 85-87.
- Chinnaraj, K., Manikandan, A., Ramu, P., Antony, S. A., & Neeraja, P. (2015). Comparative studies of microwave-and sol- gel-assisted combustion methods of Fe<sub>3</sub>O<sub>4</sub> nanostructures: structural, morphological, optical, magnetic, and catalytic properties. *Journal of Superconductivity and Novel Magnetism*, 28, 179-190.

- Chiu, W., Khiew, P., Cloke, M., Isa, D., Lim, H., Tan, T., ... & Chia, C. (2010). Heterogeneous seeded growth: synthesis and characterization of bifunctional ZF core/shell nanocrystals. *The Journal of Physical Chemistry C*, 114(18), 8212-8218.
- Chweh, A. Y., Lin, Y. B., & Swinyard, E. A. (1984). Hypnotic action of benzodiazepines: A possible mechanism. *Life sciences*, 34(18), 1763-1768.
- Cina, S. J., Collins, K. A., & Goldberger, B. A. (2011). Toxicology: what is routine for medicolegal death investigation purposes? *Academic Forensic Pathology*, 1(1), 28-31.
- Ciraulo, D. A., Sands, B. F., & Shader, R. I. (1988). Critical review of liability for benzodiazepine abuse among alcoholics. *The American journal of psychiatry*.
- Cochran, S. D., Ackerman, D., Mays, V. M., & Ross, M. W. (2004). Prevalence of non-medical drug use and dependence among homosexually active men and women in the US population. *Addiction*, 99(8), 989-998.
- Comiskey, C. M., & Snel, A. (2016). Using client's routine urinalysis records from multiple treatment systems to model five- year opioid substitution treatment outcomes. *Substance Use & Misuse*, 51(4), 498-507.
- Compton, W. M., Cottler, L. B., Ben Abdallah, A., Phelps, D. L., Spitznagel, E. L., & Horton, J. C. (2000). Substance dependence and other psychiatric disorders among drug dependent subjects: race and gender correlates. *American Journal on Addictions*, 9(2), 113-125.
- Cook, B., Creedon, T., Wang, Y., Lu, C., Carson, N., Jules, P., & Alegría, M. (2018). Examining racial/ethnic differences in patterns of benzodiazepine prescription and misuse. *Drug and alcohol dependence*, 187, 29-34. Currie CL, Wild TC, 2012 Adolescent use of prescription drugs to get high in Canada. *Can. J. Psychiatry* 57, 745–751.

Cooper Jr, J. A. D., White, D. A., & Matthay, R. A. (1986). Drug- induced pulmonary disease: Part 1: Cytotoxic drugs. *American Review of Respiratory Disease*, 133(2), 321- 340.

Cornett, E. M., Novitch, M. B., Brunk, A. J., Davidson, K. S., Menard, B. L., Urman, R. D., & Kaye, A. D. (2018). New benzodiazepines for sedation. *Best Practice & Research Clinical Anaesthesiology*, 32(2), 149-164.

Creighton, J. A., Blatchford, C. G., & Albrecht, M. G. (1979). Plasma resonance enhancement of Raman scattering by pyridine adsorbed on silver or gold sol particles of size comparable to the excitation wavelength. *Journal of the Chemical Society, Faraday Transactions 2: Molecular and Chemical Physics*, 75, 790-798.

Dåderman, A. M., & Lidberg, L. (1999). Flunitrazepam (Rohypnol) abuse in combination with alcohol causes premeditated, grievous violence in male juvenile offenders. *The journal of the American Academy of Psychiatry and the Law*, 27(1), 83-99.

Dåderman, A. M., & Lidberg, L. (1999). Flunitrazepam (Rohypnol) abuse in combination with alcohol causes premeditated, grievous violence in male juvenile

Darke, S., & Ross, J. (2000). The relationship between suicide and overdose among methadone maintenance patients. National Drug and Alcohol Research Centre, University of New South Wales.

Darke, S., Hall, W., Ross, M., & Wodak, A. (1992). Benzodiazepine use and HIV risk- taking behaviour among injecting drug users. *Drug and Alcohol Dependence*, 31(1), 31- 36.

Darke, S., Ross, J., & Cohen, J. (1994). The use of benzodiazepines among regular amphetamine users. *Addiction*, 89(12), 1683-1690.

Das, R. S., & Agrawal, Y. K. (2011). Raman spectroscopy: Recent advancements, techniques and applications. *Vibrational spectroscopy*, 57(2), 163-176.

- Dien, N. D. (2019). Preparation of various morphologies of ZnO nanostructure through wet chemical methods. *Adv. Mater. Sci*, 4, 1-5.
- Dietch, J. T., & Jennings, R. K. (1988). Aggressive dyscontrol in patients treated with benzodiazepines. *The Journal of clinical psychiatry*.
- Dijkstra, R. J., Gerssen, A., Efremov, E. V., Ariese, F., Udo, A., & Gooijer, C. (2004). Substrates for the at-line coupling of capillary electrophoresis and surface-enhanced Raman spectroscopy. *Analytica chimica acta*, 508(2), 127-134.
- Długosz, O., Szostak, K., Krupiński, M., & Banach, M. (2021). Synthesis of Fe<sub>3</sub>O<sub>4</sub>/ZnO nanoparticles and their application for the photodegradation of anionic and cationic dyes. *International Journal of Environmental Science and Technology*, 18, 561- 574.
- Doctor, E. L., & McCord, B. (2013). Comparison of aggregating agents for the surface-enhanced Raman analysis of benzodiazepines. *Analyst*, 138(20), 5926-5932.
- Donoghue, J., & Lader, M. (2010). Usage of benzodiazepines: a review. *International journal of psychiatry in clinical practice*, 14(2), 78-87.
- Dourlat, J., Liu, W. Q., Gresh, N., & Garbay, C. (2007). Novel 1, 4-benzodiazepine derivatives with antiproliferative properties on tumor cell lines. *Bioorganic & medicinal chemistry letters*, 17(9), 2527-2530.
- Drummer, O. H. (1998). Methods for the measurement of benzodiazepines in biological samples. *Journal of Chromatography B: Biomedical Sciences and Applications*, 713(1), 201-225.
- Drummer, O. H., & Gerostamoulos, J. (2002). Postmortem drug analysis: analytical and toxicological aspects. *Therapeutic drug monitoring*, 24(2), 199-209.
- Dutta, S., & Ganguly, B. N. (2012). Characterization of ZnO nanoparticles grown in presence of Folic acid template. *Journal of nanobiotechnology*, 10(1), 1-10.

- Eaton, D. L., & Gilbert, S. G. (2008). Principles of toxicology. Casarett & Doull's Toxicology. The Basic Science of Poisons. CD Klaassen (ed), 11-34.
- Edelstein, A. S., & Cammaratra, R. C. (Eds.). (1998). Nanomaterials: synthesis, properties and applications. CRC press.
- Elsohly, M. A., & Salamone, S. J. (1999). Prevalence of drugs used in cases of alleged sexual assault. *Journal of analytical toxicology*, 23(3), 141-146.
- Engin, E., Benham, R. S., & Rudolph, U. (2018). An emerging circuit pharmacology of GABAA receptors. *Trends in pharmacological sciences*, 39(8), 710-732.
- Feron, V. J., & Groten, J. P. (2002). Toxicological evaluation of chemical mixtures. *Food and chemical toxicology*, 40(6), 825-839.
- Fini, G. (2004). Applications of Raman spectroscopy to pharmacy. *Journal of Raman Spectroscopy*, 35(5), 335-337.
- Flanagan, R. J., Ruprah, M., Meredith, T. J., & Ramsey, J. D. (1990). An introduction to the clinical toxicology of volatile substances. *Drug Safety*, 5, 359- 383.
- Fleischmann, M., Hendra, P. J., & McQuillan, A. J. (1974). Raman spectra of pyridine adsorbed at a silver electrode. *Chemical physics letters*, 26(2), 163-166.
- Foitzick, M. F., Medina, N. B., García, L. C. I., & Gravielle, M. C. (2020). Benzodiazepine exposure induces transcriptional down-regulation of GABAA receptor  $\alpha 1$  subunit gene via L-type voltage- gated calcium channel activation in rat cerebrocortical neurons. *Neuroscience Letters*, 721, 134801.
- Forsman, M., Nyström, I., Roman, M., Berglund, L., Ahlner, J., & Kronstrand, R. (2009). Urinary detection times and excretion patterns of flunitrazepam and its metabolites after a single oral dose. *Journal of analytical toxicology*, 33(8), 491-501.

Fox, J. D., Waverka, K. N., & Verbeck, G. F. (2012). Gold-plating of Mylar lift films to capitalize on surface enhanced Raman spectroscopy for chemical extraction of drug residues. *Forensic science international*, 216(1-3), 141-145.

Franklin, N. M., Rogers, N. J., Apte, S. C., Batley, G. E., Gadd, G. E., & Casey, P. S. (2007). Comparative toxicity of nanoparticulate ZnO, bulk ZnO, and ZnCl<sub>2</sub> to a freshwater microalga (*Pseudokirchneriella subcapitata*): the importance of particle solubility. *Environmental science & technology*, 41(24), 8484-8490.

Fritea, L., Bănică, F., Costea, T. O., Moldovan, L., Iovan, C., & Cavalu, S. (2018). A gold nanoparticles-Graphene based electrochemical sensor for sensitive determination of nitrazepam. *Journal of Electroanalytical Chemistry*, 830, 63-71.

Gallo, M. A., & Doull, J. (1996). History and scope of toxicology. Cassarett and Doull's Toxicology. The Basic Science of Poisons (Klassen CD, ed). 5th ed. New York: McGraw-Hill, 3-11.

Gastaldi, G., Capretti, G., Focher, B., & Cosentino, C. J. I. C. (1998). Characterization and properties of cellulose isolated from the *Crambe abyssinica* hull. *Industrial Crops and Products*, 8(3), 205-218.

Gaudreault, P., Guay, J., Thivierge, R. L., & Verdy, I. (1991). Benzodiazepine poisoning: clinical and pharmacological considerations and treatment. *Drug Safety*, 6, 247-265.

Ghosh, S. P. (2012). Synthesis and characterization of zinc oxide nanoparticles by sol-gel process (Doctoral dissertation).

Ghule, K., Ghule, A. V., Chen, B. J., & Ling, Y. C. (2006). Preparation and characterization of ZnO nanoparticles coated paper and its antibacterial activity study. *Green Chemistry*, 8(12), 1034-1041.

Gochfeld, M. (1992). Principles of toxicology. *Public health and preventive medicine*, 322-323.

\

- Gordon, T., Perlstein, B., Houbara, O., Felner, I., Banin, E., & Margel, S. (2011). Synthesis and characterization of zinc/iron oxide composite nanoparticles and their antibacterial properties. *Colloids and Surfaces A: Physicochemical and Engineering Aspects*, 374(1-3), 1-8.
- Green, M. L., Gusev, E. P., Degraeve, R., & Garfunkel, E. L. (2001). Ultrathin (< 4 nm) SiO<sub>2</sub> and Si–O–N gate dielectric layers for silicon microelectronics: Understanding the processing, structure, and physical and electrical limits. *Journal of Applied Physics*, 90(5), 2057-2121.
- Greenblatt, D. J., Divoll, M., Abernethy, D. R., Ochs, H. R., & Shader, R. I. (1983). Benzodiazepine kinetics: implications for therapeutics and pharmacogeriatrics. *Drug metabolism reviews*, 14(2), 251-292.
- Greenblatt, D. J., Harmatz, J. S., von Moltke, L. L., Wright, C. E., Durol, A. L. B., Harrel-Joseph, L. M., & Shader, R. I. (2000). Comparative kinetics and response to the benzodiazepine agonists triazolam and zolpidem: evaluation of sex-dependent differences. *Journal of Pharmacology and Experimental Therapeutics*, 293(2), 435-44.
- Greenblatt, D. J., Harmatz, J. S., Zinny, M. A., & Shader, R. I. (1988). Effect of gradual withdrawal on the rebound sleep disorder after discontinuation of triazolam. *Journal of Clinical Psychopharmacology*, 8(1), 62.
- Greenblatt, D. J., Miller, L. G., & Shader, R. I. (1987). Clonazepam pharmacokinetics, brain uptake, and receptor interactions. *The Journal of Clinical Psychiatry*, 48, 4-11.
- Greenblatt, D. J., Shader, R. I., & Abernethy, D. R. (1983). Current status of benzodiazepines. *New England Journal of Medicine*, 309(7), 410-416.
- Greenblatt, D. J., Shader, R. I., & Harmatz, J. S. (1989). Implications of altered drug disposition in the elderly: studies of benzodiazepines. *The Journal of Clinical Pharmacology*, 29(10), 866-872.



- Grossi, G., Di Braccio, M., Roma, G., Ballabeni, V., Tognolini, M., Calcina, F., & Barocelli, E. (2002). 1, 5-Benzodiazepines: Part XIII. Substituted 4H-[1, 2, 4] triazolo [4, 3-a][1, 5] benzodiazepin-5-amines and 4H- imidazo [1, 2-a][1, 5] benzodiazepin-5-amines as analgesic, anti- inflammatory and/or antipyretic agents with low acute toxicity. *European journal of medicinal chemistry*, 37(12), 933- 944.
- Grover, S., Kumar, V., Avasthi, A., & Kulhara, P. (2012). First prescription of new elderly patients attending the psychiatry outpatient of a tertiary care institute in North India. *Geriatrics & gerontology international*, 12(2), 284-291.).
- Gunja, N. (2013). The clinical and forensic toxicology of Z-drugs. *Journal of Medical Toxicology*, 9, 155-162.
- Guo, L., Yang, S., Yang, C., Yu, P., Wang, J., Ge, W., & Wong, G. K. (2000). Highly monodisperse polymer-capped ZnO nanoparticles: Preparation and optical properties. *Applied physics letters*, 76(20), 2901-2903.
- Gupta, A., & Srivastava, R. (2018). Zinc oxide nanoleaves: a scalable disperser-assisted sonochemical approach for synthesis and an antibacterial application. *Ultrasonics Sonochemistry*, 41, 47-58.
- Gupta, P. K. (2016). *Fundamentals of toxicology: essential concepts and applications*. Academic Press.
- Gurney, S. M. R., Scott, K. S., Kacinko, S. L., Presley, B. C., & Logan, B. K. (2014). Pharmacology, toxicology, and adverse effects of synthetic cannabinoid drugs. *Forensic Sci Rev*, 26(1), 53-78.
- Haefely, W. (1985). Recent advances in the molecular pharmacology of benzodiazepine receptors and in the structure-activity relationships of their agonists and antagonists. *Adv. Drug Res.*, 14, 165-322.

Haiying, G., Mingjie, H., Lingyu, Z., Qingxiang, W., Haisong, W., & Bingxi, Z. (2017). Anesthetics inhibit extracellular signal-regulated Kinase1/2 phosphorylation via NMDA receptor, phospholipase C and protein kinase C in mouse hippocampal slices. *Neurochemistry International*, 103, 36-44.

Hamideh Ashrafi, Soodabeh Hassanpour, Arezoo Saadati, MohammadHasanzadeh, KhalilAnsarin, SibelAysilOzkan, NasrinShadjou, Abolghasem Jouyban (2018), Sensitive detection and determination of benzodiazepines using silver nanoparticles-N-GQDs ink modified electrode: A new platform for modern pharmaceutical analysis

Hamilton, J. T. (1967). Muscle relaxant activity of chlordiazepoxide and diazepam. *Canadian Journal of Physiology and Pharmacology*, 45(2), 191-199.

Han, B., Jones, C. M., Johnson, K., & Compton, W. M. (2018). Prevalence and correlates of benzodiazepine use, misuse, and use disorders among adults in the United States. *The Journal of clinical psychiatry*, 79(6), 1865.

Hartung, T. (2011). From alternative methods to a new toxicology. *European journal of pharmaceuticals and biopharmaceutics*, 77(3), 338-349.

He, Q. F., Zhang, Y. J., Yang, Z. L., Dong, J. C., Lin, X. M., & Li, J. F. (2023). Surface-Enhanced Raman Spectroscopy: Principles, Methods, and Applications in Energy Systems. *Chinese Journal of Chemistry*, 41(3), 355-369.

Herrera-Rivera, R., Olvera, M. D. L. L., & Maldonado, A. (2017). Synthesis of ZnO nanopowders by the homogeneous precipitation method: Use of taguchi's method for analyzing the effect of different variables. *Journal of Nanomaterials*, 2017.

Hirschtritt, M. E., Delucchi, K. L., & Olfson, M. (2018). Outpatient, combined use of opioid and benzodiazepine medications in the United States, 1993–2014. *Preventive medicine reports*, 9, 49-54.

Hoffmann, S., de Vries, R. B., Stephens, M. L., Beck, N. B., Dirven, H. A., Fowle, J. R., ... & Tsaïoun, K. (2017). A primer on systematic reviews in toxicology. *Archives of toxicology*, 91, 2551-2575.

Holzwarth, U., & Gibson, N. (2011). The Scherrer equation versus the 'Debye-Scherrer equation'. *Nature nanotechnology*, 6(9), 534-534.

Hornyak, G. L., Moore, J. J., Tibbals, H. F., & Dutta, J. (2018). *Fundamentals of nanotechnology*. CRC press.

Huang, X. H., Guo, R. Q., Wu, J. B., & Zhang, P. (2014). Mesoporous ZnO nanosheets for lithium ion batteries. *Materials Letters*, 122, 82-85.

Huang, Y., Zhang, Y., Bai, X., He, J., Liu, J., & Zhang, X. (2006). Bicrystalline zinc oxide nanocombs. *Journal of nanoscience and nanotechnology*, 6(8), 2566-2570

Huarac, J. C. B., Singh, S. P., Tomar, M. S., Peña, S., Rivera, L., & Perales-Perez, O. (2010). Synthesis of ZF core-shell nanoparticles for photodynamic therapy applications. *MRS Online Proceedings Library (OPL)*, 1257.

Hughes, W. L., & Wang, Z. L. (2004). Formation of piezoelectric single-crystal nanorings and nanobows. *Journal of the American Chemical Society*, 126(21), 6703-6709.

Hughes, W. L., & Wang, Z. L. (2005). Controlled synthesis and manipulation of ZnO nanorings and nanobows. *Applied Physics Letters*, 86(4), 043106.

Identification of illicit drugs by a combination of liquid chromatography and surface-enhanced Raman scattering spectroscopy. *Journal of molecular structure*, 661, 279-290.

Inoue, H., Maeno, Y., Iwasa, M., Matoba, R., & Nagao, M. (2000). Screening and determination of benzodiazepines in whole blood using solid-phase extraction and gas chromatography/mass spectrometry. *Forensic science international*, 113(1-3), 367-373.

Inscore, F., Shende, C., Sengupta, A., Huang, H., & Farquharson, S. (2011). Detection of drugs of abuse in saliva by surface-enhanced Raman spectroscopy (SERS). *Applied spectroscopy*, 65(9), 1004-1008.

Inscore, F., Shende, C., Sengupta, A., Huang, H., & Farquharson, S. (2011). Detection of drugs of abuse in saliva by surface-enhanced Raman spectroscopy (SERS). *Applied spectroscopy*, 65(9), 1004-1008.

iraulo, D. A., Barnhill, J. G., Greenblatt, D. J., Shader, R. I., Ciraulo, A. M., Tarmey, M. F., & Foti, M. E. (1988). Abuse liability and clinical pharmacokinetics of alprazolam in alcoholic men. *The Journal of clinical psychiatry*.

Jacobson, A. F., Goldstein, B. J., Dominguez, R. A., & Steinbook, R. M. (1983). A placebo-controlled, double-blind comparison of clobazam and diazepam in the treatment of anxiety. *The Journal of clinical psychiatry*

, D. L., & Van Duyne, R. P. (1977). Surface Raman spectroelectrochemistry: Part I. Heterocyclic, aromatic, and aliphatic amines adsorbed on the anodized silver electrode. *Journal of electroanalytical chemistry and interfacial electrochemistry*, 84(1), 1-20.

Jeong, S. H., Hwang, Y. H., & Yi, S. C. (2005). Antibacterial properties of padded PP/PE nonwovens incorporating nano-sized silver colloids. *Journal of materials science*, 40, 5413-5418.

Jeong, S. H., Yeo, S. Y., & Yi, S. C. (2005). The effect of filler particle size on the antibacterial properties of compounded polymer/silver fibers. *Journal of Materials Science*, 40, 5407-5411.

Jiang, J., Oberdörster, G., Elder, A., Gelein, R., Mercer, P., & Biswas, P. (2008). Does nanoparticle activity depend upon size and crystal phase?. *Nanotoxicology*, 2(1), 33-42.

- Johari, N., Zohari, F., & Rafati, F. (2021). ZnO and CuO nanoparticles prepared via the co-precipitation method: the evaluation of morphology and formation mechanism.
- Juhascik, M., Lan Le, N., Tomlinson, K., Moore, C., Gaensslen, R. E., & Negrusz, A. (2004). Development of an analytical approach to the specimens collected from victims of sexual assault. *Journal of analytical toxicology*, 28(6), 400-406.
- Kales, A., Soldatos, C. R., Bixler, E. O., & Kales, J. D. (1983). Rebound insomnia and rebound anxiety: a review. *Pharmacology*, 26(3), 121-137.
- Kanto, J., & Klotz, U. (1982). Intravenous benzodiazepines as anaesthetic agents: pharmacokinetics and clinical consequences. *Acta Anaesthesiologica Scandinavica*, 26(6), 554-569.
- Katoch, V., Singh, J., Sharma, N. R., & Singh, R. P. (2021). Synthesis and characterization of mesoporous zinc oxide nanoparticles. *Inorganic and Nano-Metal Chemistry*, 1-9.
- Kerker, M., Wang, D. S., & Chew, H. (1980). Surface enhanced Raman scattering (SERS) by molecules adsorbed at spherical particles. *Applied optics*, 19(19), 3373-3388.
- Kevin C. Honeychurch (2019) Review of Electroanalytical- Based Approaches for the Determination of Benzodiazepines. *Journal of Biosensors*, 9 (4), 130.
- Khoshhesab, Z. M., Sarfaraz, M., & Asadabad, M. A. (2011). Preparation of ZnO nanostructures by chemical precipitation method. *Synthesis and Reactivity in Inorganic, Metal-Organic, and Nano-Metal Chemistry*, 41(7), 814-819
- Kneipp, K., Kneipp, H., Itzkan, I., Dasari, R. R., & Feld, M. S. (2002). Surface-enhanced Raman scattering and biophysics. *Journal of Physics: Condensed Matter*, 14(18), R597.
- Kneipp, K., Moskovits, M., & Kneipp, H. (Eds.). (2006). *Surface-enhanced Raman scattering: physics and applications* (Vol. 103). Springer Science & Business Media.

- Kolekar, T. V., Yadav, H. M., Bandgar, S. S., & Deshmukh, P. Y. (2011). Synthesis by sol-gel method and characterization of ZnO nanoparticles. *Indian streams research journal*, 1(1), 1-4.
- Kołodziejczak-Radzimska, A., & Jesionowski, T. (2014). Zinc oxide—from synthesis to application: a review. *Materials*, 7(4), 2833-2881.
- Kong, X. Y., & Wang, Z. L. (2003). Spontaneous polarization- induced nanohelices, nanosprings, and nanorings of piezoelectric nanobelts. *Nano letters*, 3(12), 1625-1631.
- Koutu, V., Shastri, L., & Malik, M. M. (2016). Effect of NaOH concentration on optical properties of zinc oxide nanoparticles. *Materials Science-Poland*, 34(4), 819-827.
- Kumar, S. S., Venkateswarlu, P., Rao, V. R., & Rao, G. N. (2013). Synthesis, characterization and optical properties of zinc oxide nanoparticles. *International Nano Letters*, 3, 1-6.
- Lalzawmliana, V., Anand, A., Roy, M., Kundu, B., & Nandi, S. K. (2020). Mesoporous bioactive glasses for bone healing and biomolecules delivery. *Materials Science and Engineering: C*, 106, 110180.
- Langman, L. J., & Kapur, B. M. (2006). Toxicology: then and now. *Clinical biochemistry*, 39(5), 498-510.
- Lanje, A. S., Sharma, S. J., Ningthoujam, R. S., Ahn, J. S., & Pode, R. B. (2013). Low temperature dielectric studies of zinc oxide (ZnO) nanoparticles prepared by precipitation method. *Advanced Powder Technology*, 24(1), 331-335.
- Le Ru, E. C., & Etchegoin, P. G. (2012). Single- molecule surface-enhanced Raman spectroscopy. *Annual review of physical chemistry*, 63, 65-87.
- Le Ru, E., & Etchegoin, P. (2008). *Principles of Surface-Enhanced Raman Spectroscopy: and related plasmonic effects*. Elsevier.

- LeBeau, M., Andollo, W., Hearn, W. L., Baselt, R., Cone, E., Finkle, B., & Saady, J. (1999). Recommendations for toxicological investigations of drug-facilitated sexual assaults. *Journal of Forensic Science*, 44(1), 227-230.
- Lee, B. W., Koo, J. H., Lee, T. S., Kim, Y. H., & Hwang, J. S. (2013). Synthesis of ZnO nanoparticles via simple wet-chemical routes. In *Advanced Materials Research* (Vol. 699, pp. 133-137). Trans Tech Publications Ltd.
- Lee, B. W., Koo, J. H., Lee, T. S., Kim, Y. H., & Hwang, J. S. (2013). Synthesis of ZnO nanoparticles via simple wet-chemical routes. In *Advanced Materials Research* (Vol. 699, pp. 133-137). Trans Tech Publications Ltd.
- Leikin, J. B., & Watson, W. A. (2003). Post-mortem toxicology: what the dead can and cannot tell us. *Journal of Toxicology: Clinical Toxicology*, 41(1), 47-56.
- Leopold, N., & Lendl, B. (2003). A new method for fast preparation of highly surface-enhanced Raman scattering (SERS) active silver colloids at room temperature by reduction of silver nitrate with hydroxylamine hydrochloride. *The Journal of Physical Chemistry B*, 107(24), 5723-5727.
- Leopold, N., Baena, J. R., Bolboacă, M., Cozar, O., Kiefer, W., & Lendl, B. (2004). Raman, IR, and surface-enhanced Raman spectroscopy of papaverine: an automated setup for in situ synthesis of the silver substrate and recording of the SER spectra. *Vibrational spectroscopy*, 36(1), 47-55.
- Leroch, M., Kretschmer, M., & Hahn, M. (2011). Fungicide resistance phenotypes of *Botrytis cinerea* isolates from commercial vineyards in South West Germany. *Journal of Phytopathology*, 159(1), 63-65.
- Levine, B., & Kerrigan, S. (Eds.). (1999). *Principles of forensic toxicology* (Vol. 2). Washington, DC: American Association for Clinical Chemistry.
- Li, L. H., Deng, J. C., Deng, H. R., Liu, Z. L., & Xin, L. (2010). Synthesis and characterization of chitosan/ZnO nanoparticle composite membranes. *Carbohydrate research*, 345(8), 994-998.

- Li, Q., Mahendra, S., Lyon, D. Y., Brunet, L., Liga, M. V., Li, D., & Alvarez, P.J. (2008). Antimicrobial nanomaterials for water disinfection and microbial control: potential applications and implications. *Water research*, 42(18), 4591-4602.
- Li, X., Zhang, F., Ma, C., Deng, Y., Wang, Z., Elingarami, S., & He, N. (2012). Controllable synthesis of ZnO with various morphologies by hydrothermal method. *Journal of Nanoscience and Nanotechnology*, 12(3), 2028-2036.
- Liao, P. F., Bergman, J. G., Chemla, D. S., Wokaun, A., Melngailis, J., Hawryluk, A. M., & Economou, N. P. (1981). Surface-enhanced Raman scattering from microlithographic silver particle surfaces. *Chemical Physics Letters*, 82(2), 355-359.
- Lincot, D., & Hodes, G. (2006). Chemical solution deposition of semiconducting and non-metallic films: Proceedings of the International Symposium. The Electrochemical Society.
- Lipovsky, A., Nitzan, Y., Gedanken, A., & Lubart, R. (2011). Antifungal activity of ZnO nanoparticles—the role of ROS mediated cell injury. *Nanotechnology*, 22(10), 105101.
- Liu, A. P., Li, X., Duan, L. H., Qin, G. P., & Guo, H. H. (2010). Study of Fe<sub>3</sub>O<sub>4</sub> nano-magnetic ferrofluid by atomic force microscope. *Journal of superconductivity and novel magnetism*, 23, 967-970.
- Liu, R., Yu, H., & Huang, Y. (2005). Structure and morphology of cellulose in wheat straw. *Cellulose*, 12, 25-34.
- Lloyd, J. B. F., & Parry, D. A. (1989). Forensic applications of the determination of benzodiazepines in blood samples by microcolumn cleanup and high-performance liquid chromatography with reductive mode electrochemical detection. *Journal of analytical toxicology*, 13(3), 163-168.
- Logan, B. K., & Roper-Miller, J. D. (2012). Forensic toxicology: scope, challenges, future directions and needs. *Forensic Science: Current Issues, Future Directions*, 160-178.



- Lucotti, A., Tommasini, M., Casella, M., Morganti, A., Gramatica, F., & Zerbi, G. (2012). TLC–surface enhanced Raman scattering of apomorphine in human plasma. *Vibrational Spectroscopy*, 62, 286-291.
- Macías-Martínez, B. I., Cortés-Hernández, D. A., Zugasti-Cruz, A., Cruz-Ortíz, R., & Múzquiz-Ramos, E. M. (2016). Heating ability and hemolysis test of magnetite nanoparticles obtained by a simple co-precipitation method. *Journal of applied research and technology*, 14(4), 239-244.
- Madathil, A. N. P., Vanaja, K. A., & Jayaraj, M. K. (2007, September). Synthesis of ZnO nanoparticles by hydrothermal method. In *Nanophotonic materials IV* (Vol. 6639, pp. 47-55). SPIE.
- Mahmood, M. A., Jan, S., Shah, I. A., & Khan, I. (2016). Growth parameters for films of hydrothermally synthesized one-dimensional nanocrystals of zinc oxide. *International Journal of Photoenergy*, 2016.
- Manchester, K. R., Lomas, E. C., Waters, L., Dempsey, F. C., & Maskell, P. D. (2018). The emergence of new psychoactive substance (NPS) benzodiazepines: A review. *Drug testing and analysis*, 10(1), 37-53.
- Manthey, L., Giltay, E. J., van Veen, T., Neven, A. K., Vreeburg, S. A., Penninx, B. W., & Zitman, F. G. (2010). Long-term benzodiazepine use and salivary cortisol: the Netherlands Study of Depression and Anxiety (NESDA). *Journal of clinical psychopharmacology*, 30(2), 160-168.
- Martinaga Pintarić, L., Somogi Škoc, M., Ljoljić Bilić, V., Pokrovac, I., Kosalec, I., & Rezić, I. (2020). Synthesis, modification and characterization of antimicrobial textile surface containing ZnO nanoparticles. *Polymers*, 12(6), 1210.
- Martins, R., Nathan, A., Barros, R., Pereira, L., Barquinha, P., Correia, N., ... & Fortunato, E. (2011). Complementary metal oxide semiconductor technology with and on paper. *Advanced Materials*, 23(39), 4491-4496.
- Masaki, T., & Kim, S. (2003). Synthesis of nano-sized ZnO powders prepared by precursor process. *Journal of Ceramic Processing & Research*, 4(3), 135-139.

Maurer, H. H. (2010). Analytical toxicology. Molecular, Clinical and Environmental Toxicology: Volume 2: Clinical Toxicology, 317-338.

McKernan, R. M., Rosahl, T. W., Reynolds, D. S., Sur, C., Wafford, K. A., Atack, J. R., & Whiting, P. J. (2000). Sedative but not anxiolytic properties of benzodiazepines are mediated by the GABAA receptor  $\alpha 1$  subtype. *Nature neuroscience*, 3(6), 587-592.

Meng, Z., Berro, L. F., Sawyer, E. K., Rüedi- Bettschen, D., Cook, J. E., Li, G., ... & Rowlett, J. K. (2020). Evaluation of the anti-conflict, reinforcing, and sedative effects of YT-III-31, a ligand functionally selective for  $\alpha 3$  subunit-containing GABAA receptors. *Journal of Psychopharmacology*, 34(3), 348-357.

Merlen, A., Pardanaud, C., Gratzler, K., Coussan, S., Machon, D., Forestier, A., & Hornebecq, V. (2020). Spectral fluctuation in SERS spectra of benzodiazepin molecules: The case of oxazepam. *Journal of Raman Spectroscopy*, 51(11), 2192-2198.

Miller, L. G., Greenblatt, D. J., Barnhill, J. G., & Shader, R. I. (1988). Chronic benzodiazepine administration. I. Tolerance is associated with benzodiazepine receptor downregulation and decreased gamma-aminobutyric acidA receptor function. *Journal of Pharmacology and Experimental Therapeutics*, 246(1), 170-176.

Miller, L. G., Greenblatt, D. J., Paul, S. M., & Shader, R. I. (1987). Benzodiazepine receptor occupancy in vivo: correlation with brain concentrations and pharmacodynamic actions. *Journal of Pharmacology and Experimental Therapeutics*, 240(2), 516-522.

Mir Reza Majidi, Seyran Ghaderi, Karim Asadpour-Zeynali, Hossein Dastangoo.(2015) Synthesis of dendritic silver nanostructures supported by graphene nanosheets and its application for highly sensitive detection of diazepam, *Materials Science & Engineering C*.

Moghri Moazzen, M. A., Borghei, S. M., & Taleshi, F. (2013). Change in the morphology of ZnO nanoparticles upon changing the reactant concentration. *Applied Nanoscience*, 3, 295-302.

Mokhtari, A., Karimi- Maleh, H., Ensafi, A. A., & Beitollahi, H. (2012). Application of modified multiwall carbon nanotubes paste electrode for simultaneous voltammetric determination of morphine and diclofenac in biological and pharmaceutical samples. *Sensors and Actuators B: Chemical*, 169, 96-105.

Montalvo, G., López-Melero, L., Ortega-Ojeda, F., Peña, M. Á., & García-Ruiz, C. (2014). Raman spectral signatures for the differentiation of benzodiazepine drugs. *Analytical Methods*, 6(24), 9536-9546.

Mosier-Boss, P. A., & Lieberman, S. H. (2005). Surface-enhanced Raman spectroscopy substrate composed of chemically modified gold colloid particles immobilized on magnetic microparticles. *Analytical chemistry*, 77(4), 1031-1037.

Mostowtt, T., & McCord, B. (2017). Surface enhanced Raman spectroscopy(SERS) as a method for the toxicological analysis of synthetic cannabinoids. *Talanta*, 164, 396-402.

Musshoff, F., & Daldrup, T. (1992). A rapid solid-phase extraction and HPLC/DAD procedure for the simultaneous determination and quantification of different benzodiazepines in serum, blood and post- mortem blood. *International Journal of Legal Medicine*, 105, 105-109.

Naderi, E., Naseri, M., Rad, H. T., Emameh, R. Z., Farnoosh, G., & Taheri, R. A. (2020). In vivo and In vitro biocompatibility study of Fe<sub>3</sub>O<sub>4</sub>@ ZnO and Fe<sub>3</sub>O<sub>4</sub>@ SiO<sub>2</sub> as photosensitizer for targeted breast cancer drug delivery. *Journal of Sciences, Islamic Republic of Iran*, 31(4), 357-368.

- Nansé, G., Papirer, E., Fioux, P., Moguet, F., & Tressaud, A. (1997). Fluorination of carbon blacks: An X-ray photoelectron spectroscopy study: I. A literature review of XPS studies of fluorinated carbons. XPS investigation of some reference compounds. *Carbon*, 35(2), 175-194.
- Narayana, B., Raj, K. V., Ashalatha, B. V., & Kumari, N. S. (2006). Synthesis of some new substituted triazolo [4, 3-a][1, 4] benzodiazepine derivatives as potent anticonvulsants. *European journal of medicinal chemistry*, 41(3), 417-422.
- Neville, G. A., & Shurvell, H. F. (1990). Fourier transform Raman and infrared vibrational study of diazepam and four closely related 1, 4-benzodiazepines. *Journal of Raman spectroscopy*, 21(1), 9-19.
- Neville, G. A., Beckstead, H. D., & Shurvell, H. F. (1994). A Fourier transform-Raman and infrared vibrational study of delorazepam, fludiazepam, flurazepam, and tetrazepam. *Journal of pharmaceutical sciences*, 83(2), 143-151.
- Nuwaysir, E. F., Bittner, M., Trent, J., Barrett, J. C., & Afshari, C. A. (1999). Microarrays and toxicology: the advent of toxicogenomics. *Molecular Carcinogenesis: Published in cooperation with the University of Texas MD Anderson Cancer Center*, 24(3), 153-159.
- offenders. *The journal of the American Academy of Psychiatry and the Law*, 27(1), 83- 99.
- Ohtake, Y., Naito, A., Hasegawa, H., Kawano, K., Morizono, D., Taniguchi, M., & Tsuruya, Y. (1999). Novel vasopressin V2 receptor-selective antagonists, pyrrolo [2, 1-a] quinoxaline and pyrrolo [2, 1-c][1, 4] benzodiazepine derivatives. *Bioorganic & medicinal chemistry*, 7(6), 1247-1254.
- Padmavathy, N., & Vijayaraghavan, R. (2008). Enhanced bioactivity of ZnO nanoparticles—an antimicrobial study. *Science and technology of advanced materials*.
- Pandya, A., & Shukla, R. K. (2018). New perspective of nanotechnology: role in preventive forensic. *Egyptian Journal of Forensic Sciences*, 8, 1-11.

- Panwar, R. S., & Raina, K. K. (2009). Preparation of modified ZnO nanoparticles by sol-gel process and their characterization (Doctoral dissertation).
- Papoutsis, I. I., Athanaselis, S. A., Nikolaou, P. D., Pistos, C. M., Spiliopoulou, C. A., & Maravelias, C. P. (2010). Development and validation of an EI–GC–MS method for the determination of benzodiazepine drugs and their metabolites in blood: Applications in clinical and forensic toxicology. *Journal of pharmaceutical and biomedical analysis*, 52(4), 609-614.
- Parasuraman, S. (2011). Toxicological screening. *Journal of pharmacology & pharmacotherapeutics*, 2(2), 74.
- Park, T. W., Larochele, M. R., Saitz, R., Wang, N., Bernson, D., & Walley, A. Y. (2020). Associations between prescribed benzodiazepines, overdose death and buprenorphine discontinuation among people receiving buprenorphine. *Addiction*, 115(5), 924-932.).
- Paschoarelli, M. V., Kawai, M. S., de Lima, L. F., & de Araujo, W. R. (2023). Laser-scribing fabrication of a disposable electrochemical device for forensic detection of crime facilitating drugs in beverage samples. *Talanta*, 255, 124214.
- Peters, F. T. (2007). Stability of analytes in biosamples—an important issue in clinical and forensic toxicology?. *Analytical and bioanalytical chemistry*, 388, 1505-1519.
- Peters, F. T., Wissenbach, D. K., Busardo, F. P., Marchei, E., & Pichini, S. (2017). Method development in forensic toxicology. *Current pharmaceutical design*, 23(36), 5455-5467.
- Podporska-Carroll, J., Myles, A., Quilty, B., McCormack, D. E., Fagan, R., Hinder, S. J., ... & Pillai, S. C. (2017). Antibacterial properties of F-doped ZnO visible light photocatalyst. *Journal of hazardous materials*, 324, 39-47.
- Poklis, A. L. P. H. O. N. S. E. (1997). Forensic toxicology. dalam *Introduction to Forensic Sciences*, ed. Eckert, WG (New York: Elsevier, 1992), 107-132.

- Pourmadadi, M., Rahmani, E., Shamsabadipour, A., Mahtabian, S., Ahmadi, M., Rahdar, A., & Díez-Pascual, A. M. (2022). Role of Iron Oxide (Fe<sub>2</sub>O<sub>3</sub>) Nanocomposites in Advanced Biomedical Applications: A State-of-the-Art Review. *Nanomaterials*, 12(21), 3873.
- Prabhu, Y. T., Rao, K. V., Kumar, V. S. S., & Kumari, B. S. (2014). X-ray analysis by Williamson-Hall and size-strain plot methods of ZnO nanoparticles with fuel variation. *World Journal of Nano Science and Engineering*, 2014.
- Qian, X. M., & Nie, S. M. (2008). Single-molecule and single-nanoparticle SERS: from fundamental mechanisms to biomedical applications. *Chemical Society Reviews*, 37(5), 912-920.
- Ramalingam, S., Elsayed, A., & Singh, A. (2023). An Aflatoxin-M1 biochip using graphene quantum dot-gold hybrid nanoparticles. *Food Chemistry*, 403, 134302.
- Rana, V., Cañamares, M. V., Kubic, T., Leona, M., & Lombardi, J. R. (2011). Surface-enhanced Raman spectroscopy for trace identification of controlled substances: morphine, codeine, and hydrocodone. *Journal of forensic sciences*, 56(1), 200-207.
- Rastogi, L., & Arunachalam, J. (2011). Sunlight based irradiation strategy for rapid green synthesis of highly stable silver nanoparticles using aqueous garlic (*Allium sativum*) extract and their antibacterial potential. *Materials Chemistry and Physics*, 129(1-2), 558-563.
- Reys, L. L., & Santos, J. C. (1992). Importance of information in forensic toxicology. *The American Journal of Forensic Medicine and Pathology*, 13(1), 33- 36.
- Ridhuan, N. S. (2013). Feasibility Study of ZnO Nanorods for Sensor Application (Doctoral dissertation, Universiti Sains Malaysia).
- Rivas, L., Sanchez-Cortes, S., Stanicova, J., Garcia-Ramos, J. V., & Miskovsky, P. (1999). FT-Raman, FTIR and surface-enhanced Raman spectroscopy of the antiviral and antiparkinsonian drug amantadine. *Vibrational spectroscopy*, 20(2), 179-188.

- Roberts, K., Ursini, A., Barnaby, R., Cassarà, P. G., Corsi, M., Curotto, G., ... & van Amsterdam, F. T. (2011). Synthesis and structure–activity relationship of new 1, 5-dialkyl-1, 5-benzodiazepines as cholecystokinin-2 receptor antagonists. *Bioorganic & medicinal chemistry*, 19(14), 4257-4273.
- Robertson, J. (2005). High dielectric constant gate oxides for metal oxide Si transistors. *Reports on progress in Physics*, 69(2), 327.
- Romeiro, A., Freitas, D., Emilia Azenha, M., Canle, M., & Burrows, H. D. (2017). Effect of the calcination temperature on the photocatalytic efficiency of acidic sol-gel synthesized TiO<sub>2</sub> nanoparticles in the degradation of alprazolam. *Photochemical & Photobiological Sciences*, 16, 935-945.
- Rosi, N. L., & Mirkin, C. A. (2005). Nanostructures in biodiagnostics. *Chemical reviews*, 105(4), 1547-1562.
- Rouhi, J., Alimanesh, M., Mahmud, S., Dalvand, R. A., Ooi, C. R., & Rusop, M. (2014). A novel method for synthesis of well-aligned hexagonal cone-shaped ZnO nanostructures in field emission applications. *Materials letters*, 125, 147-150.
- Ryder, A. G. (2005). Surface enhanced Raman scattering for narcotic detection and applications to chemical biology. *Current opinion in chemical biology*, 9(5), 489- 493.
- Sabir, S., Arshad, M., & Chaudhari, S. K. (2014). Zinc oxide nanoparticles for revolutionizing agriculture: synthesis and applications. *The Scientific World Journal*, 2014.
- Sägmüller, B., Schwarze, B., Brehm, G., Trachta, G., & Schneider, S. (2003).
- Sai-Anand, G., Sivanesan, A., Benzigar, M. R., Singh, G., Gopalan, A. I., Baskar, V., ... & Vinu, A. (2019). Recent progress on the sensing of pathogenic bacteria using advanced nanostructures. *Bulletin of the Chemical Society of Japan*, 92(1), 216-244.
- Salamone, S. J. (Ed.). (2001). *Benzodiazepines and GHB: Detection and pharmacology*. Springer Science & Business Media.

- Saleh, T. A., Al-Shalalfeh, M. M., Onawole, A. T., & Al-Saadi, A. A. (2017). Ultra-trace detection of methimazole by surface-enhanced Raman spectroscopy using gold substrate. *Vibrational Spectroscopy*, 90, 96-103.
- Salve, P. S., & Mali, D. S. (2013). 1, 5-Benzodiazepine: A versatile pharmacophore. *Int.J. Pharm. Bio. Sci*, 4, 345.
- Samanta, P. K., Patra, S. K., Ghosh, A., & Chaudhuri, P. R. (2009). Visible emission from ZnO nanorods synthesized by a simple wet chemical method. *Int. J. Nanosci. Nanotechnol*, 1(1-2), 81-90.
- Sanabria, E., Cuenca, R. E., Estes, M. Á., & Maldonado, M. (2021). Benzodiazepines: Their use either as essential medicines or as toxic substances. *Toxics*, 9(2), 25.
- Santhosh, C., Velmurugan, V., Jacob, G., Jeong, S. K., Grace, A. N., & Bhatnagar, A. (2016). Role of nanomaterials in water treatment applications: a review. *Chemical Engineering Journal*, 306, 1116-1137.
- Sardana, S., & Madan, A. K. (2002). Predicting anti-HIV activity of TIBO derivatives: a computational approach using a novel topological descriptor. *Molecular modeling annual*, 8, 258-265.
- Sawai, J. (2003). Quantitative evaluation of antibacterial activities of metallic oxide powders (ZnO, MgO and CaO) by conductimetric assay. *Journal of microbiological methods*, 54(2), 177-182.
- Sawai, J., Shoji, S., Igarashi, H., Hashimoto, A., Kokugan, T., Shimizu, M., & Kojima, H. (1998). Hydrogen peroxide as an antibacterial factor in zinc oxide powder slurry. *Journal of fermentation and bioengineering*, 86(5), 521-522.



- Saxena, R., Saxena, M., & Lochab, A. (2020). Recent progress in nanomaterials for adsorptive removal of organic contaminants from wastewater. *ChemistrySelect*, 5(1), 335-353.
- Scarisoreanu, N., Matei, D. G., Dinescu, G., Epurescu, G., Ghica, C., Nistor, L. C., & Dinescu, M. (2005). Properties of ZnO thin films prepared by radio-frequency plasma beam assisted laser ablation. *Applied surface science*, 247(1-4), 518-525.
- Segawa, H., Fukuoka, T., Itoh, T., Imai, Y., Iwata, Y. T., Yamamuro, T., ... & Inoue, H. (2019). Rapid detection of hypnotics using surface-enhanced Raman scattering based on gold nanoparticle co-aggregation in a wet system. *Analyst*, 144(6), 2158-2165.
- Sha, X., Han, S. Q. G. W., Zhao, H., Li, N., Zhang, C., & Hasi, W. L. J. (2020). A rapid detection method for on-site screening of estazolam in beverages with Au@Ag core-shell nanoparticles paper-based SERS substrate. *Analytical Sciences*, 36(6), 667-671.
- Shah, A. H., Manikandan, E., Ahamed, M. B., Mir, D. A., & Mir, S. A. (2014). Antibacterial and Blue shift investigations in sol-gel synthesized  $CrxZn1-xO$  Nanostructures. *Journal of luminescence*, 145, 944-950.
- Shamhari, N. M., Wee, B. S., Chin, S. F., & Kok, K. Y. (2018). Synthesis and characterization of zinc oxide nanoparticles with small particle size distribution. *Acta Chimica Slovenica*, 65(3), 578-585.
- Shanker, U., Jassal, V., Rani, M., & Kaith, B. S. (2016). Towards green synthesis of nanoparticles: from bio-assisted sources to benign solvents. A review. *International Journal of Environmental Analytical Chemistry*, 96(9), 801-835.
- Sharma, B., Cardinal, M. F., Kleinman, S. L., Greeneltch, N. G., Frontiera, R. R., Blaber, M. G., ... & Van Duyne, R. P. (2013). High-performance SERS substrates: Advances and challenges. *MRS bulletin*, 38(8), 615-624.

- Sharma, S., Kumar, K., & Singh, G. (2017). An overview on narcotic drugs and psychotropic substances act, 1985. *J Forensic Sci Crim Invest*, 4, 555644.
- Shen, Z. C., Wu, P. F., Wang, F., Xia, Z. X., Deng, Q., Nie, T. L., ... & Chen, J. G. (2019). Gephyrin palmitoylation in basolateral amygdala mediates the anxiolytic action of benzodiazepine. *Biological psychiatry*, 85(3), 202-213.
- Shinde, S. D., Patil, G. E., Kajale, D. D., Ahire, D. V., Gaikwad, V. B., & Jain, G.H. (2012). Synthesis of ZnO nanorods by hydrothermal method for gas sensor applications. *International journal on smart sensing and intelligent systems*, 5(1), 57-70.
- Singh, K. P., Timilsina, U., Tamang, H. K., Thapa, S., & Agarwal, A. (2012). Synthesis of zinc nanoparticles by wet chemical method and study of enhancement of the antimicrobial activity of antibiotics by zinc nanoparticles. *Journal of Nepal Association for Medical Laboratory Sciences*, 11(1), 54-58.
- Singh, N., Mehra, R. M., & Kapoor, A. (2011). Synthesis and characterization of ZnO nanoparticles.
- Singh, P., Kim, Y. J., Zhang, D., & Yang, D. C. (2016). Biological synthesis of nanoparticles from plants and microorganisms. *Trends in biotechnology*, 34(7), 588-599.
- Sinha, R., Karan, R., Sinha, A., & Khare, S. K. (2011). Interaction and nanotoxic effect of ZnO and Ag nanoparticles on mesophilic and halophilic bacterial cells. *Bioresource technology*, 102(2), 1516-1520.
- Siregar, J., Sebayang, K., Yulianto, B., & Humaidi, S. (2020, March). XRD characterization of Fe<sub>3</sub>O<sub>4</sub>-ZnO nanocomposite material by the hydrothermal method. In *AIP Conference Proceedings* (Vol. 2221, No. 1, p. 110008). AIP Publishing LLC.

- Skolnick, P. (2012). Anxiolytic anxiolytics: on a quest for the Holy Grail. *Trends in pharmacological sciences*, 33(11), 611-620.
- Skopp, G. (2010). Postmortem toxicology. *Forensic science, medicine, and pathology*, 6, 314-325.
- Snure, M., & Tiwari, A. (2007). Synthesis, characterization, and green luminescence in ZnO nanocages. *Journal of Nanoscience and Nanotechnology*, 7(2), 481-485.
- Stiles, P. L., Dieringer, J. A., Shah, N. C., & Van Duyne, R. P. (2008). Surface-enhanced Raman spectroscopy. *Annu. Rev. Anal. Chem.*, 1, 601-626.
- Strom, B. L. (1987). Generic drug substitution revisited. *New England Journal of Medicine*, 316(23), 1456-1462.
- Sudha, L. K., Sukumar, R., & Uma Rao, K. (2014). Evaluation of activation energy (Ea) profiles of nanostructured alumina polycarbonate composite insulation materials. *International Journal of Materials. Mechanics and Manufacturing*, 2(1), 96-100.
- Sun, T., Qiu, J., & Liang, C. (2008). Controllable fabrication and photocatalytic activity of ZnO nanobelt arrays. *The Journal of Physical Chemistry C*, 112(3), 715-721.
- Suntako, R. (2015). Effect of zinc oxide nanoparticles synthesized by a precipitation method on mechanical and morphological properties of the CR foam. *Bulletin of Materials Science*, 38, 1033-1038.
- Thangaduraia, S., Dhanalakshmia, A., & Kannan, M. S. (2013). Separation and detection of certain benzodiazepines by thin-layer chromatography. *Malaysian Journal of Forensic Sciences*, 4(1), 47-53.
- Thirumavalavan, M., Huang, K. L., & Lee, J. F. (2013). Preparation and morphology studies of nano zinc oxide obtained using native and modified chitosans. *Materials*, 6(9), 4198-4212.

- Trachta, G., Schwarze, B., Sägmüller, B., Brehm, G., & Schneider, S. (2004). Combination of high-performance liquid chromatography and SERS detection applied to the analysis of drugs in human blood and urine. *Journal of molecular structure*, 693(1-3), 175-185.
- Tse, B. W. C., Cowin, G. J., Soekmadji, C., Jovanovic, L., Vasireddy, R. S., Ling, M. T., ... & Russell, P. J. (2015). PSMA-targeting iron oxide magnetic nanoparticles enhance MRI of preclinical prostate cancer. *Nanomedicine*, 10(3), 375-386.
- Uvarov, V. L. A. D. I. M. I. R., & Popov, I. (2007). Metrological characterization of X-ray diffraction methods for determination of crystallite size in nano-scale materials. *Materials characterization*, 58(10), 883-891.
- Vafae, M., & Ghamsari, M. S. (2007). Preparation and characterization of ZnO nanoparticles by a novel sol-gel route. *Materials Letters*, 61(14-15), 3265-3268.
- Vankeirsbilck, T., Vercauteren, A., Baeyens, W., Van der Weken, G., Verpoort, F., Vergote, G., & Remon, J. P. (2002). Applications of Raman spectroscopy in pharmaceutical analysis. *TrAC trends in analytical chemistry*, 21(12), 869-877.
- Vaseem, M., Umar, A., & Hahn, Y. B. (2010). ZnO nanoparticles: growth, properties, and applications. *Metal oxide nanostructures and their applications*, 5(1), 10- 20.
- Vinogradov, S., & Wei, X. (2012). Cancer stem cells and drug resistance: the potential of nanomedicine. *Nanomedicine*, 7(4), 597-615.
- Vinyas, M., Athul, S. J., Harursampath, D., Loja, M., & Thoi, T. N. (2019). A comprehensive review on analysis of nanocomposites: from manufacturing to properties characterization. *Materials Research Express*, 6(9), 092002.
- Wahab, R., Ansari, S. G., Kim, Y. S., Seo, H. K., Kim, G. S., Khang, G., & Shin, H. S. (2007). Low temperature solution synthesis and characterization of ZnO nano-flowers. *Materials Research Bulletin*, 42(9), 1640-1648.

- Wahid, K. A., Lee, W. Y., Lee, H. W., Teh, A. S., Bien, D. C., & Abd Azid, I. (2013). Effect of seed annealing temperature and growth duration on hydrothermal ZnO nanorod structures and their electrical characteristics. *Applied Surface Science*, 283, 629- 635.
- Wan, J., Li, H., & Chen, K. (2009). Synthesis and characterization of Fe<sub>3</sub>O<sub>4</sub>@ ZnO core-shell structured nanoparticles. *Materials Chemistry and Physics*, 114(1), 30- 32.
- Wang, H., Li, C., Zhao, H., Li, R., & Liu, J. (2013). Synthesis, characterization, and electrical conductivity of ZnO with different morphologies. *Powder technology*, 239, 266-271.
- Wang, H., Wu, X., & Guo, X. (2011). U.S. Patent No. 7,460,224. Washington, DC: U.S. Patent and Trademark Office
- Wang, Y., Gao, J., Liu, Y., Li, M., Zhang, M., He, G., & Sun, Z. (2021). Facile fabrication of ZnO nanorods modified Fe<sub>3</sub>O<sub>4</sub> nanoparticles with enhanced magnetic, photoelectrochemical and photocatalytic properties. *Optical Materials*, 111, 110608.
- Wasim, M., Khan, M. R., Mushtaq, M., Naeem, A., Han, M., & Wei, Q. (2020). Surface modification of bacterial cellulose by copper and zinc oxide sputter coating for UV-resistance/antistatic/antibacterial characteristics. *Coatings*, 10(4), 364.
- Willander, M., Nur, O., Sadaf, J. R., Qadir, M. I., Zaman, S., Zainelabdin, A., ... & Hussain, I. (2010). Luminescence from zinc oxide nanostructures and polymers and their hybrid devices. *Materials*, 3(4), 2643-2667.
- Win, K. Y., & Feng, S. S. (2005). Effects of particle size and surface coating on cellular uptake of polymeric nanoparticles for oral delivery of anticancer drugs. *Biomaterials*, 26(15), 2713-2722.
- Wittwer Jr, J. D. (1980). Application of high-pressure liquid chromatography to the forensic analysis of several benzodiazepines. *Journal of Liquid Chromatography*, 3(11), 1713-1724.

- Wright Jr, W. B., Greenblatt, E. N., Day, I. P., Quinones, N. Q., & Hardy Jr, R. A. (1980). Derivatives of 11-(1-piperazinyl)-5H-pyrrolo [2, 1-c][1, 4] benzodiazepine as central nervous system agents. *Journal of Medicinal Chemistry*, 23(4), 462-465.
- Wu, W., He, Q., & Jiang, C. (2008). Magnetic iron oxide nanoparticles: synthesis and surface functionalization strategies. *Nanoscale research letters*, 3, 397-415.
- Xia, J., Li, J., & Sun, H. (2012). Insights into ET A subtype selectivity of benzodiazepine endothelin receptor antagonists by 3D-QSAR approaches. *Journal of molecular modeling*, 18, 1299-1311.
- Xu, S., & Wang, Z. L. (2011). One-dimensional ZnO nanostructures: solution growth and functional properties. *Nano research*, 4, 1013-1098.
- Yumusak, C., Singh, T. B., Sariciftci, N. S., & Grote, J. G. (2009). Bio-organic field effect transistors based on crosslinked deoxyribonucleic acid (DNA) gate dielectric. *Applied Physics Letters*, 95(26), 341.
- Zak, A. K., Razali, R., Majid, W. A., & Darroudi, M. (2011). Synthesis and characterization of a narrow size distribution of zinc oxide nanoparticles. *International journal of nanomedicine*, 1399-1403.
- Zhou, J., Xu, N. S., & Wang, Z. L. (2006). Dissolving behavior and stability of ZnO wires in biofluids: a study on biodegradability and biocompatibility of ZnO nanostructures. *Advanced Materials*, 18(18), 2432-2435.
- Ziegler, L. D., Boston University, & United States of America. (2018). *Body Fluid Analysis by Surface Enhanced Raman Spectroscopy for Forensic Applications*.
- Zin, C. S., & Ismail, F. (2017). Co-prescription of opioids with benzodiazepine and other co-medications among opioid users: differential in opioid doses. *Journal of Pain Research*, 249-257.

## Oral presentation

- Presented in 2nd International Conference on Environment, Agriculture, Chemical and Biological Sciences ICEABS2021 on topic “Screening of abused drugs from forensic matrices by nanoparticles sensing method” and got **BEST ORAL PRESENTATION AWARD**.
- Presented in International Conference on Sustainability: Life on Earth 2021(ICS-LOE 2021) on topic “Nanoparticles sensing method for sensitive detection and determination of Benzodiazepine”.
- Presented in National Conference on Emerging trends in Plant Science for Sustainable Development (By UGC-SAP (DRS-II) IN March 2022 on topic “Nanobiotechnology based method for the detection of benzodiazepine”.
- Presented in Annual International conference on “Modernizing Forensic Sciences through Technology” held on 27-29 April, 2023 on topic “Application of Nanotechnology for ultra-sensitive detection of Benzodiazepine”.

## Publication

The image shows a screenshot of a journal article page. At the top, there is a navigation bar with the following items: Journals, Inorganic and Nano-Metal Chemistry, List of Issues, Latest Articles, and Synthesis and characterization of mesopo .... Below this, the journal title 'Inorganic and Nano-Metal Chemistry' is displayed, along with a search bar containing the text 'Enter keywords, authors, DOI, ORCID etc' and a dropdown menu for 'This Journal'. There are also buttons for 'Submit an article' and 'Journal homepage'. The main content area features the title 'Synthesis and characterization of mesoporous zinc oxide nanoparticles' in a large, bold font. Below the title, the authors 'Vaidehi Katoch, Jaskaran Singh, Neeta Raj Sharma & Ravinder Pal Singh' are listed, followed by the publication details: 'Received 27 Sep 2020, Accepted 18 Oct 2021, Published online: 01 Nov 2021'. There is a 'Check for updates' button and a DOI link: 'https://doi.org/10.1080/24701556.2021.1998121'. At the bottom, there are links for 'Full Article', 'Figures & data', 'References', 'Citations', 'Metrics', 'Reprints & Permissions', and a 'Get access' button.

# Copyright

**Extracts from the Register of Copyrights**

प्रतिलिपिचक्र कार्यालय, भारत सरकार | Copyright Office, Government Of India

Form No. CD-1 (Rev. 10/12/2023)

1. प्रवेशिका संख्या/Registration Number	<b>L-138993/2023</b>
2. आवेदन करने वाले का नाम/Name, address and nationality of the applicant	<b>LOVELY PROFESSIONAL UNIVERSITY, LOVELY PROFESSIONAL UNIVERSITY, JALANDHAR, DELHI-GT ROAD, PHAGWARA PUNJAB-144111, INDIAN</b>
3. रचना के अधिकारकर्ता का नाम/Name of the author	<b>OWNER</b>
4. रचना का विवरण/Title and description of the work	<b>LITERARY DRAMATIC WORK THE GRAPHICAL ABSTRACT PRESENT THE SURFACE COATING OF CELLULOSE MATERIAL WITH ZINC OXIDE NANOPARTICLES</b>
5. रचना का शीर्षक/Title of the work	<b>SURFACE COATING OF CELLULOSE MATERIAL WITH ZINC OXIDE NANOPARTICLES</b>
6. रचना का भाषा/Language of the work	<b>ENGLISH</b>
7. रचनाकार का नाम/Name, address and nationality of the author and if the author is deceased, date of his decease	<b>VAIDEHI KATOCH, LOVELY PROFESSIONAL UNIVERSITY, JALANDHAR, DELHI-GT ROAD, PHAGWARA PUNJAB-144111, INDIAN DR. SAURABHI SHUKLA, LOVELY PROFESSIONAL UNIVERSITY, JALANDHAR, DELHI-GT ROAD, PHAGWARA PUNJAB-144111, INDIAN</b>
8. रचना प्रकाशित है या नहीं/Whether the work is published or unpublished	<b>UNPUBLISHED</b>
9. प्रथम प्रकाशन का वर्ष/Year and country of first publication and name, address and nationality of the publisher	<b>N.A.</b>
10. रचना के अतिरिक्त अन्य प्रकाशनों का वर्ष/Year and country of subsequent publications, if any, and name, address and nationality of the publisher	<b>N.A.</b>
11. रचना के अधिकारकर्ता द्वारा प्रेषित सहमति का विवरण/Name, address and nationality of the owners of various rights comprising the copyright in the work and the extent of rights held by each, together with particulars of assignments and licenses, if any	<b>LOVELY PROFESSIONAL UNIVERSITY, LOVELY PROFESSIONAL UNIVERSITY, JALANDHAR, DELHI-GT ROAD, PHAGWARA PUNJAB-144111, INDIAN</b>
12. रचना के अधिकारकर्ता द्वारा प्रेषित सहमति का विवरण/Name, address and nationality of the assignor of the copyright and the assignee, together with particulars of the assignment	<b>N.A.</b>
13. रचना के अधिकारकर्ता द्वारा प्रेषित सहमति का विवरण/Name, address and nationality of the person in possession of the work (in the case of an architectural work, the year of completion of the work should also be shown)	<b>N.A.</b>
14. रचना के अधिकारकर्ता द्वारा प्रेषित सहमति का विवरण/Name, address and nationality of the person in possession of the work (in the case of an artistic work, the year of completion of the work should also be shown)	<b>N.A.</b>
15. रचना के अधिकारकर्ता द्वारा प्रेषित सहमति का विवरण/Name, address and nationality of the person in possession of the work (in the case of a design, the year of registration of the design should also be shown)	<b>N.A.</b>
16. रचना के अधिकारकर्ता द्वारा प्रेषित सहमति का विवरण/Name, address and nationality of the person in possession of the work (in the case of a trademark, the year of registration of the trademark should also be shown)	<b>N.A.</b>
17. रचना के अधिकारकर्ता द्वारा प्रेषित सहमति का विवरण/Name, address and nationality of the person in possession of the work (in the case of a patent, the year of registration of the patent should also be shown)	<b>N.A.</b>

THE WORK IS ORIGINAL AS DONE BY THE FACULTY AND STAFF OF LOVELY PROFESSIONAL UNIVERSITY.

Registrar of Copyrights

# Ethical Permission Letter

**Institutional Ethics Committee**  
**Punjab Institute of Medical Sciences**  
Garha Road, Jalandhar (Punjab) 144001 India  
Ph No. 0181-660600 Ext- 6035, 4005 (Email: [iec@pimsj.com](mailto:iec@pimsj.com))  
Regd. No. ECR/1413/Inst/PB/2020 Regd.No. EC/NEW/INST/2020/1234  
Reference No: DRMS/IEC/22/14

**Decision**

Protocol no. **IEC/22/14** Dated - : **17/05/22**  
Name and designation of the Applicant: **Ms. Vaidehi Katoch**

**Title of the research proposal reviewed:** Detection and determination of abused drug from urine matrices by Raman based SERS nanoparticles method.

**Along with protocol, other documents reviewed:** Patient information sheet, Informed consent form, Study Proforma

**List of IEC members who attended the meeting- clear description of their role**  
Dr. Sundeep Kaushal (Chairman), Dr. Jagminder Kaur Bajaj (Member Secretary), Dr. H.S Bains, Mrs. Parminder Berry, Dr. Bavneet Kaur Dang, Dr. Megha Sood, Dr. Tania Moudgil (Scientific Members), and Mr. Simratpal Singh (Representative of community).

**A Clear statement of decision reached:** **Approved**

**Principal Investigator has to submit progress Report every \_\_\_\_\_ months**

**Any advice by the IEC to the applicant:**  
- To first test the sample to be negative for BZD and make R value curve. Negative reports to be submitted to IEC maintaining confidentiality.

**In case of conditional decision, any requirement by IEC, including suggestions for revision and the procedure for having the application re-reviewed:** NA

**In case of rejection of the proposal, reason(s) for the rejection will be clearly stated:** NA

*(Signature)*  
Signature of the Chairman/member secretary with date

Chairman  
Institutional Ethics Committee  
PIMS, Jalandhar